

# 1 Norwegian Sea net community production estimated from O<sub>2</sub> 2 and prototype CO<sub>2</sub> optode measurements on a Seaglider

3 Luca Possenti<sup>1,5</sup>, Ingunn Skjelvan<sup>2</sup>, Dariia Atamanchuk<sup>3</sup>, Anders Tengberg<sup>4</sup>, Matthew P.  
4 Humphreys<sup>5</sup>, Socratis Loucaides<sup>6</sup>, Liam Fernand<sup>7</sup>, Jan Kaiser<sup>1</sup>

5 <sup>1</sup>Centre for Ocean and Atmospheric Sciences, School of Environmental Sciences, University of East Anglia,  
6 Norwich, UK

7 <sup>2</sup>NORCE Norwegian Research Centre, Bjerknes Centre for Climate Research, Bergen, Norway

8 <sup>3</sup>Dalhousie University, Halifax, Canada

9 <sup>4</sup>University of Gothenburg, Sweden

10 <sup>5</sup>NIOZ Royal Netherlands Institute for Sea Research, Department of Ocean Systems (OCS), ~~and Utrecht~~  
11 ~~University~~, Texel, the Netherlands

12 <sup>6</sup>National Oceanography Centre, European Way, Southampton, SO14 3ZH, UK

13 <sup>7</sup>Centre for Environment, Fisheries and Aquaculture Sciences, Lowestoft, UK, NR33 0HT

14 *Correspondence to:* Luca Possenti ([L.Possenti@uea.ac.uk](mailto:L.Possenti@uea.ac.uk)/[luca.possenti@nioz.nl](mailto:luca.possenti@nioz.nl))

15 **Abstract.** We report on a pilot study using a CO<sub>2</sub> optode deployed on a Seaglider in the Norwegian Sea ~~for 8~~  
16 ~~months (from March to October 2014)~~. The optode measurements required drift- and lag-correction, and in situ  
17 calibration using discrete water samples collected in the vicinity. We found that the optode signal correlated  
18 better with the concentration of CO<sub>2</sub>,  $c(\text{CO}_2)$ , than with its partial pressure,  $p(\text{CO}_2)$ . Using the calibrated  $c(\text{CO}_2)$   
19 and a regional parameterisation of total alkalinity ( $A_T$ ) as a function of temperature and salinity, we calculated  
20 total dissolved inorganic carbon ~~concentrations,  $C_T$  content,  $c(\text{DIC})$~~ , which had a standard deviation of 1011  
21  $\mu\text{mol kg}^{-1}$  compared with ~~direct  $C_T$  in situ~~ measurements. The glider was also equipped with an oxygen (O<sub>2</sub>)  
22 optode. The O<sub>2</sub> optode was drift-corrected and calibrated using a  $c(\text{O}_2)$  climatology for deep samples ~~( $R^2 = 0.89$ ;~~  
23  ~~$\text{RMSE} = 0.009 \mu\text{mol kg}^{-1}$ )~~. The calibrated data enabled the calculation of  ~~$C_T$ -DIC-~~ and  ~~$c(\text{O}_2)$ -~~ based net  
24 community production,  $N(C_T)$  and  $N(\text{O}_2)$ . To derive  $N$ ,  ~~$C_T$ -DIC~~ and O<sub>2</sub> inventory changes over time were  
25 combined with estimates of air-sea gas exchange, diapycnal mixing and entrainment of deeper waters. Glider-  
26 based observations captured two periods of increased Chl *a* inventory in late spring (May) and a second one in  
27 summer (June). For the May period, we found  ~~$N(C_T) = (23 \pm 4.2 \text{ DIC}) = (21 \pm 5)$~~   $\text{mmol m}^{-2} \text{ d}^{-1}$ ,  $N(\text{O}_2) = (94 \pm 2416)$   
28  $\text{mmol m}^{-2} \text{ d}^{-1}$  and an (uncalibrated) Chl *a* peak concentration of  $c_{\text{raw}}(\text{Chl } a) = 3 \text{ mg m}^{-3}$ . During the June period,  
29  $c_{\text{raw}}(\text{Chl } a)$  increased to a summer maximum of  $4 \text{ mg m}^{-3}$ , associated with  ~~$N(C_T) = (14 \pm 8.7 \text{ DIC}) = (85 \pm 5)$~~   $\text{mmol}$   
30  $\text{m}^{-2} \text{ d}^{-1}$  and  $N(\text{O}_2) = (126 \pm 25) \text{ mmol m}^{-2} \text{ d}^{-1}$ . The high-resolution dataset allowed for quantification of the changes  
31 in  $N$  before, during and after the periods of increased Chl *a* inventory. After the May period, the remineralisation  
32 of the material produced during the period of increased Chl *a* inventory decreased  ~~$N(C_T)$~~  to  ~~$(-4.3 \pm 5 \pm 5.2)$~~   
33  $\text{mmol m}^{-2} \text{ d}^{-1}$  and  $N(\text{O}_2)$  to  ~~$(0 \pm 1.62)$~~   $\text{mmol m}^{-2} \text{ d}^{-1}$ . The survey area was a source of O<sub>2</sub> and a sink of CO<sub>2</sub> for most  
34 of the summer. The deployment captured two different surface waters: influence by the Norwegian Atlantic  
35 Current (NwAC) and the Norwegian Coastal Current (NCC). The NCC was characterised by lower  $c(\text{O}_2)$  and

36  $\epsilon_T c(\text{DIC})$  than the NwAC, as well as lower  $N(\text{O}_2)$ ,  $N(\text{C}_T)$  and  $c_{\text{raw}}(\text{Chl } a)$  but higher  $N(\text{DIC})$ . Our results show  
37 the potential of glider data to simultaneously capture time and depth-resolved variability in  $\epsilon_T \text{DIC}$  and  $\text{O}_2$   
38 concentrations.

## 39 **1 Introduction**

40 Climate models project an increase in the atmospheric  $\text{CO}_2$  mole fraction driven by anthropogenic emissions  
41 from a preindustrial value of  $280 \mu\text{mol mol}^{-1}$  (Neffel et al., 1982)(Neffel et al., 1982) to  $538\text{-}936 \mu\text{mol mol}^{-1}$  by  
42 2100 (Pachauri and Reisinger, 2007). The ocean is known to be a major  $\text{CO}_2$  sink (Sabine et al., 2004; Le Quéré  
43 et al., 2009; Sutton et al., 2014)(Sabine et al., 2004; Le Quéré et al., 2009; Sutton et al., 2014); in fact, it has  
44 taken up approximately 25 % of this anthropogenic  $\text{CO}_2$  with a rate of  $(2.5 \pm 0.6) \text{ Gt a}^{-1}$  (in C equivalents)  
45 (Friedlingstein et al., 2019)(Friedlingstein et al., 2019). This uptake alters the carbonate system of seawater and  
46 is causing a decrease in seawater pH, a process known as ocean acidification (Gattuso and Hansson, 2011). The  
47 processes affecting the marine carbonate system include air-sea gas exchange, photosynthesis and respiration,  
48 advection and vertical mixing, and  $\text{CaCO}_3$  formation and dissolution. For that reason, it is important to develop  
49 precise, accurate and cost-effective tools to observe  $\text{CO}_2$  trends, variability and related processes in the ocean.  
50 Provided that suitable sensors are available, autonomous ocean glider measurements may help resolve these  
51 processes.

52 To quantify the marine carbonate system, four variables are commonly measured: total dissolved inorganic  
53 carbon concentration ( $\text{C}_T$ ), pH,  $c(\text{DIC})$ ; total alkalinity ( $A_T$ ) and the fugacity of  $\text{CO}_2$  ( $f(\text{CO}_2)$ ); and pH. At  
54 thermodynamic equilibrium, knowledge of two of the four variables is sufficient to calculate the other two.  
55 Marine carbonate system variables are primarily measured on research ships, commercial ships of opportunity,  
56 moorings, buoys and floats (Hardman-Mountford et al., 2008; Monteiro et al., 2009; Takahashi et al., 2009;  
57 Olsen et al., 2016; Bushinsky et al., 2019). Moorings equipped with submersible sensors often provide limited  
58 vertical and horizontal, but good long-term temporal resolution (Hemsley, 2015). In contrast, ship-based surveys  
59 have higher vertical and spatial resolution than moorings but limited repetition frequency because of the expense  
60 of ship operations. Ocean gliders have the potential to replace some ship surveys because they are much cheaper  
61 to operate and will increase our coastal and regional observational capacity. However, the slow glider speed of  $1\text{-}$   
62  $2 \text{ km h}^{-1}$  only allows a smaller spatial coverage than ship surveys and the sensors require careful calibration to  
63 match the quality of data provided by ship-based sampling.

64 ~~Carbonate system sensors suitable for autonomous deployment have been developed in the past decades, in  
65 particular pH sensors (Martz et al., 2010; Rérolle et al., 2013; Seidel et al., 2008) and  $p(\text{CO}_2)$  sensors (Goyet et  
66 al., 1992; Degrandpre, 1993; Körtzinger et al., 1996; Bittig et al., 2012; Atamanchuk, 2013). One of these  
67 sensors is the  $\text{CO}_2$  optode (Atamanchuk et al., 2014) which has been successfully deployed to monitor an  
68 artificial  $\text{CO}_2$  leak on the Scottish west coast (Atamanchuk, et al., 2015b), on a cabled underwater observatory  
69 (Atamanchuk, et al., 2015a), to measure lake metabolism (Peeters et al., 2016), for fish transportation (Thomas et  
70 al., 2017) and on a moored profiler (Chu et al., 2020).~~

71  $\epsilon_T$  Carbonate system sensors suitable for autonomous deployment have been developed in the past decades, in  
72 particular pH sensors (Seidel et al., 2008; Martz et al., 2010; Rérolle et al., 2013) and  $p(\text{CO}_2)$  sensors

73 [\(Atamanchuk et al., 2014; Bittig et al., 2012; Degrandpre, 1993; Goyet et al., 1992; Körtzinger et al., 1996\)](#). One  
74 [of these sensors is the CO<sub>2</sub> optode \(Atamanchuk et al., 2014\) which has been successfully deployed to monitor](#)  
75 [an artificial CO<sub>2</sub> leak on the Scottish west coast \(Atamanchuk, et al., 2015b\), on a cabled underwater observatory](#)  
76 [\(Atamanchuk et al., 2015a\), to measure lake metabolism \(Peeters et al., 2016\), for fish transportation \(Thomas et](#)  
77 [al., 2017\) and on a moored profiler \(Chu et al., 2020\).](#)

78 [c\(DIC\) and c\(O<sub>2</sub>\) measurements](#) can be used to calculate net community production ([ANCP](#)), which is defined as  
79 the difference between gross primary production ([GGPP](#)) and community respiration ([RCR](#)). At steady-state,  
80 [ANCP](#) is equal to the rate of organic carbon export and transfer from the surface into the mesopelagic and deep  
81 waters ([Lockwood et al., 2012](#)). [NCP](#) is derived by vertical integration to a specific  
82 depth, that is commonly defined relative to the mixed layer depth ( $z_{\text{mix}}$ ) or the bottom of the euphotic zone ([Plant](#)  
83 [et al., 2016](#))([Plant et al., 2016](#)). A system is defined as autotrophic when [GGPP](#) is larger than [RCR](#) (i.e. [ANCP](#) is  
84 positive) and as heterotrophic when [RCR](#) is larger than [GGPP](#) (i.e. [ANCP](#) is negative) (Ducklow and Doney,  
85 2013).

86 ~~[N can be quantified using bottle incubations or in situ biogeochemical budgets \(Sharples et al., 2006; Quay, et al,](#)~~  
87 ~~[2012; Seguro et al., 2019\). Bottle incubations involve measuring production and respiration in vitro under dark](#)~~  
88 ~~[and light conditions. Biogeochemical budgets combine O<sub>2</sub> and C<sub>T</sub> inventory changes with estimates of air-sea](#)~~  
89 ~~[gas exchange, entrainment, advection and vertical mixing \(Alkire et al., 2014; Binetti et al., 2020; Neuer et al.,](#)~~  
90 ~~[2007\).](#)~~

91 [NCP can be quantified using bottle incubations or in situ biogeochemical budgets \(Sharples et al., 2006; Quay, et](#)  
92 [al, 2012; Seguro et al., 2019\). Bottle incubations involve measuring production and respiration in vitro under](#)  
93 [dark and light conditions. Biogeochemical budgets combine O<sub>2</sub> and DIC inventory changes with estimates of air-](#)  
94 [sea gas exchange, entrainment, advection and vertical mixing \(Neuer et al., 2007; Alkire et al., 2014; Binetti et](#)  
95 [al., 2020\).](#)

96 The Norwegian Sea is a complex environment due to the interaction between the Atlantic Water (NwAC)  
97 entering from the south-west, Arctic Water coming from the north and the Norwegian Coastal Current (NCC)  
98 flowing along the Norwegian coast (Nilsen and Falck, 2006). In particular, Atlantic Water enters the Norwegian  
99 Sea through the Faroe-Shetland Channel and Iceland-Faroe Ridge (Hansen and Østerhus, 2000) with salinity  $S$   
100 between 35.1 and 35.3 and temperatures ( $\theta$ ) warmer than 6 °C (Swift, 1986). The NCC water differs from the  
101 NwAC with a surface  $S < 35$  (Saetre and Ljoen, 1972) and a seasonal  $\theta$  signal (Nilsen and Falck, 2006).

102 Biological production in the Norwegian Sea varies during the year and ~~[can be divided into 55 different](#)~~  
103 ~~[can be discerned](#)~~ (Rey, 2001): (1) winter with the smallest productivity and phytoplankton biomass; (2) a pre-  
104 bloom period; (3) the spring bloom when productivity increases and phytoplankton biomass reaches the annual  
105 maximum; (4) a post-bloom period with productivity mostly based on regenerated nutrients; (5) autumn with  
106 smaller blooms than in summer. Previous estimates of [the DIC based net community production \( \$N\(\epsilon\_T \text{ DIC}\)\$ \)](#)  
107 were based on discrete  [\$\epsilon\_T \text{ DIC}\$](#)  samples (Falck and Anderson, 2005) or were calculated from  $c(\text{O}_2)$   
108 measurements and converted to C equivalents assuming Redfield stoichiometry of production/respiration ([Falek](#)  
109 [and Gade, 1999; Kivimäe, 2007; Skjelvan et al., 2001\)](#). ~~[Glider measurements have been used to estimate  \$N\$ \(Falck](#)~~  
110 ~~[and Gade, 1999; Skjelvan et al., 2001; Kivimäe, 2007\)](#)~~. ~~[Glider measurements have been used to estimate NCP in](#)~~

111 other ocean regions (~~Nicholson et al., 2008; Alkire et al., 2014; Haskell et al., 2019; Binetti et al.,~~  
112 ~~2020~~)(Nicholson et al., 2008; Alkire et al., 2014; Haskell et al., 2019; Binetti et al., 2020); however, as far as we  
113 know, this is the first study of net community production in the Norwegian Sea using a high-resolution glider  
114 dataset ( $>10^6$  data points; 40 s time resolution) and the first anywhere estimating  $\Delta NCP$  from a glider-mounted  
115 sensor directly measuring the marine carbonate system.

## 116 2 Material and methods

### 117 ~~2.12.1~~ List of symbols (unit)

118	$A_T$	total alkalinity ( $\mu\text{mol kg}^{-1}$ )
119	$b$	backscatter signal (engineering units)
120	$c$	amount content ( $\mu\text{mol kg}^{-1}$ )
121	$C$	amount concentration ( $\text{mmol m}^{-3}$ )
122	Chl $a$	chlorophyll $a$
123	DIC	dissolved inorganic carbon
124	$E$	entrainment flux ( $\text{mmol m}^{-2} \text{d}^{-1}$ )
125	$F_V$	diapycnal eddy diffusion flux ( $\text{mmol m}^{-2} \text{d}^{-1}$ )
126	$f(\text{CO}_2)$	fugacity of $\text{CO}_2$ ( $\mu\text{atm}$ )
127	$I$	inventory ( $\text{mmol m}^{-2}$ )
128	$K_z$	diapycnal eddy diffusivity ( $\text{m}^2 \text{s}^{-1}$ )
129	$N$	net community production ( $\text{mmol m}^{-2} \text{d}^{-1}$ )
130	$p(\text{CO}_2)$	partial pressure of $\text{CO}_2$ ( $\mu\text{atm}$ )
131	$S$	practical salinity ()
132	$t$	time (s)
133	$U$	wind speed ( $\text{m s}^{-1}$ )
134	$x$	dry mole fraction ( $\text{mol mol}^{-1}$ )
135	$z_{\text{DCM}}$	depth of the deep chlorophyll maximum (m)
136	$z_{\text{lim}}$	integration depth (m)
137	$z_{\text{mix}}$	mixed layer depth (m)
138	$\Phi$	air-sea flux ( $\text{mmol m}^{-2} \text{d}^{-1}$ )
139	$\varphi$	$\text{CO}_2$ optode CalPhase ( $^\circ$ )
140	$\sigma_0$	potential density ( $\text{kg m}^{-3}$ )
141	$\theta$	Celsius temperature ( $^\circ\text{C}$ )
142	$\tau$	response time (s)

143

### 144 2.2 Glider sampling

145 Kongsberg Seaglider 564 was deployed in the Norwegian Sea on 16 March 2014 at  $63.00^\circ \text{N}$ ,  $3.86^\circ \text{E}$  and  
146 recovered on 30 October 2014 at  $62.99^\circ \text{N}$ ,  $3.89^\circ \text{E}$ . The Seaglider was equipped with a prototype Aanderaa  
147 4797  $\text{CO}_2$  optode, an Aanderaa 4330F oxygen optode (~~Tengberg et al., 2006~~)(Tengberg et al., 2006), a Seabird  
148 CTD and a combined backscatter/chlorophyll  $a$  fluorescence sensor (Wetlabs Eco Puck BB2FLVMT). The  
149 mean sampling intervals for each sensor varied with depth (Table 1). ~~On average in the top 100 m the CTD~~  
150 ~~performed an in situ measurement every 24 s, the  $\text{O}_2$  optode every 49 s, the  $\text{CO}_2$  optode every 106 s and the~~

151 fluorescence sensor every 62 s. The sampling interval increased in depths between 100 to 500 m to 31 s for the  
 152 CTD, 153 s for the O<sub>2</sub>-optode and 233 s for the CO<sub>2</sub>-optode. The sampling interval reached its maximum at  
 153 depths between 500 to 1000 m where was 42 s for the CTD, 378 s for the O<sub>2</sub>-optode and 381 s for the CO<sub>2</sub>  
 154 optode.

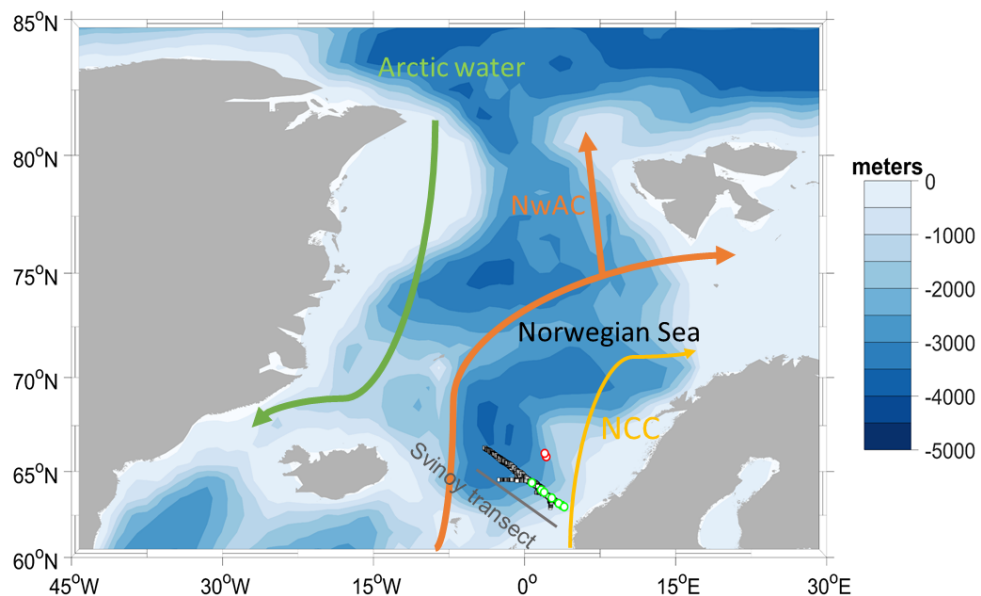
155 **Table 1.** Average sampling interval of Seabird CTD, Aanderaa 4330F oxygen optode, Aanderaa 4797 CO<sub>2</sub>  
 156 optode and a combined backscatter/chlorophyll *a* fluorescence sensor (Wetlabs Eco Puck BB2FLVMT) in the  
 157 top 100 m, from 100 to 500 and from 500 to 1000 m.

Depth / m	$t(\text{CTD}) / \text{s}$	$t(\text{O}_2) / \text{s}$	$t(\text{CO}_2) / \text{s}$	$t(\text{Chl } a) / \text{s}$
0 – 100 m	24	49	106	62
100 – 500 m	31	153	233	-
500 – 1000 m	42	378	381	-

158

159 The deployment followed the Svinøy trench, from the open sea towards the Norwegian coast. The glider covered  
 160 a 536 km long transect 8 times (4 times in each direction) for a total of 703 dives (Figure 1).

161



162

163 **Figure 1:** Map of the glider deployment and the main water masses/currents. The black dots are the glider dives,  
 164 the green and the red dots are the water samples collected along the glider section and at Ocean Weather Station  
 165 M (OWSM<sub>7</sub>), respectively. The three main water masses (Skjelvan et al., 2008)(Skjelvan et al., 2008) are the  
 166 Norwegian Coastal Current (yellow), the Norwegian Atlantic Current (NwAC, orange) and Arctic Water (green).

167

168

169 **2.23 Discrete sampling**

170 During the glider deployment, 70 discrete water samples from various depths (5, 10, 20, 30, 50, 100, 300, 500  
 171 and 1000 m) were collected on 45 different cruises on the R/V Haakon Mosby along the southern half of the

172 glider transect on 18 March, 5 May, 6 and 14 June, and 30 October 2014. Samples for  $\epsilon_{TC}(DIC)$  and  $A_T$  were  
173 collected from 10 L Niskin bottles following the standard operational procedure (SOP) 1 of Dickson et al.  
174 (2007). The  $\epsilon_{TC}(DIC)$  and  $A_T$  samples were preserved with saturated  $HgCl_2$  solution (final  $HgCl_2$  concentration:  
175  $15 \text{ mg dm}^{-3}$ ) and analysed within 14 days after the collection. Nutrient samples from the same Niskin bottles  
176 were preserved with chloroform (Hagebo and Rey, 1984).  $\epsilon_{TC}(DIC)$  and  $A_T$  were analysed on shore according to  
177 SOP 2 and 3b (Dickson et al., 2007) using a VINDTA 3D (Marianda) with a CM5011 coulometer (UIC  
178 instruments) and a VINDTA 3S (Marianda), respectively. The precision of the samples'  $c(DIC)$  and  $A_T$  values  
179 was  $1 \mu\text{mol kg}^{-1}$  for both, based on duplicate samples and running Certified Reference Material (CRM) batch  
180 numbers 118 and 138 provided by professor A. Dickson, Scripps Institution of Oceanography, San Diego, USA  
181 (Dickson et al., 2003). Nutrients were analysed on shore using an Alpkem Auto Analyzer. In addition, 43 water  
182 samples were collected at Ocean Weather Station M (OWSM) on 5 different cruises on 22 March on R/V  
183 Haakon Mosby, on 9 May on R/V G.O. Sars, on 14 June on R/V Haakon Mosby, on 2 August and on 13  
184 November 2014 on R/V Johan Hjort from 10, 30, 50, 100, 200, 500, 800 and 1000 m depth. The OWSM  
185 samples were preserved and analysed for  $A_T$  and  $\epsilon_{TC}(DIC)$  as the Svinøy samples. No phosphate and silicate  
186 samples were collected at OWSM. Temperature ( $\theta$ ) and salinity ( $S$ ) profiles were measured at each station using  
187 a SeaBird 911 plus CTD. pH and  $f(CO_2)$  were calculated using the MATLAB toolbox CO2SYS (Van Heuven et  
188 al., 2014)(Van Heuven et al., 2011), with the following constants:  $K_1$  and  $K_2$  carbonic acid dissociation constants  
189 of Lueker et al. (2000), Lueker et al. (2000),  $K(HSO_4^-/SO_4^{2-})$  bisulfate dissociation constant of Dickson (1990)  
190 and borate to chlorinity ratio of Lee et al. (2010). In Lee et al. (2010). The precision of  $A_T$  and  $c(DIC)$  led to an  
191 uncertainty in the calculated  $c(CO_2)$  of  $0.28 \mu\text{mol kg}^{-1}$ . For the OWSM calculations, we used nutrient  
192 concentrations from the Svinøy section at a time as close as possible to the OWSM sampling as input. In the case  
193 of the glider, we derived a parameterisation for phosphate and silicate concentration as a function of sample  
194 depth and time. This parameterisation had an uncertainty of  $1.3$  and  $0.13 \mu\text{mol kg}^{-1}$  and a  $R^2$  of  $0.6$  and  $0.4$ , for  
195 silicate and phosphate concentrations, respectively. The uncertainty was calculated as the root mean square  
196 difference between measured and parameterised concentrations. This nutrient concentration uncertainty  
197 contributed an uncertainty of  $0.04 \mu\text{mol kg}^{-1}$  in the calculation of  $c(CO_2)$ , which is negligible- and smaller than  
198 the uncertainty caused by  $A_T$  and  $c(DIC)$ .

### 199 **2.34 Oxygen optode calibration**

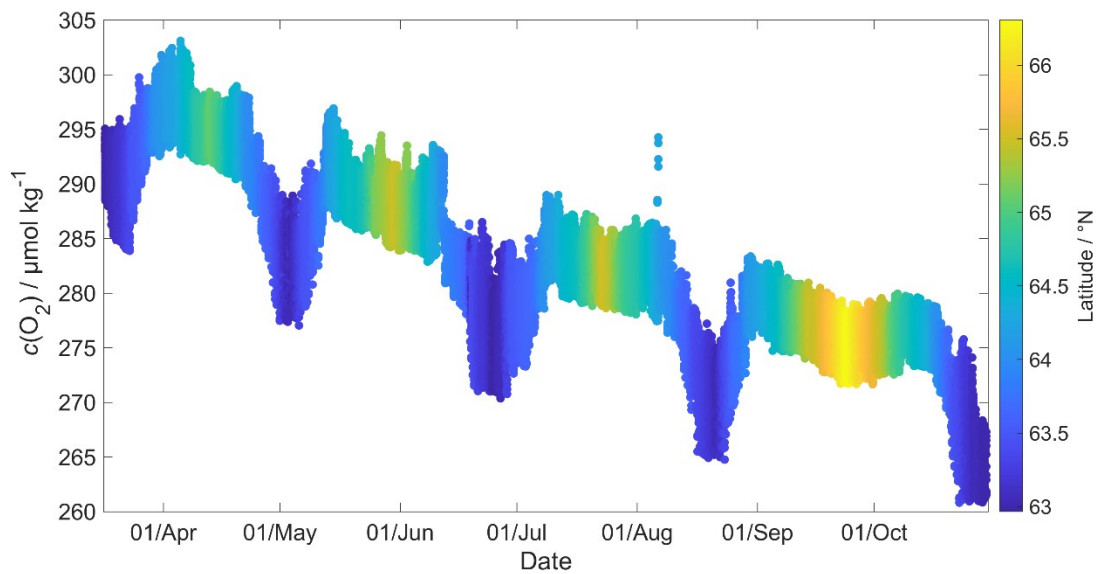
200 The last oxygen optode calibration before the deployment was performed in 2012 as a two-point calibration at  
201  $9.91 \text{ }^\circ\text{C}$  in air-saturated water and at  $20.37 \text{ }^\circ\text{C}$  in anoxic  $Na_2SO_3$  solution. Oxygen optodes are known to be  
202 affected by drift (Bittig et al., 2015)Bittig et al., 2015), which is even worse for the fast-response foils used in the  
203 4330F optode for glider deployments. It has been suggested that it is necessary to calibrate and drift correct the  
204 optode using discrete samples or in-air measurements (Nicholson and Feen, 2017). Unfortunately, no discrete  
205 samples were collected at glider deployment or recovery.

206 To overcome this problem, we used archived data to correct for oxygen optode drift. These archived  
207 concentration data (designated  $c_c(O_2)$ ) were collected at OWSM between 2001 and 2007 (downloaded from  
208 ICES data base) and in the glider deployment region between 2000 and 2018 (extracted from GLODAPv2;  
209 Olsen et al., 2016)Olsen et al., 2016). To apply the correction, we used the oxygen samples corresponding to a  
210 potential density  $\sigma_0 > 1028 \text{ kg m}^{-3}$  (corresponding to depths between 427 and 1000 m), because waters of these  
211 potential densities were always well below the mixed layer and therefore subject to limited seasonal and

212 interannual variability, as evidenced by the salinity  $S$  and potential temperature  $\theta$  of these samples:  $S$  varied from  
213 34.88 to 34.96, with a mean of  $34.90 \pm 0.01$ ;  $\theta$  varied from 0.45 to  $-0.76$  °C, with a mean of  $(-0.15 \pm 0.36)$  °C.

214 Figure 2 shows that the glider oxygen concentration ( $c_G(\text{O}_2)$ ) corresponding to  $\sigma_0 > 1028 \text{ kg m}^{-3}$  was  
215 characterised by two different water masses separated at a latitude of about  $64^\circ \text{ N}$ . We used the samples  
216 collected north of  $64^\circ \text{ N}$  to derive the glider optode correction because this reflects the largest area covered by  
217 the glider. We did not use the southern region because the archived samples from there covered only 5 days. For  
218 each day of the year with archived samples, we calculated the median concentration of the glider and the  
219 archived samples. Figure 3 shows a plot of the ratio between  $c_C(\text{O}_2)/c_G(\text{O}_2)$  against the day of the year and a  
220 linear fit, which is used to calibrate  $c_G(\text{O}_2)$  and correct for drift.

221



222

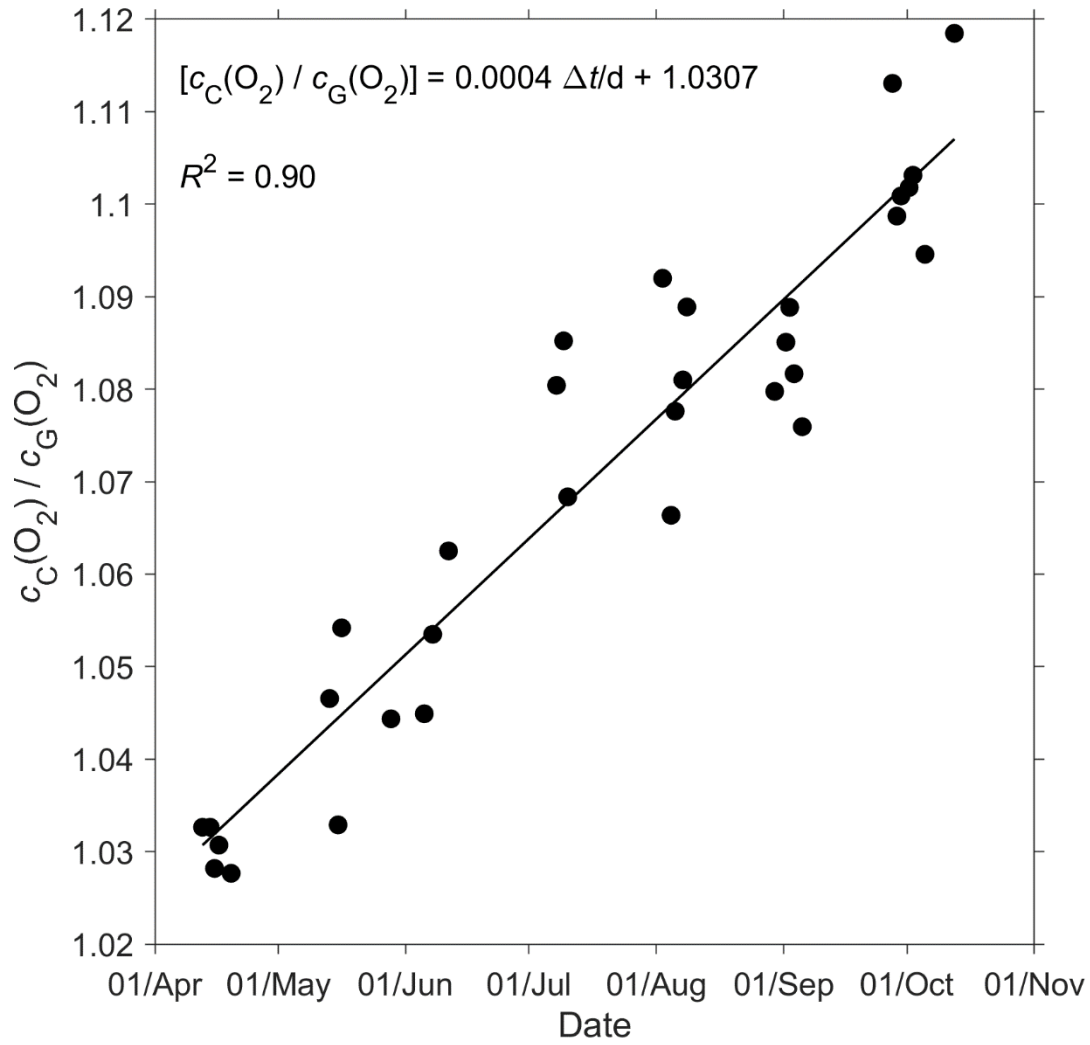
223 **Figure 2:** Glider oxygen concentration,  $c_G(\text{O}_2)$ , for  $\sigma_0 > 1028 \text{ kg m}^{-3}$  coloured by latitude.

224

225 No lag correction was applied because the  $\text{O}_2$  optode had a fast response foil and showed no detectable lag ( $< 10$   
226 s), based on a comparison between descent and ascent profiles.

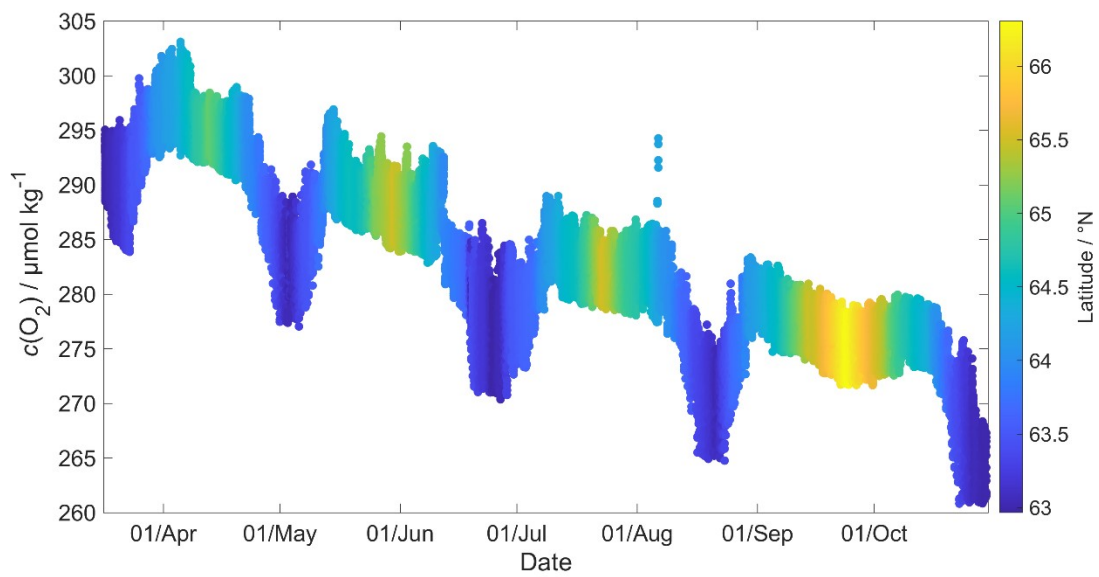
227

228



229  
230

Figure 3:- The

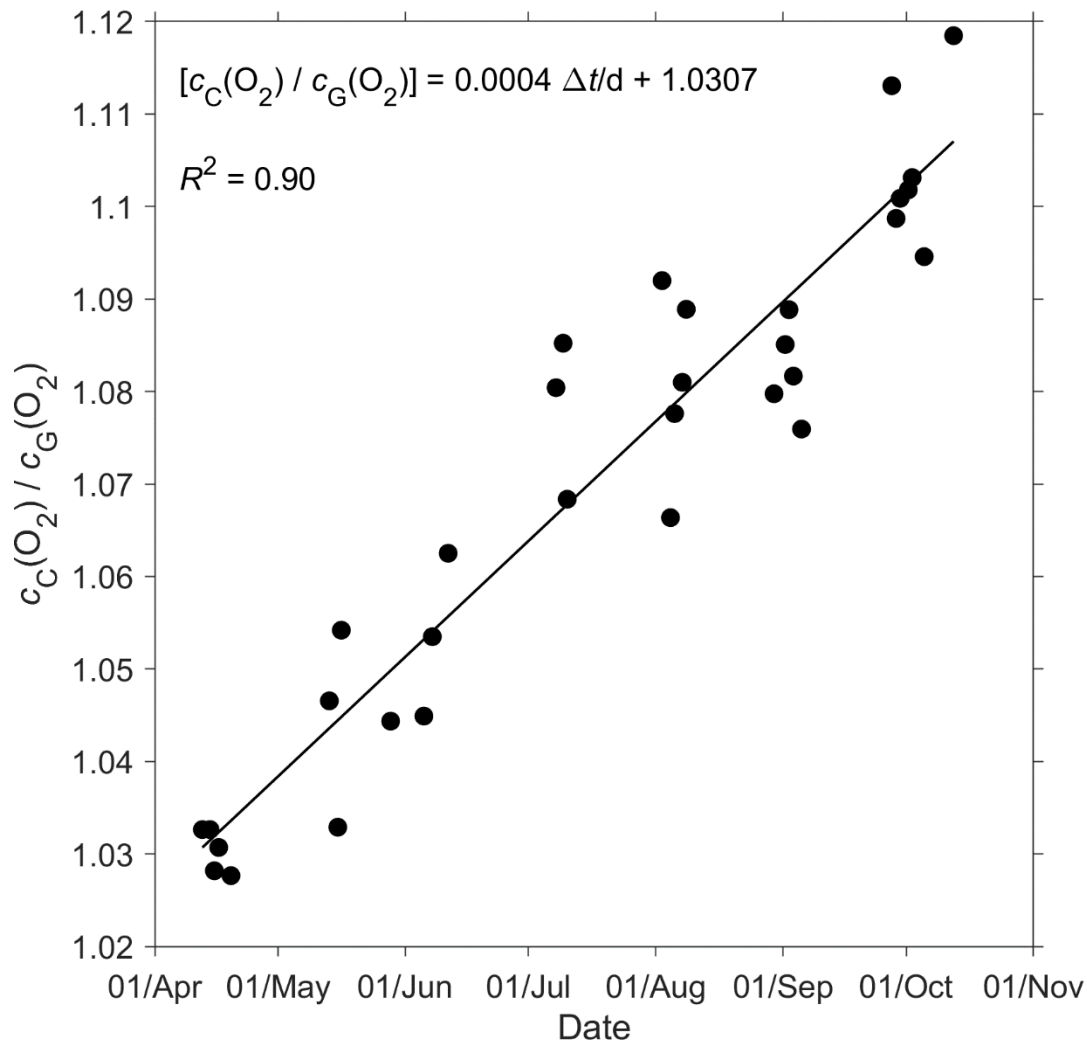


231

232

Figure 2: Glider oxygen concentration,  $c_G(\text{O}_2)$ , for  $\sigma_\theta > 1028 \text{ kg m}^{-3}$  coloured by latitude.





233

234 **Figure 3:** A linear fit of the ratio between the daily median of the discrete oxygen samples ( $c_C(O_2)$ ) and glider  
 235 oxygen data ( $c_G(O_2)$ ) for  $\sigma_0 > 1028 \text{ kg m}^{-3}$  was used to derive the  $c_G(O_2)$  drift and initial offset at deployment.

236 The time difference  $\Delta t$  is calculated with respect to the deployment day ~~of the 16th of~~ on 16 March.

237

### 238 **2.45 CO<sub>2</sub> optode measurement principle**

239 The CO<sub>2</sub> optode consists of an optical and a temperature sensor incorporated into a pressure housing. The optical  
 240 sensor has a sensing foil comprising two fluorescence indicators (luminophores), one of which is sensitive to pH  
 241 changes and the other is not and thus used as a reference. The excitation and emission spectra of the two  
 242 fluorescence indicators overlap, but the reference indicator has a longer fluorescence lifetime than the pH  
 243 indicator. These two fluorescence lifetimes are combined using an approach known as Dual Lifetime  
 244 Referencing (DLR) ([Klimant et al., 2001](#); [von Bültzingslöwen et al., 2002](#))([Klimant et al., 2001](#); [von](#)  
 245 [Bültzingslöwen et al., 2002](#)). From the phase shift ( $\varphi$ ), the partial pressure of CO<sub>2</sub>,  $p(\text{CO}_2)$ , is parameterised as an  
 246 eight-degree polynomial ([Atamanchuk et al., 2014](#))([Atamanchuk et al., 2014](#)):

$$247 \log [p(\text{CO}_2)/\mu\text{atm}] = C_0 + C_1 \varphi + \dots + C_8 \varphi^8 \quad (1)$$

248 where  $C_0$  to  $C_8$  are temperature-dependent coefficients.

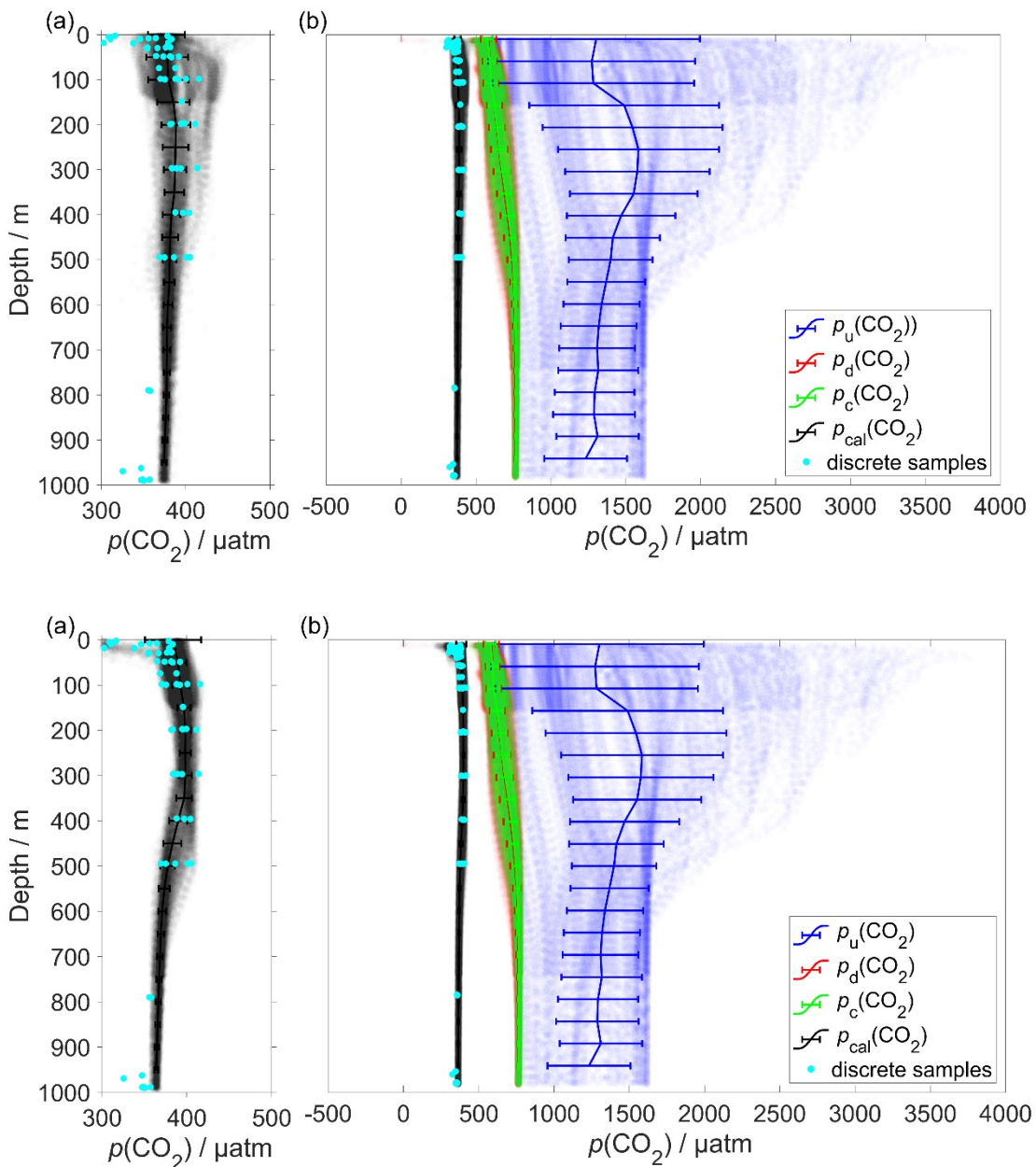
249 The partial pressure of CO<sub>2</sub> is linked to the CO<sub>2</sub> concentration,  $c(\text{CO}_2)$ , and the fugacity of CO<sub>2</sub>,  $f(\text{CO}_2)$ , via the  
 250 following relationship:

$$251 \quad c(\text{CO}_2) = p(\text{CO}_2) / [1 - p(\text{H}_2\text{O}) / p] \quad F(\text{CO}_2) = K_0(\text{CO}_2) f(\text{CO}_2) \quad (2)$$

252 where  $F(\text{CO}_2)$  is the solubility function (Weiss and Price, 1980),  $p(\text{H}_2\text{O})$  is the water vapour pressure,  $p$  is the  
 253 total gas tension (assumed to be near 1 atm) and  $K_0(\text{CO}_2)$  is the solubility coefficient.  $F$  and  $K_0$  vary according to  
 254 temperature and salinity.

### 255 2.56 CO<sub>2</sub> optode lag and drift correction and calibration

256 The CO<sub>2</sub> optode was fully functional between dives 31 (on 21 March 2014) and 400 (on 24 July 2014). After  
 257 dive 400, the CO<sub>2</sub> optode stopped sampling in the top 150 m. Figure 4 shows the outcome of each calibration  
 258 step ~~described in this section (steps 1 and 2) and section 2.6 (step 3)~~: 0) uncalibrated optode output (blue dots),  
 259 1) drift correction (red dots), 2) lag correction (green dots) and 3) calibration using discrete water samples (black  
 260 dots).



261  
262

263

264 **Figure 4:** Panel a) shows in black the calibrated  $p(\text{CO}_2)$  ( $p_{\text{cal}}(\text{CO}_2)$ ) and in azure the discrete samples. b) Plot of  
 265  $p(\text{CO}_2)$  versus depth where the vertical continuous lines are the mean every 50 m and the error bars represent the  
 266 standard deviation. Blue colour shows  $p_{\text{d}}(\text{CO}_2)$  without any correction; red shows  $p_{\text{d}}(\text{CO}_2)$  corrected for drift,  
 267 green represents  $p_{\text{c}}(\text{CO}_2)$  corrected for drift and lag; black shows  $p_{\text{cal}}(\text{CO}_2)$  calibrated against water samples  
 268 (azure dots) collected during the deployment (section 2.6).  $p_{\text{cal}}(\text{CO}_2)$  had a mean standard deviation of 22  $\mu\text{atm}$   
 269 and a mean bias of 1.8.4  $\mu\text{atm}$  compared with the discrete samples.

270

271 In order to correct for the drift occurring during the glider mission, we selected the  $\text{CO}_2$  optode measurements in  
 272 water with  $\sigma_0 > 1028 \text{ kg m}^{-3}$  (just as for  $\text{O}_2$ ; section 2.34). We calculated the median of the raw optode phase  
 273 shift data ("CalPhase"  $\varphi_{\text{cal}}$ ) for each Seagliders dive. Then, we calculated a drift coefficient ( $m_i$ ) as the ratio  
 274 between the median  $\varphi_{\text{cal}}$  for a given dive divided by the median  $\varphi_{\text{cal}}$  of dive 31. Drift-corrected  $\varphi_{\text{cal,d}}$  values were  
 275 calculated by dividing the raw  $\varphi_{\text{cal}}$  by the specific  $m_i$  for each dive.

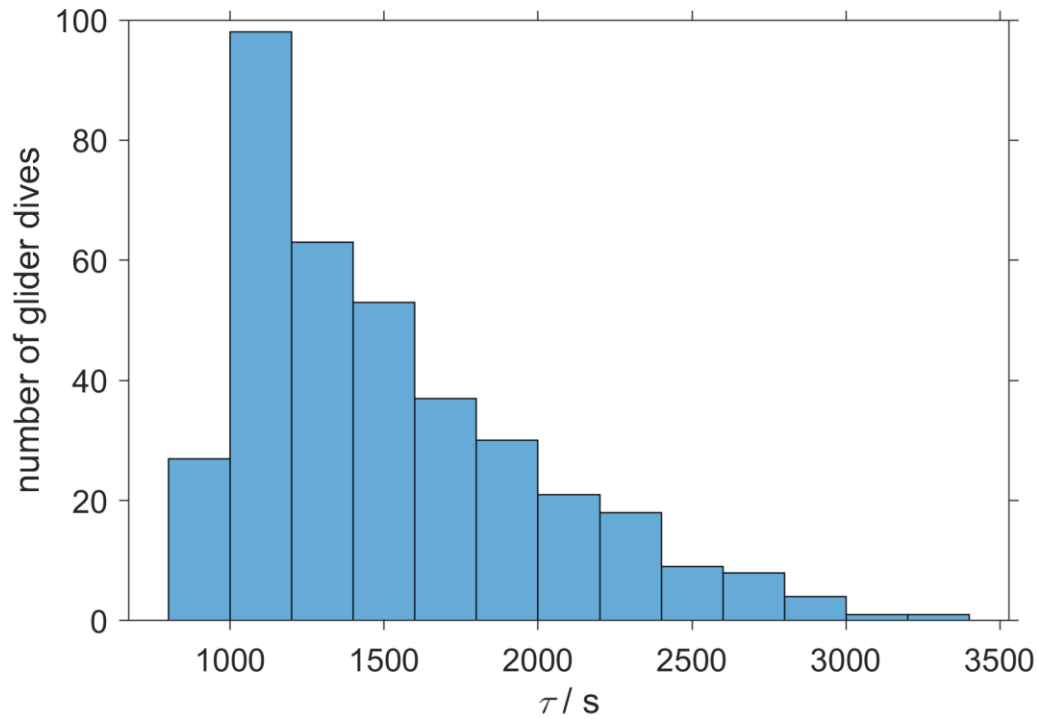
276 The  $\text{CO}_2$  optode was also affected by lag (~~Atamanchuk et al., 2014~~)(Atamanchuk et al., 2014) caused by the  
 277 slow response of the optode to ambient  $c(\text{CO}_2)$  changes in time and depth. The lag created a discrepancy  
 278 between the depth profiles obtained during glider ascents and descents. To correct for this lag we applied the  
 279 method of Miloshevich et al. (2004), which was previously used by ~~Fiedler et al. (2013)~~Fiedler et al. (2013) and  
 280 ~~Atamanchuk et al. (2015b)~~Atamanchuk et al. (2015b) to correct the lag of the Contros HydroC  $\text{CO}_2$  sensor  
 281 (Fiedler et al., 2013; Saderne et al., 2013). This  $\text{CO}_2$  sensor has a different measurement principle (infrared  
 282 absorption) than the  $\text{CO}_2$  optode, but both rely on the diffusion of  $\text{CO}_2$  through a gas-permeable membrane.

283 To apply the lag correction, the sampling interval ( $\Delta t$ ) needs to be sufficiently small compared to the sensor  
 284 response time ( $\tau$ ) and the ambient variability (Miloshevich, 2004). Before the lag correction,  $\varphi_{\text{cal,d}}$  was  
 285 ~~rLOWESS~~-smoothed to remove any outliers and "kinks" in the profile using the Matlab function rLOWESS. The  
 286 smoothing function applies a local regression every 9 points using a weighted robust linear least-squares fit.  
 287 Subsequently,  $\tau$  was determined such that the following lag-correction equation (Miloshevich, 2004) minimised  
 288 the  $\varphi_{\text{cal,d}}$  difference between each glider ascent and the following descent:

$$289 \quad p_{\text{c}}(\text{CO}_2, t_1) = \frac{p_{\text{d}}(\text{CO}_2, t_1) - p_{\text{d}}(\text{CO}_2, t_0) e^{-\Delta t/\tau}}{1 - e^{-\Delta t/\tau}} \quad (3)$$

290 where  $p_{\text{d}}(\text{CO}_2, t_0)$  is the drift-corrected value measured by the optode at time  $t_0$ ,  $p_{\text{d}}(\text{CO}_2, t_1)$  is the measured value  
 291 at time  $t_1$ ,  $\Delta t$  is the time between  $t_0$  and  $t_1$ ,  $\tau$  is the response time, and  $p_{\text{c}}(\text{CO}_2, t_1)$  is the lag-corrected value at  $t_1$ .

292 We calculated a  $\tau$  value for each glider dive and used the median of  $\tau$  (1384 s, 25<sup>th</sup> quartile: 1101 s; 75<sup>th</sup> quartile:  
 293 1799 s) (Figure 5), which was larger than  $\Delta t$  (258 s) and therefore met the requirement to apply the Miloshevich  
 294 (2004) method. To apply the lag correction the glider needs to sample same water mass during the ascent and  
 295 descent. The difference between the ascent and descent was minimal because was  $(0.13 \pm 0.33) ^\circ\text{C}$  for  $\theta$  and  
 296  $0.02 \pm 0.04$  for  $S$ . This lag correction reduced the average difference between ~~the~~ glider ascent and descent from  
 297  $(71 \pm 30) \mu\text{atm}$  to  $(21 \pm 26) \mu\text{atm}$ .



298

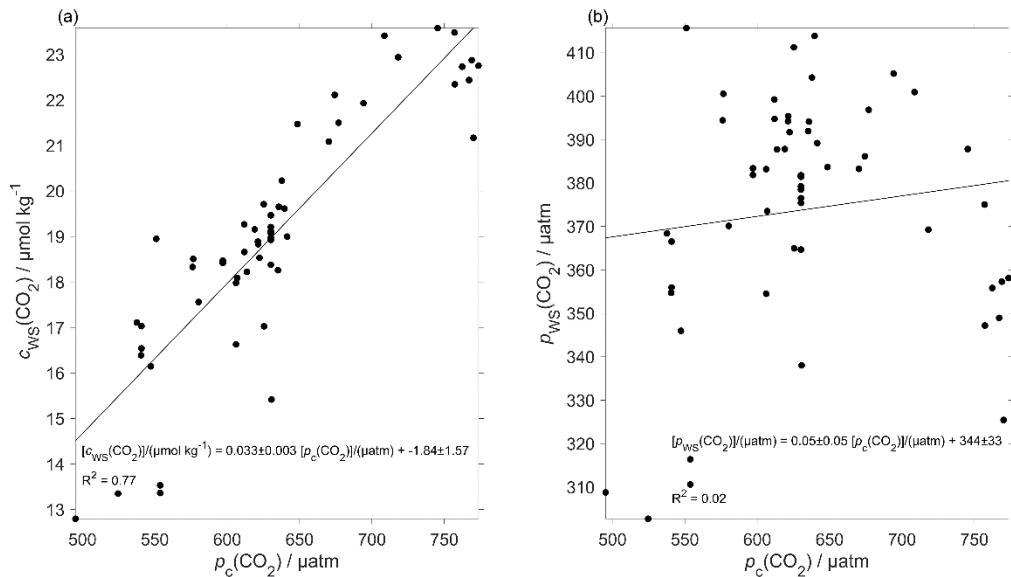
299 **Figure 5:** The histogram shows the distribution of the  $\tau$  calculated from glider dive 31 to 400 to correct the CO<sub>2</sub>  
 300 optode drift using the algorithm of Miloshevich (2004).

301

302

303 The CO<sub>2</sub> optode output was calibrated using the discrete samples collected throughout the mission. Using the  
 304 discrete sample time and potential density  $\sigma_0$ , we selected the closest CO<sub>2</sub> optode output. ~~Figure 6 shows a~~  
 305 ~~linear regression between optode output and  $c(\text{CO}_2)$  from the discrete samples ( $c_{\text{ws}}(\text{CO}_2)$ ), which~~ was used to  
 306 calibrate the optode output  $p_c(\text{CO}_2)$  in terms of  $c(\text{CO}_2)$ . ~~We used  $c(\text{CO}_2)$  because it~~ had a better correlation than  
 307  ~~$p(\text{CO}_2)$  ( $R^2 = 0.77$  vs.  $R^2 = 0.02$ ). The residual difference in  $c(\text{CO}_2)$  between glider and water samples had a~~  
 308 ~~standard deviation of  $1.3 \mu\text{mol kg}^{-1}$ .~~

309

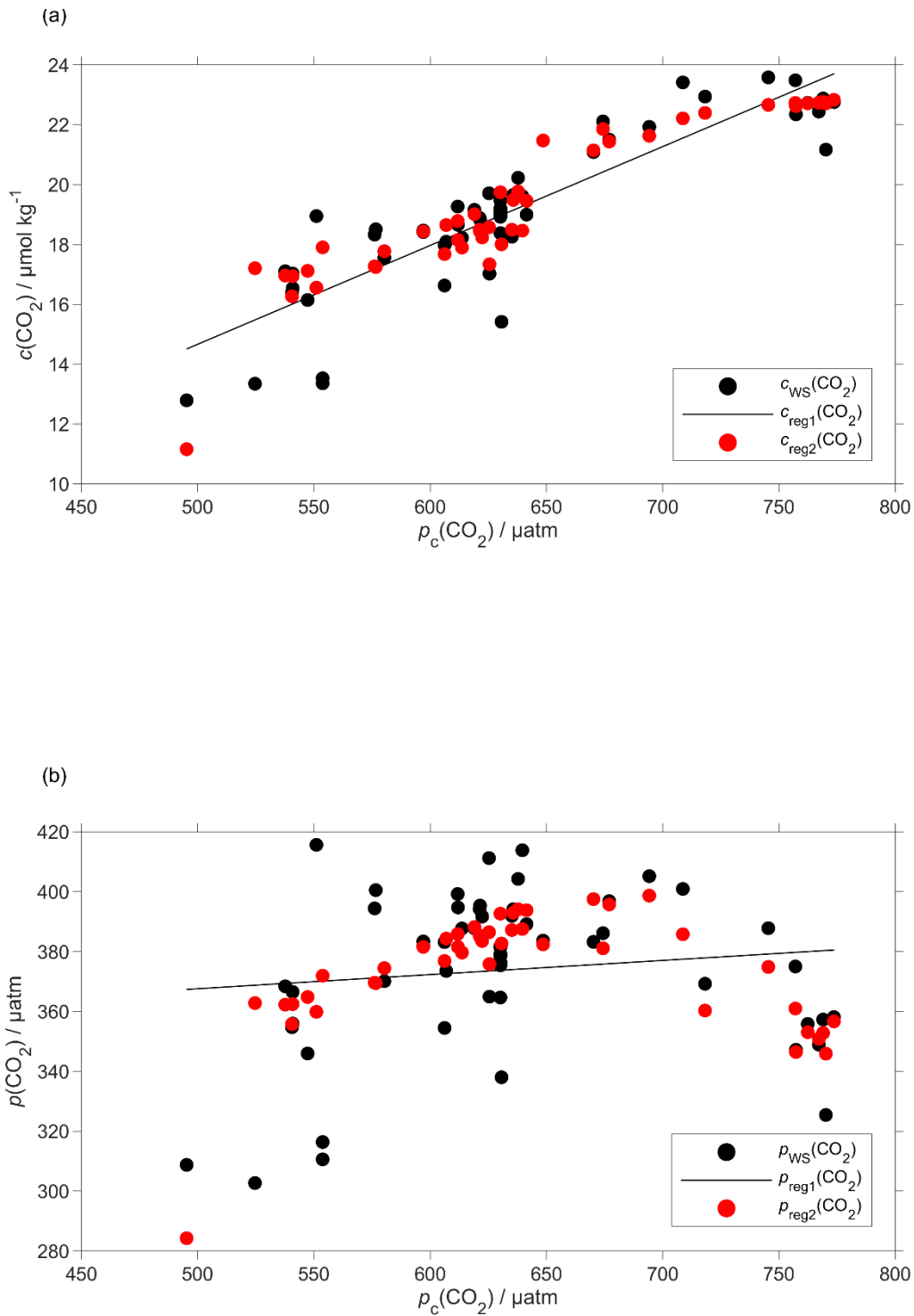


310  
311  
312  
313  
314

**Figure 6:** Calibration of the CO<sub>2</sub>-optode using a) CO<sub>2</sub>-concentration of the discrete samples ( $c_{ws}(CO_2)$ ) against the glider output with the linear regression line and b) CO<sub>2</sub>-partial pressure of the discrete samples ( $p_{ws}(CO_2)$ ) against the glider output with the linear regression line.

315  
316  
317  
318  
319  
320

Plotting the regression residuals ( $c_r(CO_2)$ , calculated as the difference between  $c_{ws}(CO_2)$  and the value predicted by the regression) revealed a quadratic relation between the regression residuals and water temperature ( $\theta$ ). We have therefore included  $\theta$  and  $\theta^2$  in the optode calibration (Figure 6a). This second calibration increased the correlation coefficient  $R^2$  from 0.77 to 0.90 and decreased the standard deviation of the regression residuals from 1.3 to 0.8  $\mu\text{mol kg}^{-1}$ . Even with the explicit inclusion of temperature in the calibration, the CO<sub>2</sub> optode response remained more closely related to  $c(CO_2)$  than  $p(CO_2)$  (Figure 6b).



321

322 **Figure 6:** Regression (black lines, reg1) of the CO<sub>2</sub> optode output  $p_c(\text{CO}_2)$  against a) co-located concentration  
 323  $c_{\text{WS}}(\text{CO}_2)$  that has an uncertainty of  $0.28 \mu\text{mol kg}^{-1}$  b) and partial pressure  $p_{\text{WS}}(\text{CO}_2)$  of CO<sub>2</sub> in discrete water  
 324 samples (black dots). Also shown are the values predicted by including  $\theta$  and  $\theta^2$  in the regression used for optode  
 325 calibration (red dots, reg2). The regression equations are:

326 a) reg1:  $c_{\text{WS}}(\text{CO}_2)/(\mu\text{mol kg}^{-1}) = (0.033 \pm 0.003)p_c(\text{CO}_2)/\mu\text{atm} - 1.8 \pm 1.6$  ( $R^2 = 0.77$ )

327 a) reg2:  $c_{\text{WS}}(\text{CO}_2)/(\mu\text{mol kg}^{-1}) = (0.12 \pm 0.14)\theta/^\circ\text{C} - (0.071 \pm 0.011)(\theta/^\circ\text{C})^2 + (0.0094 \pm 0.0048)p_c(\text{CO}_2)/\mu\text{atm}$   
 328  $+ 16 \pm 4$  ( $R^2 = 0.90$ ).

329 b) reg1:  $p_{\text{WS}}(\text{CO}_2)/\mu\text{atm} = (0.05 \pm 0.05)p_c(\text{CO}_2)/\mu\text{atm} + 344 \pm 33$  ( $R^2 = 0.02$ )

330 b) reg2:  $p_{\text{WS}}(\text{CO}_2)/\mu\text{atm} = (21 \pm 3)\theta/^\circ\text{C} - (1.9 \pm 0.2)(\theta/^\circ\text{C})^2 + (0.2 \pm 0.1)p_c(\text{CO}_2)/\mu\text{atm} + 209 \pm 76$  ( $R^2 = 0.60$ ).

331

332 **2.7 Regional algorithm to estimate  $A_T$**

333 To calculate  $C_T$ , we used two variables: glider  $c(\text{CO}_2)$  derived as described in section 2.6 and  $A_T$  derived using a  
334 regional algorithm based on  $S$  and  $\theta$  in the top 1000 m. The algorithm followed the approach of Lee et al. (2006)  
335 and was derived using 663 water samples collected at OWSM from 2004 to 2014 and GLODAPv2 (Olsen et al.,  
336 2016) data from 2000 in the deployment region. Discrete samples with  $S < 33$  were removed because these  
337 values were lower than the minimum  $S$  measured by the glider. The derived  $A_T$  parameterisation is:

338 
$$A_{T,\text{reg}} / (\mu\text{mol kg}^{-1}) = 2317.03 + 33.12 (S - 35) + 7.94 (S - 35)^2 + 0.96 (\theta / ^\circ\text{C} - 20) + 0.01 (\theta / ^\circ\text{C} - 20)^2 \quad (4)$$

339 The parameterisation has an uncertainty of  $8.2 \mu\text{mol kg}^{-1}$  calculated as the standard deviation of the residual  
340 difference between actual and parameterised  $A_T$ .

341 To test this parameterisation, we compared the predicted  $A_{T,\text{reg}}$  values with discrete measurements ( $A_{T,\text{WS}}$ )  
342 collected close in terms of time, potential density ( $\sigma_\theta$ ) and distance to the glider transect ( $n = 60$ ). These discrete  
343 samples and the glider had mean temperature and salinity differences of  $(0.17 \pm 0.68) ^\circ\text{C}$  and  $0.03 \pm 0.013$ ,  
344 respectively. The mean difference between  $A_{T,\text{WS}}$  and  $A_{T,\text{reg}}$  was  $(2.1 \pm 6.5) \mu\text{mol kg}^{-1}$ .

345 This  $A_T$  parameterisation was used in CO2SYS (Van Heuven et al., 2011) to calculate  $C_T$  from  $A_{T,\text{reg}}$  and the  
346 calibrated  $c(\text{CO}_2)$ ,  $c_{G,\text{cal}}(\text{CO}_2)$ . These calculated  $C_{T,\text{cal}}$  values were compared with  $C_{T,\text{WS}}$ . To calculate  $c(\text{DIC})$ , we  
347 used two variables: (1) glider  $c(\text{CO}_2)$  derived as described in section 2.6 and (2)  $A_T$  derived using a regional  
348 algorithm based on  $S$  and  $\theta$  depths of less than 1000 m. The algorithm followed the approach of Lee et al. (2006)  
349 and was derived using 663 water samples collected at OWSM from 2004 to 2014 and GLODAPv2 (Olsen et al.,  
350 2016) data from the year 2000 in the deployment region. Discrete samples with  $S < 33$  were removed because  
351 these values were lower than the minimum  $S$  measured by the glider. The derived  $A_T$  parameterisation is:

352 
$$A_{T,\text{reg}} / (\mu\text{mol kg}^{-1}) = 2317.03 + 33.12 (S - 35) + 7.94 (S - 35)^2 + 0.96 (\theta / ^\circ\text{C} - 20) + 0.01 (\theta / ^\circ\text{C} - 20)^2 \quad (4)$$

353 The parameterisation has an uncertainty of  $8.2 \mu\text{mol kg}^{-1}$  calculated as the standard deviation of the residual  
354 difference between actual and parameterised  $A_T$ .

355 To test this parameterisation, we compared the predicted  $A_{T,\text{reg}}$  values with discrete measurements ( $A_{T,\text{WS}}$ )  
356 collected close in terms of time, potential density ( $\sigma_\theta$ ) and distance to the glider transect ( $n = 60$ ). These discrete  
357 samples and the glider had mean temperature and salinity differences of  $(0.17 \pm 0.68) ^\circ\text{C}$  and  $0.03 \pm 0.013$ ,  
358 respectively. The mean difference between  $A_{T,\text{WS}}$  and  $A_{T,\text{reg}}$  was  $(2.1 \pm 6.5) \mu\text{mol kg}^{-1}$ .

359 This  $A_T$  parameterisation was used in CO2SYS (Van Heuven et al., 2011) to calculate  $c(\text{DIC})$  from  $A_{T,\text{reg}}$  and the  
360 calibrated  $c(\text{CO}_2)$ ,  $c_{G,\text{cal}}(\text{CO}_2)$ . These calculated  $c_{G,\text{cal}}(\text{DIC})$  values were compared with  $c_{\text{WS}}(\text{DIC})$  of the same set  
361 of discrete samples used to calibrate  $c_{G,\text{cal}}(\text{CO}_2)$ , the only difference being that instead of the actual total  
362 alkalinity of the water sample ( $A_{T,\text{WS}}$ ), we used  $A_{T,\text{reg}}$ . The mean difference between  $c_{T,\text{G},\text{cal}}(\text{DIC})$  and

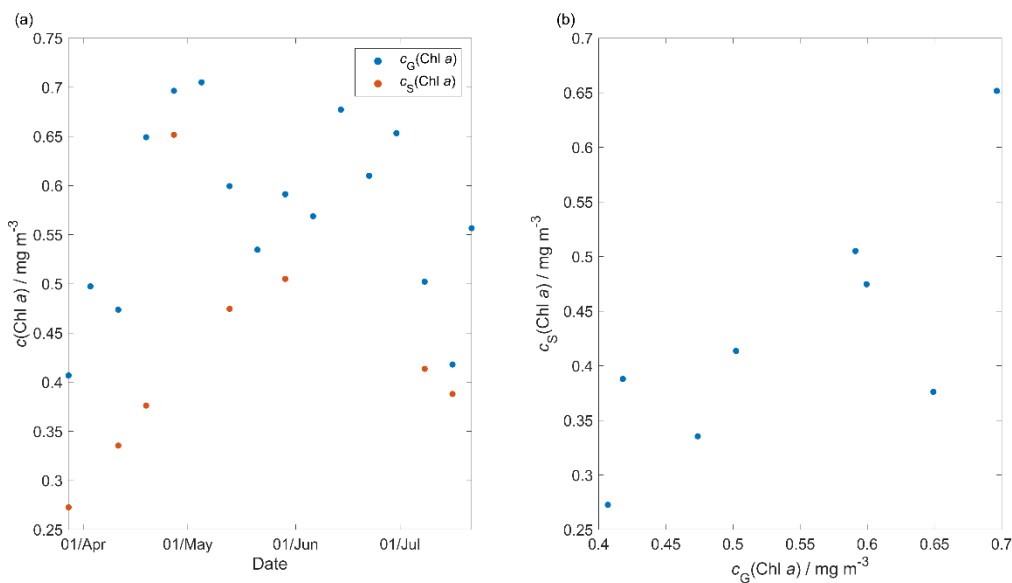
363  $c_{T,reg}c_{WS}(DIC)$  was  $(4.5 \pm 103 \pm 11)$   $\mu\text{mol kg}^{-1}$ , with the non-zero bias and the standard deviation due to the  
 364 uncertainties in the  $A_{Treg}$  parameterisation and the  $c_{G,cal}(CO_2)$  calibration.

## 365 2.78 Quality control of other measurement variables

366 The thermal lag of the glider conductivity sensor was corrected using the method of Gourcuff (2014). Single-  
 367 point outliers in conductivity were removed and replaced by linear interpolation. The glider CTD salinity was  
 368 affected by presumed particulate matter stuck in the conductivity cell (Medeot et al., 2011)(Medeot et al., 2011)  
 369 during dives 147, 234, 244, 251, 272, 279, 303, 320 and 397 and sensor malfunction caused a poor match  
 370 between glider ascent and descent during a dives 214, 215, 235 and 243. These dives were removed from the  
 371 subsequent analysis.

372 Glider-reported chlorophyll concentrations,  $c_{raw}(\text{Chl } a)$ , were computed using the factory coefficients.  $c_{raw}(\text{Chl } a)$   
 373 was affected by photochemical quenching during the daytime dives. To correct for quenching, we used the  
 374 method of Hemsley et al. (2015)Hemsley et al. (2015) based on the night-time relationship between fluorescence  
 375 and optical backscatter. This relationship was established in the top 60 meters and the night-time values were  
 376 selected between sunset and sunrise. We calculated a linear fit between  $c_{raw}(\text{Chl } a)$  measured at night,  $c_N(\text{Chl } a)$ ,  
 377 and the backscatter signal measured at night ( $b_N$ ). The slope and the intercept were then used to derive corrected  
 378 daytime  $c_D(\text{Chl } a)$ . The glider-reported chlorophyll concentration has not been calibrated against in situ samples  
 379 and is not expected to be accurate, even after correction for quenching. However, it should give an indication of  
 380 the depth of the deep chlorophyll concentration maximum ( $z_{DCM}$ ) and the direction of chlorophyll concentration  
 381 change (up/down). 8 day-means of  $c_{raw}(\text{Chl } a)$  were compared with satellite 8 day-composite chlorophyll  
 382 concentration (Figure 7) from Ocean Colour CCI (<https://esa-oceancolour-cci.org/>) and gave a mean  
 383 difference of  $(0.12 \pm 0.08)$   $\text{mg m}^{-3}$ .

384



385

386 **Figure 7:** Comparison between the 8 day-glider  $c(\text{Chl } a)$  ( $c_G(\text{Chl } a)$ ) mean and the 8 day-satellite  $c(\text{Chl } a)$   
 387 ( $c_S(\text{Chl } a)$ ) download from Ocean Colour CCI (<https://esa-oceancolour-cci.org/>), as time-series (panel a) and  
 388 scatter plot (panel b).



389 **2.89 Calculation of oxygen-based net community production  $N(O_2)$**

390 Calculating net community production  $N$  from glider data is challenging because the glider continuously moves  
 391 through different water masses. For that reason we subdivided the transect by binning the data into  $0.1^\circ$  latitude  
 392 intervals to derive  $O_2$  concentration changes every two transects. The changes were calculated between transects  
 393 in the same direction of glider travel (e.g. transects 1 and 3, both in N-S direction) to have approximately the  
 394 same time difference (40-58 days) at every latitude. If instead we had used two consecutive transects, this would  
 395 lead to a highly variable time difference of near-0 to about 50 days along the transect.

396 We calculated  $N(O_2)$  (in  $\text{mmol m}^{-2} \text{d}^{-1}$ ) from the oxygen inventory changes ( $I(O_2)$ ) corrected for air-sea  
 397 exchange  $\Phi(O_2)$ , normalised to  $z_{\text{mix}}$  when  $z_{\text{mix}}$  was deeper than the integration depth of  $z_{\text{lim}} = 45 \text{ m}$ , entrainment  
 398  $E(O_2)$  and diapycnal eddy diffusion  $F_v(O_2)$ :

399 
$$N(O_2) = \frac{I(O_2)}{\Delta t} + \Phi(O_2) \frac{\min(z_{\text{lim}}, z_{\text{mix}})}{z_{\text{mix}}} - E(O_2) - F_v(O_2)$$
  
 400 (5)

401 The inventory changes were calculated as the difference between two transects of the integrated  ~~$e(O_2)$  in the top~~  
 402 ~~45 m. A constant~~ oxygen concentration  $C(O_2)$ .  $C(O_2)$  (in  $\text{mmol m}^{-3}$ ) was derived from the oxygen content  $c(O_2)$   
 403 (in  $\mu\text{mol kg}^{-1}$ ) by multiplication with the water density (about  $1027 \text{ kg m}^{-3}$ , but we used the actual values). A  
 404 default integration depth of 45 m was chosen to capture the deepest extent of the deep chlorophyll maximum  
 405 ( $z_{\text{DCM}}$ ) found during the deployment, which likely represents the extent of the euphotic zone.

406 The inventory changes for every latitude bin were calculated using the following equation:

407 
$$I(O_2) = \frac{\int_{\theta}^{45 \text{ m}} C_{n+1}(z) dz - \int_{\theta}^{45 \text{ m}} C_n(z) dz}{t_{n+1} - t_n} \Delta t = \frac{\int_0^{45 \text{ m}} C_{n+1}(O_2, z) dz - \int_0^{45 \text{ m}} C_n(O_2, z) dz}{t_{n+1} - t_n}$$
  
 408 (6)

409 where  $n$  is the transect number,  $t$  is the day of the year and  $C(O_2, z)$  is the vertical  ~~$e(O_2)$  concentration~~ profile.  
 410  ~~$I(O_2)$  is defined as the changes of the integrated  $c(O_2)$  to  $z_{\text{lim}}$  in the same latitude bin between two dives.~~

411 The air-sea flux of oxygen,  $\Phi(O_2)$  was calculated for each glider dive using the median  ~~$eC(O_2)$~~ ,  $\theta$  and  $S$  in the  
 412 top 10 m. We followed the method of Woolf and Thorpe (1991) that includes the effect of bubble equilibrium  
 413 supersaturation in the calculations:

414 
$$\Phi(O_2) = k_w(O_2) \{ (eC(O_2) - [1 + A_{\text{bub}}(O_2)] e_{\text{sat}} C_{\text{sat}}(O_2)) \}$$
 (7)

415 where  $k_w(O_2)$  is the gas transfer coefficient,  $A_{\text{bub}}(O_2)$  is the increase of equilibrium saturation due to bubble  
 416 injection and  $e_{\text{sat}} C_{\text{sat}}(O_2)$  is the oxygen saturation.  $e_{\text{sat}} C_{\text{sat}}(O_2)$  was calculated from  $S$  and  $\theta$  using the solubility  
 417 coefficients of Benson and Krause Jr (1984), as fitted by Garcia and Gordon (1992).  $A_{\text{bub}}(O_2)$  was calculated  
 418 from the following equation:

419 
$$A_{\text{bub}}(O_2) = 0.01 \left( \frac{U}{U_0} \right)^2$$
 (8)

420 where  $U$  is 10 m-wind speed with 1 hour resolution (ECMWF ERA5,  
 421 <https://www.ecmwf.int/en/forecasts/datasets/reanalysis-datasets/era5>) and  $U_0$  represents the wind speed when the  
 422 oxygen concentration is 1 % supersaturated and has a value of  $9 \text{ m s}^{-1}$  (Woolf and Thorpe, 1991).  $U$  has a spatial

423 resolution of 0.25° latitude and 0.25° longitude and was interpolated to the glider position at the beginning of the  
 424 dive.

425 The transfer velocity  $k_w(O_2)$  was calculated based on Wanninkhof (2014):

$$426 \frac{k_w(O_2)}{\text{cm h}^{-1}} = 0.251 \left( \frac{Sc(O_2)}{660} \right)^{-0.5} \left( \frac{U}{\text{m s}^{-1}} \right)^2 \quad (9)$$

427 The Schmidt number,  $Sc(O_2)$ , was calculated using the parameterisation of Wanninkhof (2014). ~~To account for~~  
 428 ~~wind speed variability,  $k_w(O_2)$  applied to calculate  $N(O_2)$  was a weighted mean based on the varying daily mean~~  
 429 ~~wind speed  $U$  in the time interval between  $t_n$  and  $t_{n+1}$  ( $\Delta t$ ) used to calculate  $\frac{\Delta I(O_2)}{\Delta t}$  using a 5 points median  $z_{\text{mix}}$  and~~  
 430 ~~for 50 days to calculate  $\Phi(O_2)$  (section 3.2) (Reuer et al., 2007). To account for wind speed variability,  $k_w(O_2)$~~   
 431 ~~applied to calculate  $N(O_2)$  was a weighted mean. This value was calculated using the varying daily-mean wind~~  
 432 ~~speed  $U$  in the time interval between  $t_n$  and  $t_{n+1}$  ( $\Delta t$ ) (50 days) using a 5 point-median  $z_{\text{mix}}$  (section 3.2) (Reuer et~~  
 433 ~~al., 2007). The time interval is the same as used to calculate  $\frac{\Delta I(O_2)}{\Delta t}$ .~~

434 The entrainment flux,  $E(O_2)$ , was calculated as the oxygen flux when the mixed layer depth deepens in time and  
 435 is greater than  $z_{\text{lim}}$  at time  $t_2$ :

$$436 E(O_2) = \frac{I(O_2, t_1, z_{\text{mix}}(t_2)) \frac{z_{\text{lim}}}{z_{\text{mix}}(t_2)} - I(O_2, t_1, z_{\text{lim}})}{t_2 - t_1} \quad (10)$$

437 where  $t_2 - t_1$  represents the change in time,  $z_{\text{mix}}$  is the mixed layer depth,  $I(O_2, t_1, z_{\text{mix}}(t_2))$ , is the expected  
 438 inventory that would result from a mixed layer deepening to  $z_{\text{mix}}(t_2)$  between  $t_2$  and  $t_1$ , and  $I(O_2, t_1, z_{\text{lim}})$  is the  
 439 original inventory at  $t_1$ .

440 The effect of diapycnal eddy diffusion ( $F_v$ ) was calculated at  $z_{\text{mix}}$  when it was deeper than  $z_{\text{lim}}$  and at  $z_{\text{lim}}$  when  
 441  $z_{\text{mix}}$  was shallower than  $z_{\text{lim}}$ , using the following equation:

$$442 F_v(O_2) = K_z \frac{\partial \epsilon(O_2)}{\partial z} \frac{\partial C(O_2)}{\partial z}$$

443 (11)

444 ~~for a vertical eddy diffusivity ( $K_z$ ) of  $10^{-5} \text{ m}^2 \text{ s}^{-1}$  (Naveira Garabato et al., 2004). The effect of  $F_v(O_2)$  on  $N(O_2)$~~   
 445 ~~was negligible (Figure A2b) with a median of  $(-0.06 \pm 0.34) \text{ mmol m}^{-2} \text{ d}^{-1}$ .~~

446 2.9 for a vertical eddy diffusivity ( $K_z$ ) of  $10^{-5} \text{ m}^2 \text{ s}^{-1}$  (Naveira Garabato et al., 2004). The effect of  $F_v(O_2)$  on  
 447  $N(O_2)$  was negligible (Figure A2b) with a median of  $(-0.1 \pm 0.5) \text{ mmol m}^{-2} \text{ d}^{-1}$ .

#### 448 **2.10 Calculation of dissolved inorganic carbon-based net community production, $N(\underline{C_T \text{ DIC}})$**

449  $N(\underline{C_T \text{ DIC}})$  was expressed in  $\text{mmol m}^{-2} \text{ d}^{-1}$  and was calculated from ~~the  $\underline{C_T \text{ DIC}}$~~  inventory changes  
 450  ~~$\Delta(\underline{C_T \text{ DIC}})/\Delta t$~~ , air-sea flux of  $\text{CO}_2$ ,  $\Phi(\text{CO}_2)$ , entrainment  $E(\underline{C_T \text{ DIC}})$  and diapycnal diffusion  $F_v(\underline{C_T \text{ DIC}})$ :

$$451 N(\underline{C_T}) = -I(\underline{C_T}) - (\text{DIC}) = -\frac{\Delta(\text{DIC})}{\Delta t} - \Phi(\text{CO}_2) \frac{\min(z_{\text{lim}}, z_{\text{mix}})}{z_{\text{mix}}} + E(\underline{C_T}) + (\text{DIC}) + F_v(\underline{C_T}) - (\text{DIC})$$

452 (12)

453 Firstly,  $\Phi(\text{CO}_2)$  was calculated using the 10 m wind speed with 1 hour resolution downloaded from ECMWF  
 454 ERA5. As for oxygen, we selected the closest wind speed data point at the beginning of each glider dive. We  
 455 used the monthly mean atmospheric  $\text{CO}_2$  dry mole fraction ( $x(\text{CO}_2)$ ) downloaded from the Greenhouse Gases  
 456 Reference Network Site (<https://www.esrl.noaa.gov/gmd/ccgg/ggrn.php>) closest to the deployment at Mace  
 457 Head, County Galway, Ireland (~~Dlugokencky et al., 2015~~), ([Dlugokencky et al., 2015](#)). Using  $x(\text{CO}_2)$  we  
 458 calculated the air-saturation concentration  $e_{\text{atm}}C_{\text{atm}}(\text{CO}_2)$ :

$$459 \quad e_{\text{atm}}C_{\text{atm}}(\text{CO}_2) = x(\text{CO}_2) p_{\text{baro}} F(\text{CO}_2) \quad (13)$$

460 where  $p_{\text{baro}}$  is the mean sea level pressure and  $F(\text{CO}_2)$  is the  $\text{CO}_2$  solubility function (in  $\text{mol dm}^{-3} \text{atm}^{-1}$ )  
 461 calculated from surface  $\theta$  and  $S$  (Weiss and Price, 1980).

462 The seawater  $c(\text{CO}_2)$  at the surface was calculated using the median in the top 10 meters between the glider  
 463 ascent and descent of the following dive  $c(\text{CO}_2)$ . From this,  $\Phi(\text{CO}_2)$  was calculated:

$$464 \quad \Phi(\text{CO}_2) = k(\text{CO}_2) [eC(\text{CO}_2) - e_{\text{atm}}C_{\text{atm}}(\text{CO}_2)]. \quad (14)$$

465  $k(\text{CO}_2)$  was calculated using the parameterisation of Wanninkhof (2014):

$$466 \quad \frac{k(\text{CO}_2)}{\text{cm h}^{-1}} = 0.251 \left( \frac{Sc(\text{CO}_2)}{660} \right)^{-0.5} \left( \frac{U}{\text{m s}^{-1}} \right)^2 \quad (15)$$

467  $Sc(\text{CO}_2)$  is the dimensionless Schmidt number at the seawater temperature (Wanninkhof, 2014). To account for  
 468 wind speed variability,  $k_w(\text{CO}_2)$  applied to calculate  $N(\Theta_2 \text{DIC})$  was a weighted mean based on the varying daily-  
 469 mean wind speed  $U$  in the time interval between  $t_n$  and  $t_{n+1}$  ( $\Delta t$ ) used to calculate  $\frac{\Delta I(\text{CO}_2)}{\Delta t}$  and for 40 50 days  
 470 to calculate  $\Phi(\text{CO}_2)$  (section 3.2) (Reuer et al., 2007).

471 The DIC inventory changes were calculated in the top 45 m with the following equation:

$$472 \quad \frac{\Delta I(\text{DIC})}{\Delta t} = \frac{\int_0^{45 \text{ m}} C_{n+1} dz - \int_0^{45 \text{ m}} C_n dz}{t_{n+1} - t_n} \frac{\Delta I(\text{DIC})}{\Delta t} = \frac{\int_0^{45 \text{ m}} C_{n+1}(\text{DIC}, z) dz - \int_0^{45 \text{ m}} C_n(\text{DIC}, z) dz}{t_{n+1} - t_n}$$

473 (16)

474 Just as for  $C(\text{O}_2)$ ,  $C(\text{DIC})$  (in  $\text{mmol m}^{-3}$ ) was derived from the DIC content  $c(\text{DIC})$  (in  $\mu\text{mol kg}^{-1}$ ) by  
 475 multiplication with the water density (about  $1027 \text{ kg m}^{-3}$ , but we used the actual values).

476 The entrainment flux,  $E(C_{\text{T}} \text{DIC})$ , was calculated as the oxygenDIC flux when the mixed layer depth deepens in  
 477 time and is greater than  $z_{\text{lim}}$  at time  $t_2$ :

$$478 \quad E(C_{\text{T}}) = \frac{I(C_{\text{T}}, z_{\text{mix}}(t_2)) \frac{z_{\text{lim}}}{z_{\text{mix}}(t_2)} - I(C_{\text{T}}, z_{\text{lim}})}{t_2 - t_1} E(\text{DIC}) = \frac{I(\text{DIC}, t_1, z_{\text{mix}}(t_2)) \frac{z_{\text{lim}}}{z_{\text{mix}}(t_2)} - I(\text{DIC}, t_1, z_{\text{lim}})}{t_2 - t_1}$$

479 (17)

480 As for oxygen, the effect of diapycnal eddy diffusion ( $F_v$ ) was calculated at  $z_{\text{mix}}$  when it was deeper than  $z_{\text{lim}}$  and  
 481 at  $z_{\text{lim}}$  when  $z_{\text{mix}}$  was shallower than  $z_{\text{lim}}$ , using the following equation:

$$482 \quad F_v(C_{\text{T}}) = K_z \frac{\partial c(C_{\text{T}})}{\partial z} \text{DIC} = K_z \frac{\partial C(\text{DIC})}{\partial z}$$

483 (18)

484 for a  $K_z$  of  $10^{-5} \text{ m s}^{-2}$  (Naveira Garabato et al., 2004). The effect of  $F_v(C_T)$  was negligible (Figure A2a) with a  
 485 median of  $(0.07 \pm 0.3) \text{ mmol m}^{-2} \text{ d}^{-1}$ .

486 The contribution of horizontal advection to  $N(C_T)$  was considered minimal over the timescales we calculated  
 487 inventory changes because previous studies have shown that changes in  $C_T$  during summer are mainly controlled  
 488 by biology and air-sea interactions (Gislefoss et al., 1998). For that reason, previous studies that estimated  $N$  in  
 489 the Norwegian Sea have also neglected advective fluxes (Falck and Anderson, 2005; Falck and Gade, 1999;  
 490 Kivimäe, 2007; Skjelvan et al., 2001).

491 for a  $K_z$  of  $10^{-5} \text{ m}^2 \text{ s}^{-1}$  (Naveira Garabato et al., 2004). The effect of  $F_v(\text{DIC})$  was negligible (Figure A2a) with a  
 492 median of  $(0.1 \pm 0.3) \text{ mmol m}^{-2} \text{ d}^{-1}$ .

493 The contribution of horizontal advection to  $N(\text{DIC})$  was considered minimal over the timescales we calculated  
 494 inventory changes because previous studies have shown that changes in  $C(\text{DIC})$  during summer are mainly  
 495 controlled by biology and air-sea interactions (Gislefoss et al., 1998). For that reason, previous studies that  
 496 estimated  $N$  in the Norwegian Sea have also neglected advective fluxes (Falck and Anderson, 2005; Falck and  
 497 Gade, 1999; Kivimäe, 2007; Skjelvan et al., 2001).

498 Uncertainties in  $N(C_T \text{ DIC})$  and  $N(\text{O}_2)$  were evaluated with a Monte-Carlo approach. The uncertainties of the  
 499 input variables are shown in Table 2; we repeated the analysis 1000 times. The total uncertainty in  $N$  was  
 500 calculated as the standard deviation of the 1000 Monte-Carlo simulations.

501

502

503

504 **Table 2.** Uncertainty associated with  $N(C_T \text{ DIC})$  and  $N(\text{O}_2)$  input variables calculated by a Monte Carlo approach

Variable	Error	Reference/Method
$C_T \text{ DIC}$	$\pm 0.11 \text{ } \mu\text{mol kg}^{-1}$	Standard deviation <del>vs</del> of the <u>differences to discrete</u> water samples.
$S$	0.01	Standard deviation of glider salinities for $\sigma_0 > 1028 \text{ kg m}^{-3}$ and latitude $> 64^{\circ} 64' \text{ N}$
$\theta$	0.3 °C	Standard deviation of glider temperature for $\sigma_0 > 1028 \text{ kg m}^{-3}$ and latitude $> 64^{\circ} 64' \text{ N}$
$e_{\text{atm}} C_{\text{atm}}(\text{CO}_2)$	$1.5 \text{ } \mu\text{mol kg}^{-1}$ $\pm \text{mmol m}^{-3}$	Standard deviation of $e_{\text{atm}} C_{\text{atm}}(\text{CO}_2)$
$e_C(\text{CO}_2)$	$\pm 0.8 \text{ mmol m}^{-3}$ $\mu\text{mol kg}^{-1}$	<del>Error is the standard</del> Standard deviation <del>vs</del> of the <u>differences to discrete</u> water samples.
$k_w(\text{CO}_2)$	20 %	(Wanninkhof, 2014)
$k_w(\text{O}_2)$		

$z_{\text{mix}}$	9 m	Standard deviation <del>compared with</del> for $z_{\text{mix}}$ based on thresholds $\Delta T = 0.1$ °C (Sprintall and Roemmich, 1999), 0.2 °C (Thompson, 1976) and 0.8 °C ( <del>Kara et al., 2000</del> )(Kara et al., 2000).
$c(\text{O}_2)$	$2.4 \mu\text{mol kg}^{-1}$	Standard deviation of glider oxygen concentrations for $\sigma_0 > 1028 \text{ kg m}^{-3}$ and latitude $> 64^{\circ}64' \text{ N}$

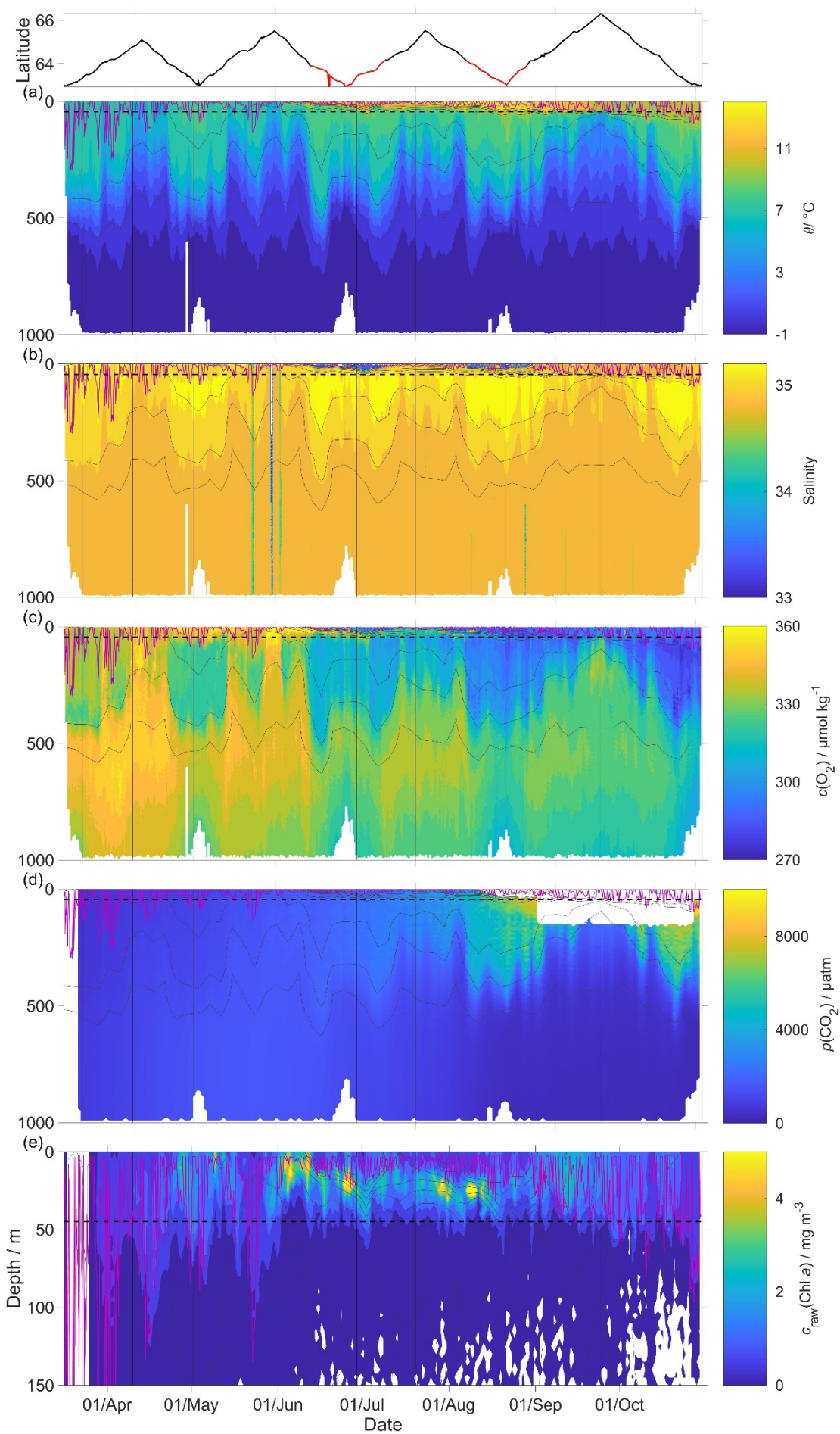
505

506

507 **3 Results**

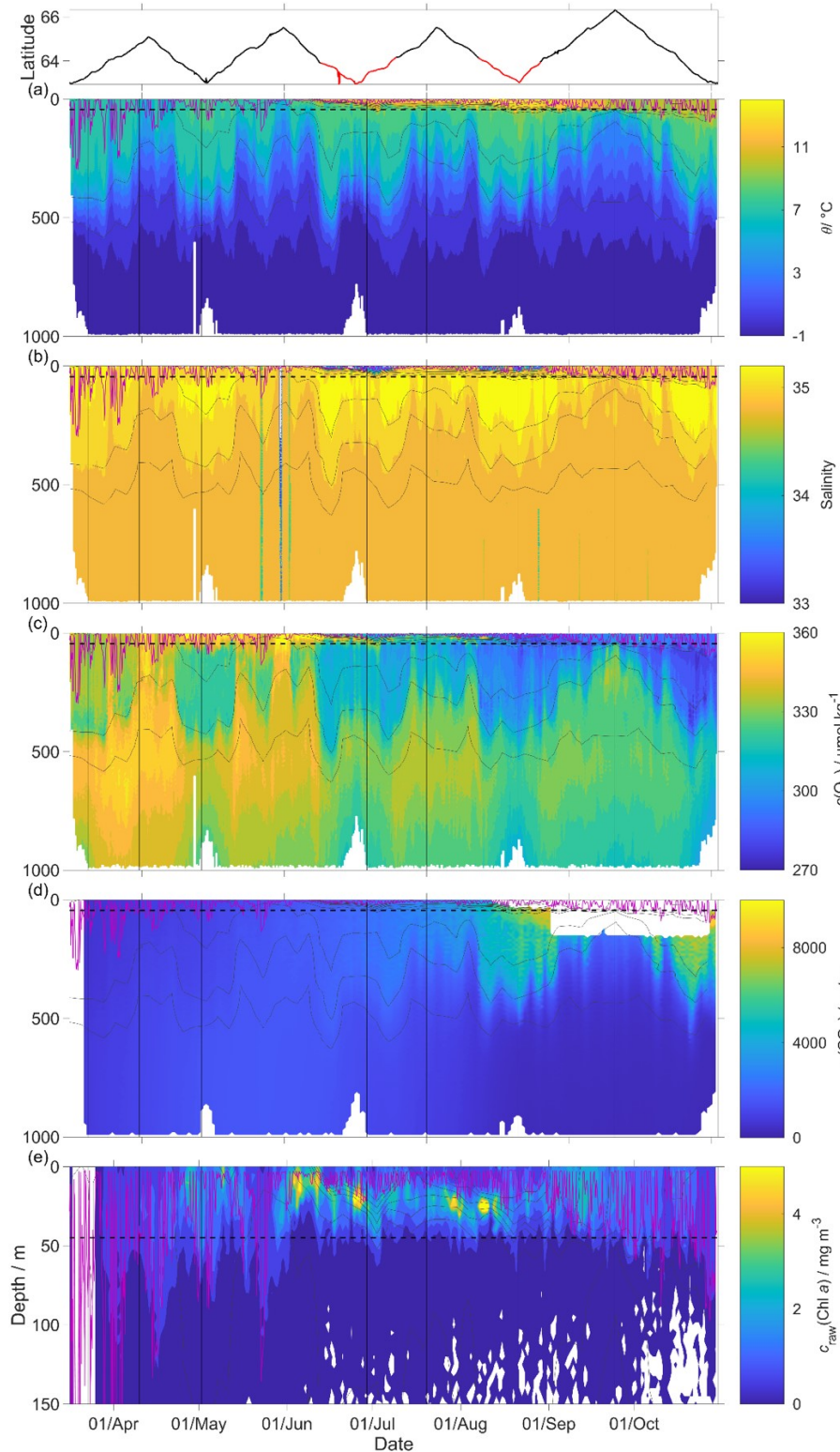
508 The uncorrected ~~temperature  $\theta$ , salinity  $S$ ,  $c(\text{O}_2)$ ,  $p(\text{CO}_2)$  and  $c_{\text{raw}}(\text{Chl } a)$~~  presented in Figure 8 were analysed up  
509 to dive 400 (24 July 2014). For the following dives, the  $\text{CO}_2$  optode stopped sampling in the first 150 m (Figure  
510 8d). Instead, the uncorrected temperature  $\theta$ , salinity  $S$ ,  $c(\text{O}_2)$  and  $c_{\text{raw}}(\text{Chl } a)$  were analysed for all the dives (30  
511 October 2014). The raw optode  $c(\text{O}_2)$  data was calibrated and drift-corrected and  $c(\text{CO}_2)$  was drift-, lag-corrected  
512 and recalibrated, then used to quantify the temporal and spatial changes in  $N$  and  $\Phi$  together with the quenching  
513 corrected  $c_{\text{raw}}(\text{Chl } a)$  to evaluate net community production changes.

514



516  
517  
518  
519  
520  
521  
522  
523  
524  
525

**Figure 8:** Raw glider data for all 703 dives with latitude of the glider trajectory at the top (black: NwAC; red: NCC, separated by a  $S$  of 35). a) temperature  $\theta$ , b) salinity  $S$ , c) oxygen concentration  $c(\text{O}_2)$ , d) uncorrected  $\text{CO}_2$  optode output  $p_a(\text{CO}_2)$  and e) chlorophyll  $a$  concentration  $c_{\text{raw}}(\text{Chl } a)$ . The white space means that the sensors did not measure any data. The pink line is  $z_{\text{mix}}$  calculated using a threshold criterion of  $\Delta\theta = 0.5^\circ\text{C}$  to a median  $\theta$  of the top 5 m of the glider profile (Obata et al., 1996; United States National Environmental Satellite and Information Service, Monterey and Levitus, 1997; Foltz et al., 2003), the black dotted line  $z_{\text{lim}}$  used as depth limit to calculate the net community production ( $N$ ) and black contour lines are the isopycnals.



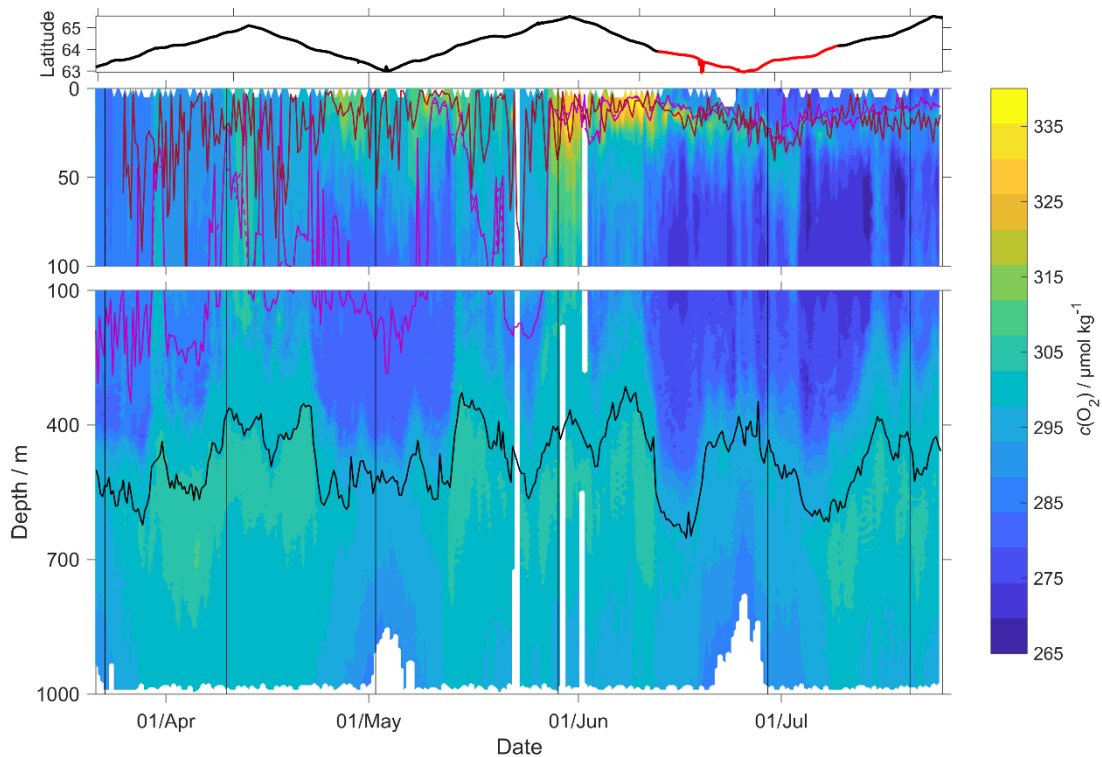
526

527 **Figure 8:** Raw glider data for all 703 dives with latitude of the glider trajectory at the top (black: NwAC; red:  
 528 NCC, separated by a  $S$  of 35). a) temperature  $\theta$ , b) salinity  $S$ , c) oxygen concentration  $c_G(\text{O}_2)$ , d) uncorrected  $\text{CO}_2$   
 529 optode output  $p_{\text{O}_2}(\text{CO}_2)$  and e) chlorophyll  $a$  concentration  $c_{\text{raw}}(\text{Chl } a)$ . The white space means that the sensors did  
 530 not measure any data. The pink line is  $z_{\text{mix}}$  calculated using a threshold criterion of  $\Delta\theta = 0.5^\circ\text{C}$  to the median  $\theta$   
 531 in the top 5 m (Obata et al., 1996; United States. National Environmental Satellite and Information Service,  
 532 Monterey and Levitus, 1997; Foltz et al., 2003). Black dotted line designates  $z_{\text{lim}}$ , used as depth limit to calculate  
 533  $N$ . Black contour lines represent isopycnals.

### 534 3.1 $\text{O}_2$ and $\text{CO}_2$ optode calibration

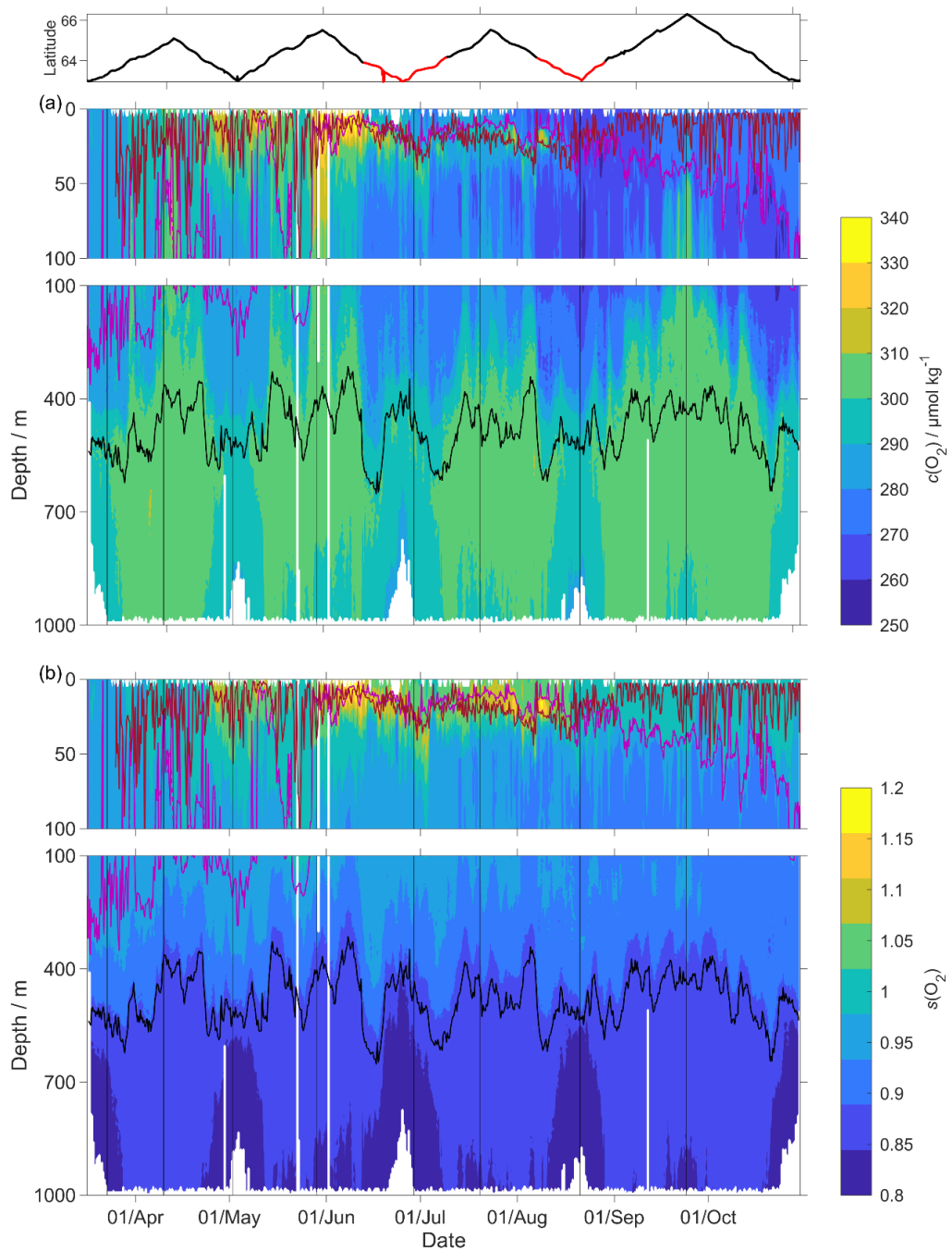
535 The  $\text{O}_2$  optode drift caused a continuous and unexpected decrease of the uncorrected  $c(\text{O}_2)$  continually  
 536 decreased  $c_G(\text{O}_2)$  from 290 to 282  $\mu\text{mol kg}^{-1}$  for  $\sigma_0 > 1028 \text{ kg m}^{-3}$  (Figure 8c). The ratio  $c_C(\text{O}_2)/c_G(\text{O}_2)$  against day  
 537 of the year used for the drift correction had a good correlation with time ( $R^2 = 0.90$ ), showing a continuous  
 538 increase of  $0.0004 \text{ d}^{-1}$  (Figure 3), equivalent to a decrease in the measured glider  $\text{O}_2$  concentration of  $0.11 \mu\text{mol}$   
 539  $\text{kg}^{-1} \text{ d}^{-1}$ . It was possible to apply the correction because  $c_C(\text{O}_2)$  had low temporal variability for the chosen  
 540 potential density  $\sigma_0 > 1028 \text{ kg m}^{-3}$ . The  $c_C(\text{O}_2)$  values from OWSM and GLODAPv2 had a mean of  
 541 ~~(304.6305±3.4)~~  $\mu\text{mol kg}^{-1}$ , varying from 294 to 315  $\mu\text{mol kg}^{-1}$  (Figure A1). The drift correction reduced the  
 542 variability of  $c_G(\text{O}_2)$  in the selected potential density range from a standard deviation of 7.3  $\mu\text{mol kg}^{-1}$  to a  
 543 standard deviation of 2.4  $\mu\text{mol kg}^{-1}$  (Figure 99a).

544  
 545



546 **Figure 9:**  $c(\text{O}_2)$  contour plot with  $z_{\text{DCM}}$  (red line) and the  $z_{\text{mix}}$  (pink line) and  $z_{\text{mix}}$  using 5 points median (pink  
 547 dotted line) calculated using a threshold criterion of  $\Delta\theta = 0.5^\circ\text{C}$  to median  $\theta$  of the top 5 m of the glider profile  
 548 (Obata et al., 1996; United States. National Environmental Satellite and Information Service, Monterey and  
 549 Levitus, 1997; Foltz et al., 2003), in black  $\sigma_0 = 1028 \text{ kg m}^{-3}$  and at the top the latitude trajectory of the glider in  
 550 black NwAC and in red NCC.  
 551





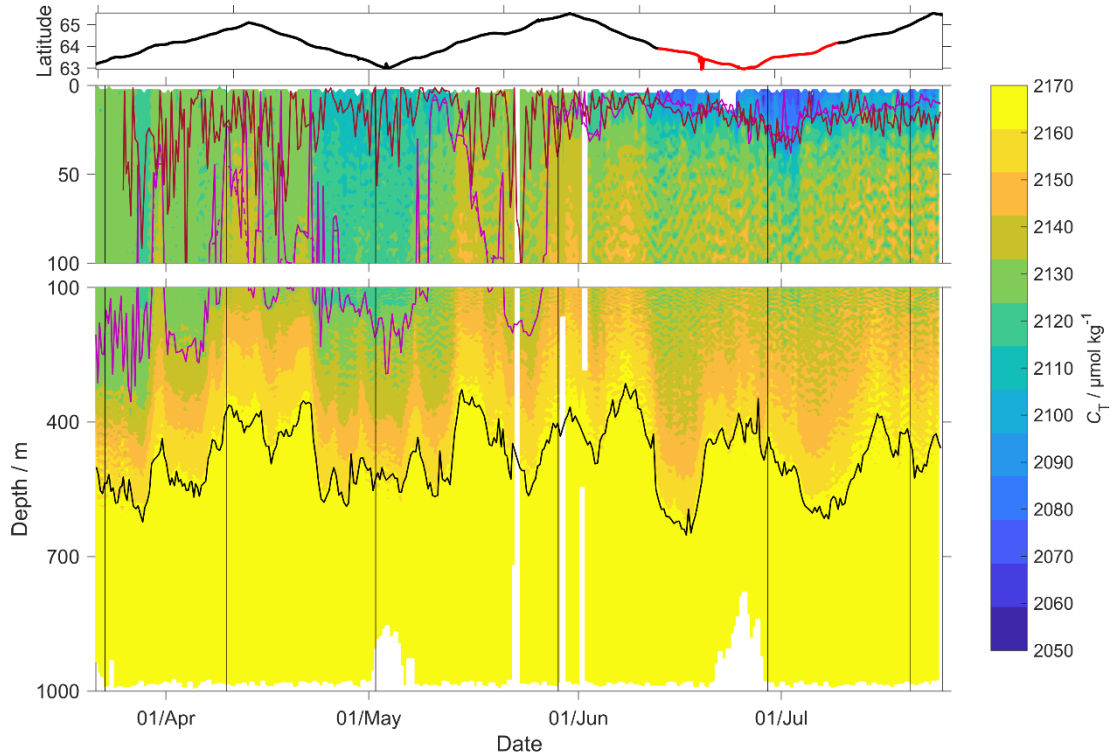
552

553 **Figure 9:** a)  $c(\text{O}_2)$ ; b)  $s(\text{O}_2) = c(\text{O}_2)/c_{\text{sat}}(\text{O}_2)$  with  $z_{\text{DCM}}$  (red line),  $z_{\text{mix}}$  (pink line) 5-point median  $z_{\text{mix}}$  (pink dotted  
 554 line). Black line:  $\sigma_0 = 1028 \text{ kg m}^{-3}$ . Top panel: glider latitude (black: NwAC; red: NCC).

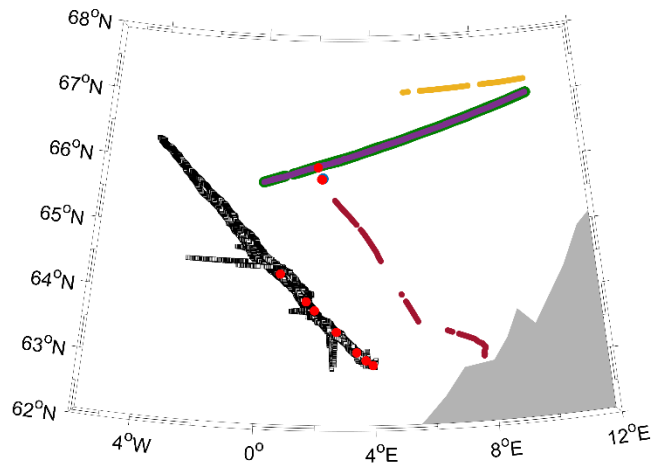
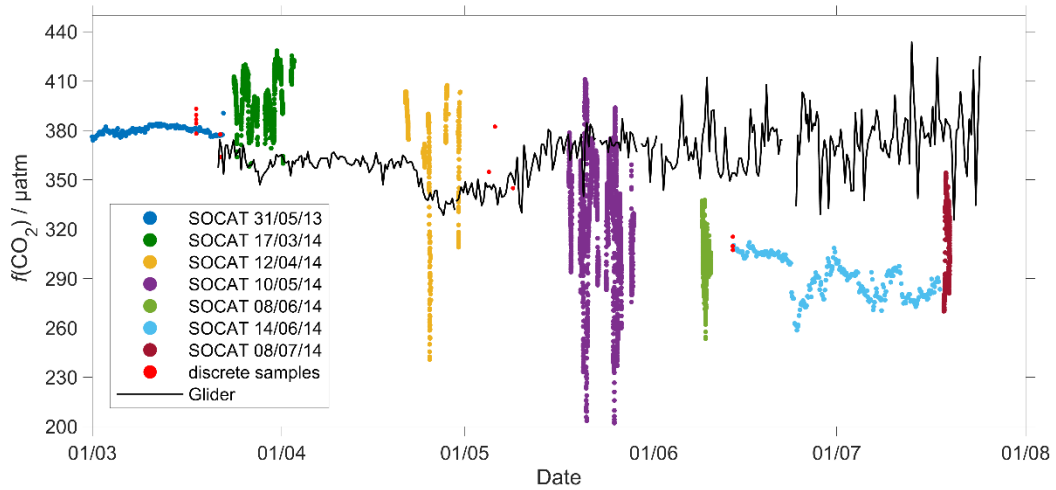
555 Following drift, lag and scale corrections, glider fugacity  $f_G(\text{CO}_2)$  derived from Eq. 2 had a mean difference of  
 556  $(82 \pm 22) \mu\text{atm}$  to the discrete samples ( $n = 55$ ; not shown) and  $C_T(\text{DIC})$  had a standard deviation of  $10 \mu\text{mol kg}^{-1}$   
 557 and a mean difference of  $1.5(3 \pm 11) \mu\text{mol kg}^{-1}$  (Figure 10).  $p(\text{CO}_2)$  and  $f(\text{CO}_2)$  are almost identical, but  $f(\text{CO}_2)$   
 558 takes into account of the non-ideal nature of the gas phase. The optode was able to capture the temporal and  
 559 spatial variability showing that NCC had a lower DIC concentration of  $C_T$  than NwAC. Restricting the  $f(\text{CO}_2)$   
 560 comparison to the discrete samples in the top 10 m gave a mean difference of  $(21 \pm 21) \mu\text{atm}$  ( $n = 86$ ). We  
 561 also compared glider  $f_G(\text{CO}_2)$  with SOCAT  $f(\text{CO}_2)$  (Bakker et al., 2016) (Bakker et al., 2016) data in the region  
 562 during the deployment (Figure 11). Until during the beginning of June whole deployment, there was general  
 563 agreement between  $f_G(\text{CO}_2)$  and  $f_{\text{SOCAT}}(\text{CO}_2)$ . Afterwards,  $f_G(\text{CO}_2)$  varied between  $326204$  and  $434391 \mu\text{atm}$   
 564 while  $f_{\text{SOCAT}}(\text{CO}_2)$  varied between  $259202$  and  $354428 \mu\text{atm}$  (Figure 11).

565 Our results are in agreement with Jeansson et al. (2011) who found the surface NCC was the region with the  
 566 lowest  $C_T$  values ( $2083 \mu\text{mol kg}^{-1}$ ) in the Norwegian Sea. This was confirmed during our deployment because  
 567  $C_T$  was  $(2100 \pm 18) \mu\text{mol kg}^{-1}$  in the NCC region and  $(2150 \pm 23)$  Jeansson et al. (2011) who found the surface NCC  
 568 was the region with the lowest  $c(\text{DIC})$  values ( $2083 \mu\text{mol kg}^{-1}$ ) in the Norwegian Sea. This was confirmed  
 569 during our deployment because  $c(\text{DIC})$  was  $(2081 \pm 39) \mu\text{mol kg}^{-1}$  in the NCC region and  $(2146 \pm 27) \mu\text{mol kg}^{-1}$  in  
 570 the NwAC region (Figure 10) and  $c(\text{O}_2)$  was  $> 300 \mu\text{mol kg}^{-1}$  in the NwAC and  $< 280 \mu\text{mol kg}^{-1}$  in the NCC.

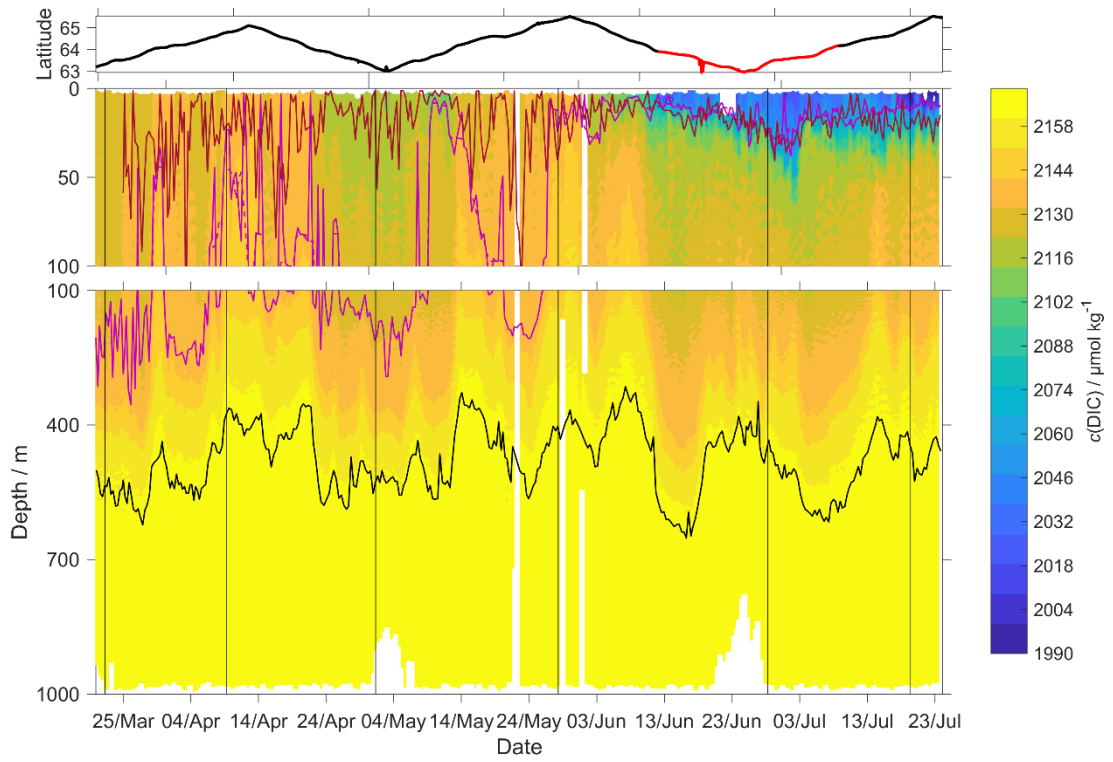
571  
 572



573 **Figure 10:**  $C_T$  contour plot with  $z_{\text{DCM}}$  (red line) and the  $z_{\text{mix}}$  (pink line) and  $z_{\text{mix}}$  using 5 points median (pink  
 574 dotted line) calculated using a threshold criterion of  $\Delta\theta = 0.5^\circ\text{C}$  to median  $\theta$  of the top 5 m of the glider profile  
 575 (Obata et al., 1996; United States. National Environmental Satellite and Information Service, Monterey and  
 576 Levitus, 1997; Foltz et al., 2003), in black  $\sigma_\theta = 1028 \text{ kg m}^{-3}$  and at the top the latitude trajectory of the glider in  
 577 black NwAC and in red NCC.  
 578  
 579



580 **Figure 11:** The plot represents the surface  $f(\text{CO}_2)$  from 2014 SOCAT and from the glider. The black dots are the  
 581 median of the glider  $f(\text{CO}_2)$  in the top 10 meters calculated using the ascent of the single dive and the descent of  
 582 the next dive. The red dots are the water samples collected during the deployment and the remaining dots are  
 583 from the SOCAT cruises in the area during the deployment. On the bottom there is the map of the glider and  
 584 SOCAT data positions.  
 585



586

587 **Figure 10: c(DIC) contour plot with  $z_{\text{DCM}}$  (red line),  $z_{\text{mix}}$  (pink line) 5-point median  $z_{\text{mix}}$  (pink dotted line). Black**

588 **line:  $\sigma_0 = 1028 \text{ kg m}^{-3}$ . Top panel: glider latitude (black: NwAC; red: NCC).**

589

590

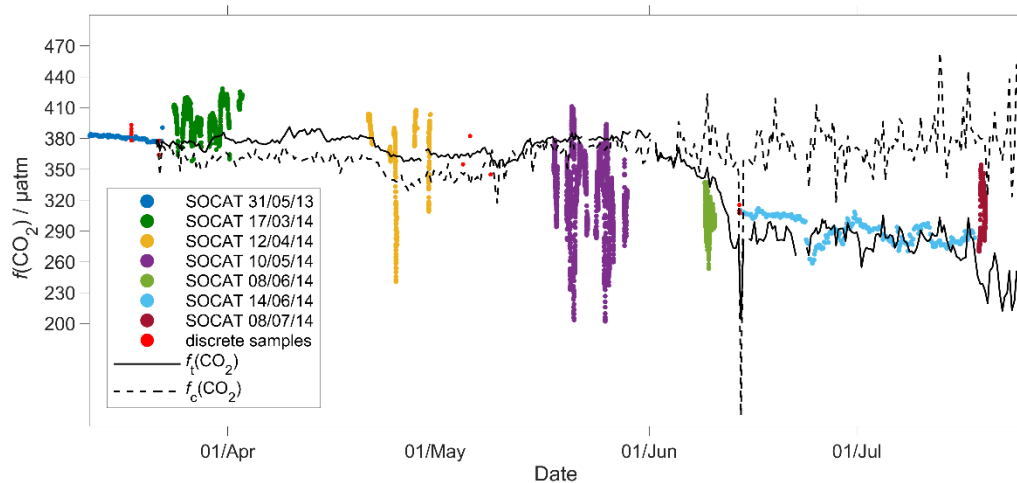
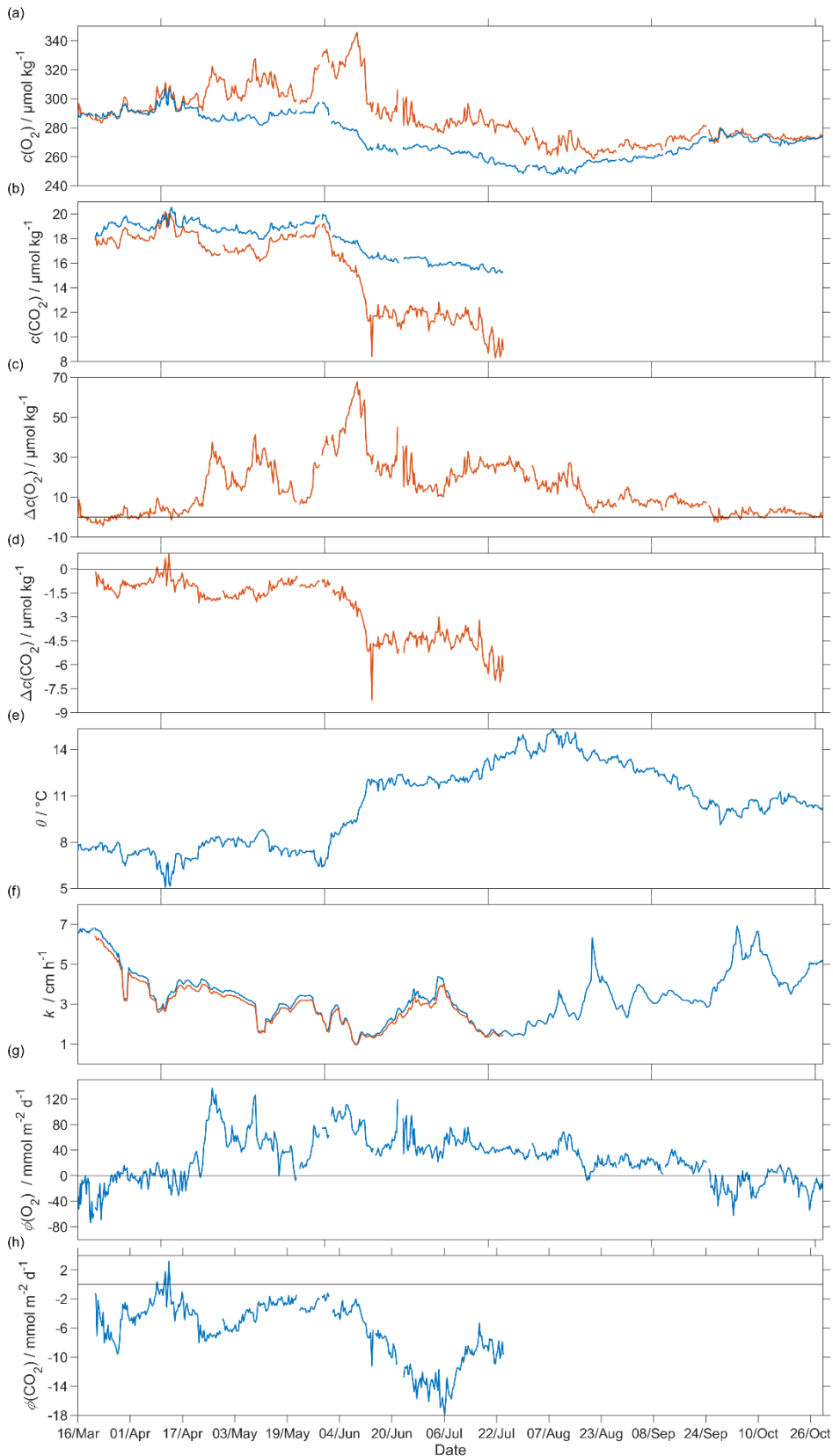


**Figure 11:** Comparison between surface  $f(\text{CO}_2)$  from 2014 SOCAT and  $\text{CO}_2$  optode on the glider. Top panel: The black lines are the median glider  $f(\text{CO}_2)$  in the top 10 meters, with  $f_c(\text{CO}_2)$  (dotted line) corresponding to regression 1 (Figure 6a) and  $f_i(\text{CO}_2)$  (continuous line) to regression 2 (Figure 6a). Discrete samples collected during the deployment are shown as red dots, with the other coloured dots representing cruises in the SOCAT database (Bakker et al., 2016). Bottom panel: Glider and SOCAT data positions (same colours as in the top panel).

### 3.2 Air-sea exchange

The surface water was supersaturated with oxygen all summer (Figure 12). From May, this supersaturation drove a continuous  $\text{O}_2$  flux from the sea to the atmosphere. However, the flux varied throughout the deployment having a median of  $4425 \text{ mmol m}^{-2} \text{ d}^{-1}$  (5<sup>th</sup> centile:  $-1631 \text{ mmol m}^{-2} \text{ d}^{-1}$ ; 95<sup>th</sup> centile:  $10388 \text{ mmol m}^{-2} \text{ d}^{-1}$ ). Prior to the spring period of increased Chl  $a$  inventory, the supersaturation varied between 0 to  $10 \text{ } \mu\text{mol kg}^{-1}$ .  $\Phi(\text{O}_2)$  had a median of  $-1.4 \text{ mmol m}^{-2} \text{ d}^{-1}$  (5<sup>th</sup> centile:  $-49 \text{ mmol m}^{-2} \text{ d}^{-1}$ ; 95<sup>th</sup> centile:  $23 \text{ mmol m}^{-2} \text{ d}^{-1}$ ). Then, during the spring period of increased Chl  $a$  inventory, the surface concentration increased by over  $35 \text{ } \mu\text{mol kg}^{-1}$ , causing a peak in  $\Phi(\text{O}_2)$  of  $140 \text{ mmol m}^{-2} \text{ d}^{-1}$ . A second period of increased Chl  $a$  inventory was encountered in June and had a larger  $\Phi(\text{O}_2)$  up to  $118 \text{ mmol m}^{-2} \text{ d}^{-1}$ , driven by supersaturation of  $68 \text{ } \mu\text{mol kg}^{-1}$ . The fluxes were smaller than during the first period of increased Chl  $a$  spring and were associated by an increase of  $c_{\text{raw}}(\text{Chl } a)$  from  $2.5 \text{ mg m}^{-3}$  to the summer maximum of  $4.0 \text{ mg m}^{-3}$ . However, prior to the spring period of increased Chl  $a$

610 inventory,  $\Phi(\text{O}_2)$  showed a few days of influx into seawater caused by a decrease of  $\theta$  from 7.6 °C to 5.9 °C that  
611 increased  $e_{\text{sat}}C_{\text{sat}}(\text{O}_2)$ . The influx at the beginning of the deployment is partly due to the  $\Delta_{\text{bub}}(\text{O}_2)$  correction that  
612 ~~increased  $[1 + \Delta_{\text{bub}}(\text{O}_2)]e_{\text{sat}}(\text{O}_2)$  to values larger than  $e(\text{O}_2)$  for  $U > 10 \text{ m s}^{-1}$ ; resulted in  $[1 + \Delta_{\text{bub}}(\text{O}_2)]c_{\text{sat}}(\text{O}_2) \geq$~~   
613  $e(\text{O}_2)$  for  $U > 10 \text{ m s}^{-1}$ . In August the surface supersaturation decreased to  $2.3 \text{ } \mu\text{mol kg}^{-1}$  and  $\Phi(\text{O}_2)$  decreased to  
614 a monthly minimum of  $-7.6 \text{ mmol m}^{-2} \text{ d}^{-1}$ . In the second half of September the surface water became  
615 undersaturated by  $-2.6 \text{ } \mu\text{mol kg}^{-1}$ , causing  $\text{O}_2$  uptake with a median flux of  $-13 \text{ mmol m}^{-2} \text{ d}^{-1}$  (5<sup>th</sup> centile:  $-39$   
616  $\text{mmol m}^{-2} \text{ d}^{-1}$ ; 95<sup>th</sup> centile:  $10 \text{ mmol m}^{-2} \text{ d}^{-1}$ ).



617

618 **Figure 12:** Air-sea flux of O<sub>2</sub> and CO<sub>2</sub> during spring and summer for CO<sub>2</sub> and during spring, summer and  
 619 autumn for O<sub>2</sub>, a)  $c_{\text{sat}}(\text{O}_2)$  in blue and  $c(\text{O}_2)$  in red, b)  $c_{\text{sat}}(\text{CO}_2)$  in blue and  $c(\text{CO}_2)$  in red, c)  $\Delta c(\text{O}_2) = c(\text{O}_2) -$   
 620  $c_{\text{sat}}(\text{O}_2)$ , d)  $\Delta c(\text{CO}_2) = c(\text{CO}_2) - c_{\text{sat}}(\text{CO}_2)$ , e) sea surface temperature, f)  $k_w(\text{O}_2)$  in blue and  $k_w(\text{CO}_2)$  in red  
 621 normalised back to 50 days (Reuer et al., 2007), g) oxygen air-sea flux  $\Phi(\text{O}_2)$  and h) CO<sub>2</sub> air-sea flux  $\Phi(\text{CO}_2)$ .  
 622 The flux from sea to air is positive while that from air to sea is negative.

623

624 The CO<sub>2</sub> flux from March to July was always from the air to the sea (Figure 12), with a median of ~~-3.95.2~~ mmol  
625 m<sup>-2</sup> d<sup>-1</sup> (5<sup>th</sup> centile: ~~-4.14~~ mmol m<sup>-2</sup> d<sup>-1</sup>; 95<sup>th</sup> centile: ~~0.3-1.5~~ mmol m<sup>-2</sup> d<sup>-1</sup>). An opposite flux direction is expected  
626 for  $\Phi(\text{O}_2)$  and  $\Phi(\text{CO}_2)$  during the productive season when net community production is the main driver of  
627 concentration changes. After the summer period of increased Chl *a* inventory, the flux had a median of ~~-4.11~~  
628 mmol m<sup>-2</sup> d<sup>-1</sup> (5<sup>th</sup> centile: ~~-5.116~~ mmol m<sup>-2</sup> d<sup>-1</sup>; 95<sup>th</sup> centile: ~~1.7-6.8~~ mmol m<sup>-2</sup> d<sup>-1</sup>), in agreement with previous  
629 studies that classified the Norwegian Sea as a CO<sub>2</sub> sink (~~Skjelvan et al., 2005; Takahashi et al., 2002~~)(~~Takahashi~~  
630 ~~et al., 2002; Skjelvan et al., 2005~~).  $\Phi(\text{CO}_2)$  for the discrete samples from 18 March to 14 June ( $n = 13$ ) varied  
631 from 0.1 to ~~-~~13 mmol m<sup>-2</sup> d<sup>-1</sup>.

632

633

634

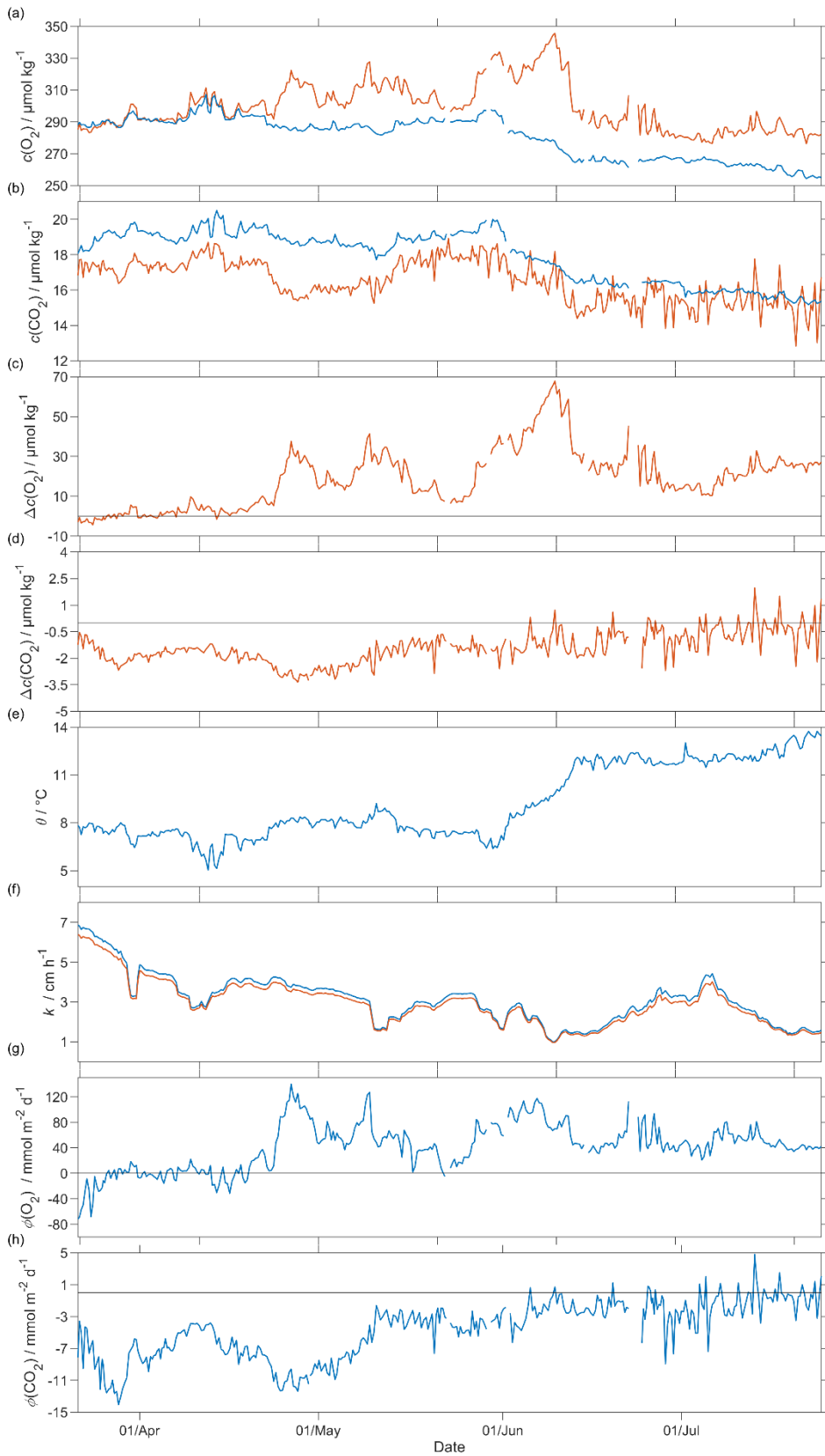
635

636

637

638





639  
640  
641

**Figure 12:** Oxygen and CO<sub>2</sub> air-sea flux where a) shows in blue  $c_{\text{sat}}(\text{O}_2)$  and in red  $c(\text{O}_2)$ , b) shows in blue  $c_{\text{sat}}(\text{CO}_2)$  and in red  $c(\text{CO}_2)$ , c)  $\Delta c(\text{O}_2) = c(\text{O}_2) - c_{\text{sat}}(\text{O}_2)$ , d)  $\Delta c(\text{CO}_2) = c(\text{CO}_2) - c_{\text{sat}}(\text{CO}_2)$ , e) sea surface

642 temperature  $\theta$ , f)  $k_w(\text{O}_2)$  (blue) and  $k(\text{CO}_2)$  normalised back to 50 days (Reuer et al., 2007), g) oxygen air-sea  
643 flux  $\Phi(\text{O}_2)$ , and h)  $\text{CO}_2$  air-sea flux  $\Phi(\text{CO}_2)$ . The flux from sea to air is positive while that from air to sea is  
644 negative.

### 646 3.3 $N(\text{O}_2)$

647 ~~We calculated  $N(\text{O}_2)$  and  $N(\text{C}_T)$  using an integration depth of  $z_{\text{lim}} = 45$  m because the mean deep chlorophyll~~  
648 ~~maximum (DCM) depth was  $z_{\text{DCM}} = (20 \pm 18)$  m (Figure 9). For comparison, the mixed layer depth was deeper~~  
649 ~~and varied more strongly and had a mean value of  $z_{\text{mix}} = (68 \pm 78)$  m, using a threshold criterion of  $\Delta\theta = 0.5$  °C to~~  
650 ~~the median  $\theta$  value of the top 5 m of the glider profile (Obata et al., 1996; United States. National Environmental~~  
651 ~~Satellite and Information Service, Monterey and Levitus, 1997; Foltz et al., 2003). Using a 5 points moving~~  
652 ~~median maintained the same mean value of  $z_{\text{mix}}$  but decreased the variability  $=(68 \pm 75)$  m.~~

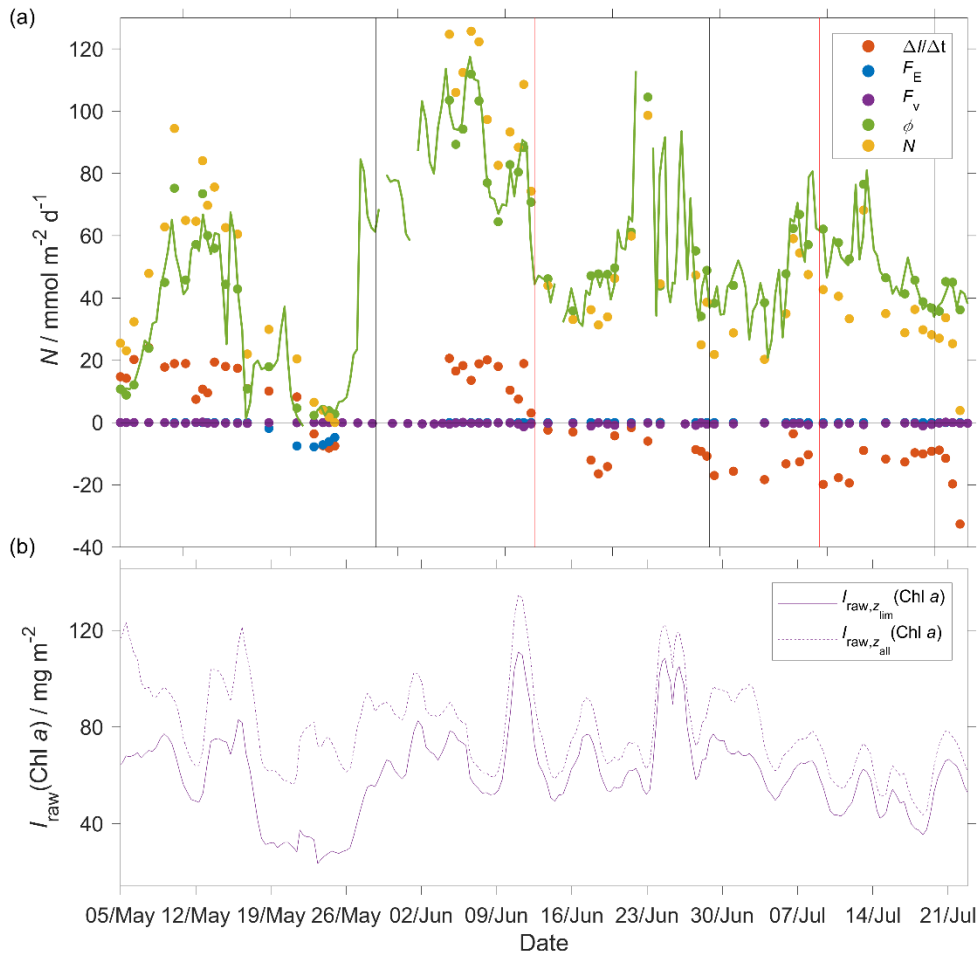
653 To capture the entire euphotic zone, we calculated  $N(\text{O}_2)$  and  $N(\text{DIC})$  using an integration depth of  $z_{\text{lim}} = 45$  m  
654 because the mean deep chlorophyll maximum (DCM) depth was  $z_{\text{DCM}} = (20 \pm 18)$  m (Figure 9). For comparison,  
655 the mixed layer depth was deeper, varied more strongly and had a mean value of  $z_{\text{mix}} = (68 \pm 78)$  m, using a  
656 threshold criterion of  $\Delta\theta = 0.5$  °C to the median  $\theta$  value in the top 5 m of the glider profile (Obata et al., 1996;  
657 United States. National Environmental Satellite and Information Service, Monterey and Levitus, 1997; Foltz et  
658 al., 2003).

659 The two  $N$  values were calculated as the difference in inventory changes between two transects when the glider  
660 moved in the same direction. ~~This method was used in order to have similar time interval between repeat~~  
661 ~~occupations of the same transect position to calculate the inventory changes and entrainment.~~

662 During the deployment, we sampled two periods of increased Chl  $a$  inventory, the first one in May and a second  
663 one in June. The chlorophyll  $a$  inventory ( $I_{\text{raw},z_{\text{lim}}}(\text{Chl } a)$ ) was calculated integrating  $c_{\text{raw}}(\text{Chl } a)$  to  $z_{\text{lim}}$ . ~~The~~  
664 ~~fluorometer was not calibrated for that reason to  $T_{\text{O}}$  remove any outliers we used a five-point moving mean of~~  
665  $I_{\text{raw},z_{\text{lim}}}(\text{Chl } a)$ .

666 The  $N(\text{O}_2)$  changes ~~of  $N(\text{O}_2)$~~  were dominated by  $\Phi(\text{O}_2)$  that had an absolute median of 4734  $\text{mmol m}^{-2} \text{d}^{-1}$  (5<sup>th</sup>  
667 centile: 4.13  $\text{mmol m}^{-2} \text{d}^{-1}$ ; 95<sup>th</sup> centile: 10386  $\text{mmol m}^{-2} \text{d}^{-1}$ ), followed by  $I(\text{O}_2)$  that had a median of 1215  $\text{mmol}$   
668  $\text{m}^{-2} \text{d}^{-1}$  (5<sup>th</sup> centile: 2.83  $\text{mmol m}^{-2} \text{d}^{-1}$ ; 95<sup>th</sup> centile: 2029  $\text{mmol m}^{-2} \text{d}^{-1}$ ),  $F_v(\text{O}_2)$  that had an absolute median of  
669 0.23  $\text{mmol m}^{-2} \text{d}^{-1}$  (5<sup>th</sup> centile: 0  $\text{mmol m}^{-2} \text{d}^{-1}$ ; 95<sup>th</sup> centile: 1.09  $\text{mmol m}^{-2} \text{d}^{-1}$ ) and  $E(\text{O}_2)$  that had a median of 0  
670  $\text{mmol m}^{-2} \text{d}^{-1}$  (5<sup>th</sup> centile: 0.12  $\text{mmol m}^{-2} \text{d}^{-1}$ ; 95<sup>th</sup> centile: 0.4  $\text{mmol m}^{-2} \text{d}^{-1}$ ).

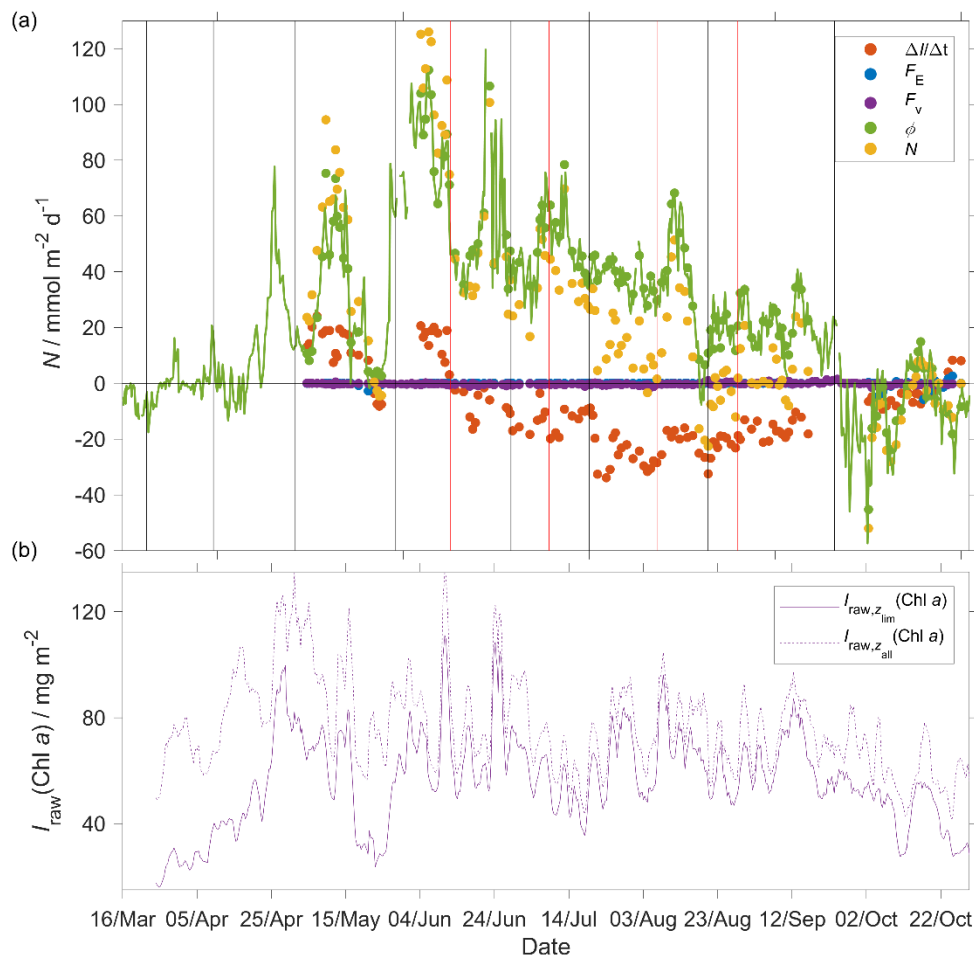
671 At the beginning of May,  $I_{\text{raw},z_{\text{lim}}}(\text{Chl } a)$  increased to 97  $\text{mg m}^{-2}$  and  
672  
673



674 **Figure 13:** a) Each component of the  $N(O_2)$  calculation: in red  $I(O_2)$ ,  $E(O_2)$  in blue, in violet  $F_v(O_2)$ ,  $\Phi(O_2)$  in  
 675 green dots and the green line is  $\Phi(O_2)$  continuous timeseries calculated using  $k_w(O_2)$  weighted 50 days and in  
 676 yellow  $N(O_2) = I(O_2) + \Phi(O_2) \frac{\min(z_{lim}, z_{mix})}{z_{mix}} - E(O_2) - F_v(O_2)$  b) the violet continuous line is the  $e_{raw}(\text{Chl } a)$   
 677 inventory in the top 45 m,  $z_{lim}$ , ( $I_{raw,z_{lim}}(\text{Chl } a)$ ) and the dotted line in all the water column,  $z_{all}$ ,  
 678 ( $I_{raw,z_{all}}(\text{Chl } a)$ ). The black vertical lines represent each glider transect and between the two vertical red lines  
 679 when the glider was in NCC.  
 680  
 681

682  $N(O_2) = (95 \pm 16) \text{ mmol m}^{-2} \text{ d}^{-1}$ . After this period,  $I_{raw,z_{lim}}(\text{Chl } a)$  decreased to  $49 \text{ mg m}^{-2}$  and  $N(O_2) = (-4.6 \pm 1.6)$   
 683  $\text{mmol m}^{-2} \text{ d}^{-1}$ . During the summer  $I_{raw,z_{lim}}(\text{Chl } a)$  increased to  $110 \text{ mg m}^{-2}$ , which caused a sharp increase of  
 684  $N(O_2)$  to  $(126 \pm 25) \text{ mmol m}^{-2} \text{ d}^{-1}$ .  $I_{raw,z_{lim}}(\text{Chl } a)$  remained higher than  $50 \text{ mg m}^{-2}$  until the end of June when  
 685  $N(O_2)$  was  $(31 \pm 9) \text{ mmol m}^{-2} \text{ d}^{-1}$ . The passage of the glider from NwAC to NCC accompanied by a drop of  
 686 surface  $c(O_2)$  from  $330$  to  $280 \mu\text{mol kg}^{-1}$  (Figure 9) that resulted in lower  $\Phi(O_2)$  and  $N(O_2)$  values (Figure 13). At  
 687 the same time  $I_{raw,z_{lim}}(\text{Chl } a)$  decreased to  $35 \text{ mg m}^{-2}$  showing that the decrease of  $N(O_2)$  depended on the  
 688 passage to NCC and a decrease of biological production. After the beginning of August,  $I_{raw,z_{lim}}(\text{Chl } a)$   
 689 decreased to  $49 \text{ mg m}^{-2}$  and  $N(O_2)$  turned negative with a minimum of  $(-23 \pm 25) \text{ mmol m}^{-2} \text{ d}^{-1}$ . In October during  
 690 the last glider transect  $I_{raw,z_{lim}}(\text{Chl } a)$  continued decreasing to  $27 \text{ mg m}^{-2}$  leading to the minimum  $N(O_2)$  of  $(-$   
 691  $52 \pm 11) \text{ mmol m}^{-2} \text{ d}^{-1}$ .

692 Integrating At the beginning of May,  $I_{\text{raw},z_{\text{lim}}}(\text{Chl } a)$  increased to  $97 \text{ mg m}^{-2}$  and  $N(\text{O}_2) = (94 \pm 16) \text{ mmol m}^{-2} \text{ d}^{-1}$ .  
 693 After this period from March to October gives a flux of  $4.9 \text{ mol m}^{-2} \text{ a}^{-1}$  (Table 3; discussed in section 4.2).



694  
 695 **Figure 13:** a) Components of the  $N(\text{O}_2)$  calculation:  $\Delta I(\text{O}_2)/\Delta t$  (red),  $E(\text{O}_2)$  (blue),  $F_v(\text{O}_2)$  (violet),  $\Phi(\text{O}_2)$  (green)  
 696 with  $k_w(\text{O}_2)$  weighted over 50 days,  $N(\text{O}_2)$  (yellow). b) Chl  $a$  inventory in the top 45 m,  $I_{\text{raw},z_{\text{lim}}}(\text{Chl } a)$  (violet),  
 697 Chl  $a$  inventory for the whole water column,  $I_{\text{raw},z_{\text{all}}}(\text{Chl } a)$  (violet dotted line). The black vertical lines  
 698 represent each glider transect. Between the two vertical red lines, the glider was in the NCC region.  
 699

### 700 3.4 N(DIC)

701 In the case of  $N(\text{DIC})$  the main drivers were the inventory changes with an absolute median of  $29 \text{ mmol m}^{-2} \text{ d}^{-1}$   
 702 (5<sup>th</sup> centile:  $1.3 \text{ mmol m}^{-2} \text{ d}^{-1}$ ; 95<sup>th</sup> centile:  $57 \text{ mmol m}^{-2} \text{ d}^{-1}$ ), followed by  $\Phi(\text{CO}_2)$  that had an absolute median of  
 703  $7.0 \text{ mmol m}^{-2} \text{ d}^{-1}$  (5<sup>th</sup> centile:  $0.8 \text{ mmol m}^{-2} \text{ d}^{-1}$ ; 95<sup>th</sup> centile:  $15 \text{ mmol m}^{-2} \text{ d}^{-1}$ ),  $F_v(\text{DIC})$  that had an absolute  
 704 median of  $0.2 \text{ mmol m}^{-2} \text{ d}^{-1}$  (5<sup>th</sup> centile:  $0 \text{ mmol m}^{-2} \text{ d}^{-1}$ ; 95<sup>th</sup> centile:  $1.3 \text{ mmol m}^{-2} \text{ d}^{-1}$ ) and  $E(\text{DIC})$  had a median  
 705 of  $0 \text{ mmol m}^{-2} \text{ d}^{-1}$  (5<sup>th</sup> centile:  $0 \text{ mmol m}^{-2} \text{ d}^{-1}$ ; 95<sup>th</sup> centile:  $3.4 \text{ mmol m}^{-2} \text{ d}^{-1}$ ). During the period of increased Chl  
 706  $a$  inventory  $N(\text{DIC})$  was  $(21 \pm 4.5) \text{ mmol m}^{-2} \text{ d}^{-1}$ . Later  $I_{\text{raw},z_{\text{lim}}}(\text{Chl } a)$  decreased to  $30 \text{ mg m}^{-2}$  driving  $N(\text{DIC})$  to  
 707 negative values with a minimum of  $(-2.7 \pm 5.0) \text{ mmol m}^{-2} \text{ d}^{-1}$ . In the next transect, the glider measured the  
 708 maximum  $I_{\text{raw},z_{\text{lim}}}(\text{Chl } a)$  of  $111 \text{ mg m}^{-2}$  that increased  $N(49 \text{ mg m}^{-2} \text{ DIC})$  to  $(85 \pm 4.5) \text{ mmol m}^{-2} \text{ d}^{-1}$ . This  
 709 maximum was reached during a transect when the glider moved in NCC that had a  $c(\text{DIC})$  of  $2080 \text{ } \mu\text{mol kg}^{-1}$  at  
 710 the surface compared with the  $2150 \text{ } \mu\text{mol kg}^{-1}$  in NwAC and drove a continuous positive  $N(\text{O}_2) = (0 \pm 1.6 \text{ DIC})$   
 711 that had a minimum of  $(36 \pm 7.4) \text{ mmol m}^{-2} \text{ d}^{-1}$  (Figure 14).

712 Using the mean of  $N(\text{O}_2)$  assuming an  $N(\text{O}_2) = 0$  in the rest of the year lead to an annual value of  $4 \text{ mol m}^{-2} \text{ a}^{-1}$   
 713 (Table 3) discussed in section 4.2.

714 Integrating  $N(\text{DIC})$  from March to July gives a flux of  $3.3 \text{ mol m}^{-2} \text{ a}^{-1}$  (Table 3,  ~~$N$~~  discussed in section 4.2).

715  
 716 **Table 3. Net community production ( $N$ ) estimates in the Norwegian Sea.** ~~The previous studies dataset had data~~  
 717 ~~collected by several cruises in different years, (with integration depth  $z_{\text{lim}}$ ).~~ Falck and Anderson (2005) used  
 718 ~~historical year-round~~ data from 1960 to 2000 ~~collected all the year in the area from between~~  $62^\circ$  ~~to~~ and  $70^\circ$  N and  
 719 from 1991 to 1994 ~~collected~~ at OWSM. Skjelvan et al., (2001) used data collected all the year from  $67.5^\circ$  N  $9^\circ$  E  
 720 ~~to~~  $71.5^\circ$  N  $1^\circ$  E and along  $74.5^\circ$  N from  $7$  to  $15^\circ$  E from 1957 to 1970 and from 1991 to 1998. Skjelvan et al.  
 721 (2001) used year-round data from 1957 to 1970 and from 1991 to 1998 between  $67.5^\circ$  N  $9^\circ$  E and  $71.5^\circ$  N  $1^\circ$  E  
 722 and along  $74.5^\circ$  N from  $7$  to  $15^\circ$  E. Kivimäe (2007) used ~~the oxygen measured at OWSM all the year~~ year-round  
 723 ~~data~~ from 1955 to 2005 and Falck and Gade (1999) used ~~data collected all the year in all the Norwegian Sea~~  
 724 ~~from 1955 to 1988~~ year-round data from 1955 to 1988 in all of the Norwegian Sea. While the previous studies  
 725 report annual  $N$  estimates, the present study derives  $N(\text{O}_2)$  between March and October and  $N(\text{DIC})$  between  
 726 March and July.

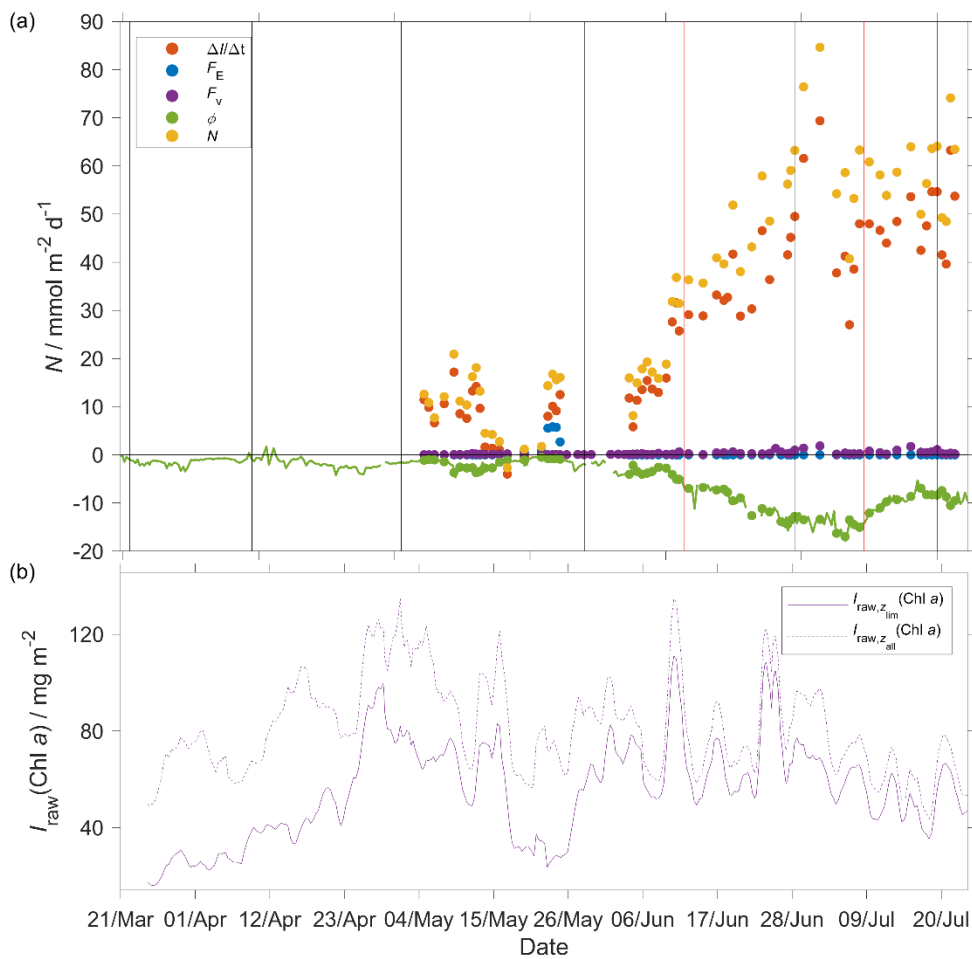
727

Study	<del><math>N(\text{DIC})</math></del> / $\text{mol m}^{-2} \text{ a}^{-1}$	$N(\text{O}_2)$ / $\text{mol m}^{-2} \text{ a}^{-1}$	$N(\text{O}_2) /$ $N(\text{DIC})$	$z_{\text{lim}} /$ m	Variables used to derive $N$
(Falck and Anderson, 2005), <u>annual</u>	3.4	—		100	$c(\text{NO}_3^-)$ , $c(\text{PO}_4^{3-})$ , <del><math>\epsilon_{\text{TC}}(\text{DIC})</math></del>
<del>(Skjelvan et al., 2001)</del> (Skjelvan et al., 2001), <u>annual</u>	<del>2.0</del>	2.6		300	$c(\text{O}_2)$ , $c(\text{PO}_4^{3-})$
(Kivimäe, 2007), <u>annual</u>	<del>8.6</del>	11 (4.7 to 18.3)		$z_{\text{mix}}$ until 100 m	$c(\text{O}_2)$
(Falck and Gade, 1999), <u>annual</u>	<del>3.0</del>	3.9		30	$c(\text{O}_2)$
This study, <u>March to July</u>	<del>3.1</del> 0	4.0 <sub>1</sub>	1.3	30	$c(\text{O}_2)$ , <del><math>\epsilon_{\text{TC}}(\text{DIC})</math></del>
This study, <u>March to July</u>	0.9 <sub>3.3</sub>	4.0 <sub>2</sub>	1.3	45	$c(\text{O}_2)$ , <del><math>\epsilon_{\text{TC}}(\text{DIC})</math></del>
This study, <u>March to July</u>	0.4 <sub>3.3</sub>	3.7	1.1	100	$c(\text{O}_2)$ , <del><math>\epsilon_{\text{TC}}(\text{DIC})</math></del>
<u>This study, March to October</u>		5.0			
<u>This study, March to October</u>		4.9			
<u>This study, March to October</u>		3.6			

728

729 **3.4  $N(C_T)$**

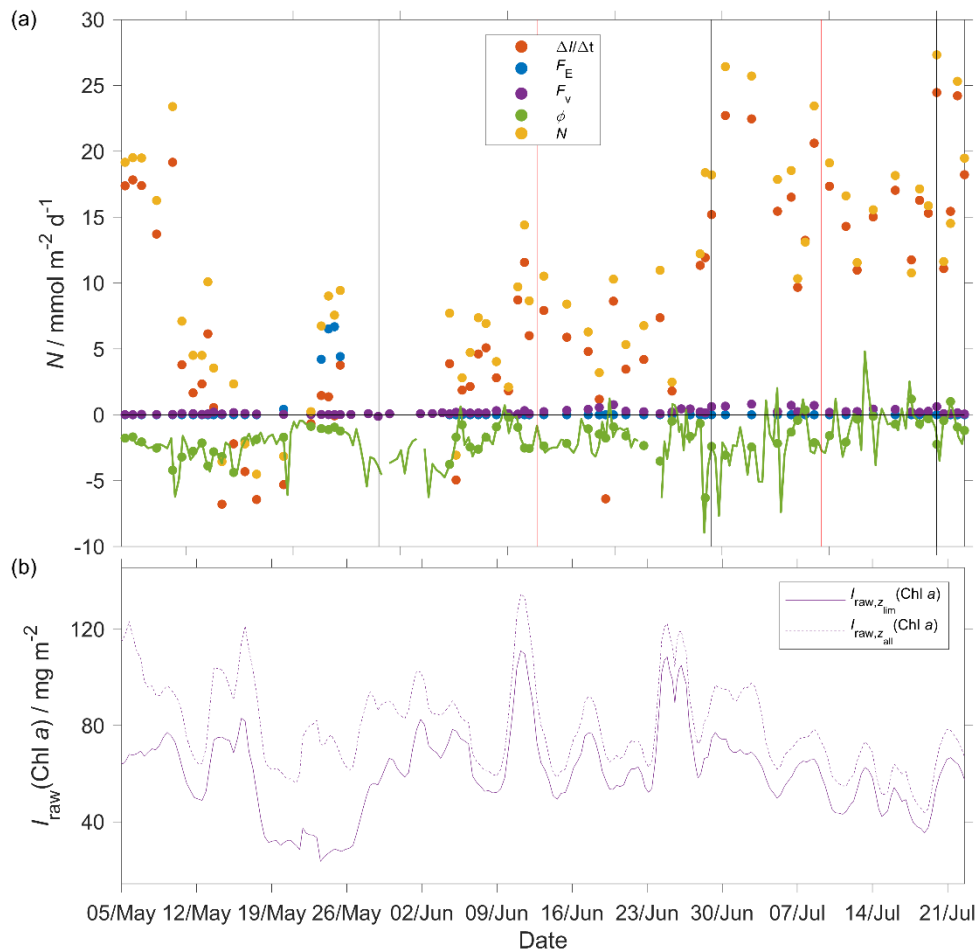
730 In the case of  $N(C_T)$  the main driver were the inventory changes with an absolute median of  $7.6 \text{ mmol m}^{-2} \text{ d}^{-1}$  (5<sup>th</sup>  
 731 centile:  $1 \text{ mmol m}^{-2} \text{ d}^{-1}$ ; 95<sup>th</sup> centile:  $23 \text{ mmol m}^{-2} \text{ d}^{-1}$ ), followed by  $\Phi(\text{CO}_2)$  that had an absolute median of  $1.7$   
 732  $\text{mmol m}^{-2} \text{ d}^{-1}$  (5<sup>th</sup> centile:  $0.3 \text{ mmol m}^{-2} \text{ d}^{-1}$ ; 95<sup>th</sup> centile:  $4 \text{ mmol m}^{-2} \text{ d}^{-1}$ ),  $F_v(C_T)$  that had an absolute median of  
 733  $0.2 \text{ mmol m}^{-2} \text{ d}^{-1}$  (5<sup>th</sup> centile:  $0 \text{ mmol m}^{-2} \text{ d}^{-1}$ ; 95<sup>th</sup> centile:  $0.7 \text{ mmol m}^{-2} \text{ d}^{-1}$ ) and  $E(C_T)$  had a median of  $0 \text{ mmol}$   
 734  $\text{m}^{-2} \text{ d}^{-1}$  (5<sup>th</sup> centile:  $0 \text{ mmol m}^{-2} \text{ d}^{-1}$ ; 95<sup>th</sup> centile:  $3.3 \text{ mmol m}^{-2} \text{ d}^{-1}$ ). During the period of increased Chl *a* inventory  
 735  $N(C_T)$  was  $(23 \pm 4.2) \text{ mmol m}^{-2} \text{ d}^{-1}$ . Later  $I_{\text{raw},z_{\text{lim}}}(\text{Chl } a)$  decreased to  $30 \text{ mg m}^{-2}$  driving  $N(C_T)$  to negative values  
 736 with a minimum of  $(-4.5 \pm 5.2) \text{ mmol m}^{-2} \text{ d}^{-1}$ . In the next transect, the glider measured the maximum  
 737  $I_{\text{raw},z_{\text{lim}}}(\text{Chl } a)$  of  $111 \text{ mg m}^{-2}$  that increased  $N(C_T)$  to  $(14 \pm 8.7) \text{ mmol m}^{-2} \text{ d}^{-1}$ . In the next transect the glider  
 738 moved in NCC that had a  $C_T$  of  $2075 \text{ } \mu\text{mol kg}^{-1}$  at the surface compared with the  $2130 \text{ } \mu\text{mol kg}^{-1}$  in NwAC and  
 739 drove a continuous positive  $N(C_T)$  that had a maximum of  $(26 \pm 3.7) \text{ mmol m}^{-2} \text{ d}^{-1}$  (



740  
 741 **Figure 14).**

742 Using the mean of  $N(C_T)$  with the assumption that during the rest of year  $N(C_T) = 0$ , we calculated the annual  
 743  $N(C_T)$  of  $0.9 \text{ mol m}^{-2} \text{ a}^{-1}$  (Table 3) that its implications are discussed in section 4.2.

744  
 745



746 **Figure 14:** a) Each component of the  $N(C_T)$  calculation:  $\Delta I(DIC)/\Delta t$  (red dots),  $E(C_T \text{ in DIC})$  (blue dots),  $F_v(C_T \text{ in } CO_2)$  (violet dots),  $\Phi(C_T \text{ in } CO_2)$  (green dots and the green line is  $\Phi(O_2)$  continuous time series calculated using  $k$  with  $k_w(CO_2)$  weighted over 50 days and in  $N(DIC)$  (yellow dots)  $N(C_T) = -I(C_T) - \Phi(CO_2) \frac{\min(z_{lim}, z_{mix})}{z_{mix}} + E(C_T) + F_v(C_T)$ . b) the violet continuous line is the  $I_{raw, z_{lim}}(Chl a)$  inventory in the top 45 m,  $I_{raw, z_{lim}}(Chl a)$  (violet dotted line) and the  $I_{raw, z_{all}}(Chl a)$  (violet dotted line) in all the water column,  $I_{raw, z_{all}}(Chl a)$ . The black vertical lines represent each glider transect and between. Between the two vertical red lines when the glider was in the NCC region.

## 756 4 Discussion

### 757 4.1 Sensor performance

758 This study presents data from the first glider deployment with a  $CO_2$  optode. The initial uncalibrated  $p_{CO_2}$  measured by the  $CO_2$  optode had a median of 604  $\mu atm$  (5<sup>th</sup> centile: 566  $\mu atm$ ; 95<sup>th</sup> centile: 768  $\mu atm$  when), whereas the  $p(CO_2)$  of discrete samples varied from 302 to 421  $\mu atm$ . This discrepancy was caused by sensor drift prior to and during deployment of the optode.

762 We applied corrections for drift (using deep-water samples as a reference point), sensor lag and calibrated the  
763 CO<sub>2</sub> optode against co-located discrete samples throughout the water column.

764 ~~Atamanchuk (2014)~~Atamanchuk (2014) reported that the sensor was affected by a lag that varied from 45 to 264  
765 s depending on temperature. These values were determined in an actively stirred beaker. However, in this study  
766 the sensor was mounted on a glider and was not actively pumped, which increased the response time to ~~(1384 s,~~  
767 ~~23 min~~ (25<sup>th</sup> quartile: ~~1101 s~~18 min; 75<sup>th</sup> quartile: ~~1799 s~~30 min). Also, the optode was affected by a continuous  
768 drift from 637 to 5500  $\mu\text{atm}$  that is larger than the drift found by Atamanchuk et al. (2015a) that increased by 75  
769  $\mu\text{atm}$  after 7 months.

770 In this study, the drift- and lag-corrected sensor output showed a better correlation with the CO<sub>2</sub> concentration  
771  $c(\text{CO}_2)$  than with  $p(\text{CO}_2)$ . The latter two quantities are related to each other by the solubility that varies with  $\theta$   
772 and  $S$  (Weiss, 1974) (Eq. 2). The better correlation with  $c(\text{CO}_2)$  was probably related due to an inadequate  
773 temperature-parameterisation of the sensor calibration function. ~~The sensor output depends on the~~  
774 ~~changes~~Including temperature and temperature squared in pH that are directly related to the changes of the  
775 calibration gave a better fit for both  $c(\text{CO}_2)$  in the membrane and indirectly than with  $p(\text{CO}_2)$ , via Henry's  
776 Law but overall still a lower calibration residual for the former. ~~The sensor output depends on the changes in pH~~  
777 ~~that are directly related to the changes of  $c(\text{CO}_2)$  in the membrane and – indirectly –  $p(\text{CO}_2)$ , via Henry's Law.~~  
778 The calibration is supposed to correct for the temperature-dependence of the sensor output (Atamanchuk et al.,  
779 2014). So the fact, that the sensor output correlated better with  $c(\text{CO}_2)$  than  $p(\text{CO}_2)$  is perhaps due to a fortuitous  
780 cancellation of an inadequate temperature-parameterisation and the Henry's Law relationship between  $c(\text{CO}_2)$   
781 than  $p(\text{CO}_2)$ .

782 The calibrated optode output captured the  $\epsilon_{\text{T}c(\text{DIC})}$  changes in space and time with a standard deviation of ~~1011~~  
783  $\mu\text{mol kg}^{-1}$  compared with the discrete samples.  $\epsilon_{\text{T}c(\text{DIC})}$  decreased from ~~2100~~2130  $\mu\text{mol kg}^{-1}$  to ~~2050~~2000  $\mu\text{mol}$   
784  $\text{kg}^{-1}$  and increased with depth to 2170  $\mu\text{mol kg}^{-1}$ . This shows the potential of the sensor for future studies that  
785 aim to analyse the carbon cycle using a high-resolution dataset.

786 The optode-derived CO<sub>2</sub> fugacity  $f_{\text{G}}(\text{CO}_2)$  had a mean bias of (~~1.8~~±22)  $\mu\text{atm}$  compared with the discrete samples.  
787 These values are comparable with a previous study when the CO<sub>2</sub> optode was tested for 65 days on a wave-  
788 powered Profiling ~~er~~AWLERcRAWLER (PRAWLER) from 3 to 80 m (~~Chu et al., 2020~~)(Chu et al., 2020),  
789 which had an uncertainty between 35 and 72  $\mu\text{atm}$ . The PRAWLER optode was affected by a continuous drift of  
790 5.5  $\mu\text{atm d}^{-1}$  corrected using a regional empirical algorithm that uses  $c(\text{O}_2)$ ,  $\theta$ ,  $S$  and  $\sigma_{\text{o}}$  to estimate  $A_{\text{T}}$  and  
791  $\epsilon_{\text{T}c(\text{DIC})}$ .

## 792 4.2 Norwegian Sea net community production

793 Increases in  $N(\text{O}_2)$  and  $N(\epsilon_{\text{T}c(\text{DIC})})$  were associated with increases in depth-integrated  $c_{\text{raw}}(\text{Chl } a)$ , designated as  
794 periods of increased Chl  $a$  inventory  ~~$\epsilon_{\text{T}c(\text{DIC})}$~~  $I_{\text{raw}}(\text{Chl } a)$ , at the beginning of May and in June. During ~~the first period of~~  
795 ~~increased Chl  $a$  inventory at the beginning of~~ May surface  ~~$\epsilon_{\text{T}c(\text{DIC})}$~~  $c_{\text{raw},1} I_{\text{raw}}(\text{Chl } a)$  reached ~~3~~135  $\text{mg m}^{-3}$ . ~~The second~~  
796 ~~period of increased Chl  $a$  inventory in~~. In June lasted longer and  ~~$\epsilon_{\text{T}c(\text{DIC})}$~~  $c_{\text{raw},2} I_{\text{raw}}(\text{Chl } a)$  increased to ~~4~~reached again  
797 ~~135~~  $\text{mg m}^{-3}$ . Between ~~these~~ two periods of increased Chl  $a$  inventory,  $N(\epsilon_{\text{T}c(\text{DIC})})$  briefly turned negative  
798 values and  $N(\text{O}_2)$  reached the deployment minimum, indicating ~~that~~ remineralisation of the high Chl  $a$  inventory  
799 material ~~was a dominant process~~ during this period. ~~Even though they are uncalibrated, the spring~~The period of  
800 increased Chl  $a$  inventory  ~~$\epsilon_{\text{T}c(\text{DIC})}$~~  $c_{\text{raw}}(\text{Chl } a)$  values are in agreement ~~coincided~~ with the study of Rey (2001) who found



801  $c_{\text{raw}}(\text{Chl } a) = 3 \text{ mg m}^{-3}$  at the beginning of May. The largest period of increased Chl  $a$  inventory when the top 50  
 802 m  $\theta$  increased a surface temperature increase from 7 °C to 11 °C and  $z_{\text{mix}}$  shoaled shoaling of the mixed layer from  
 803 200 m to 20 m. During this period,  $c(\text{O}_2)$  reached a summer maximum of 340  $\mu\text{mol kg}^{-1}$  and  $C_{\text{T}}c(\text{DIC})$  decreased  
 804 to the summer minimum at 2070 of 1990  $\mu\text{mol kg}^{-1}$ . In both cases, the main components of the  $N$  changes were  
 805 the inventory and air-sea flux, while the smallest driver was the entrainment. Also, the glider sampled two  
 806 different water masses characterised by different  $C_{\text{T}}c(\text{DIC})$  and  $c(\text{O}_2)$ . This led to might be the cause of the  
 807 smaller values of  $N(\text{O}_2)$  and higher values  $N(C_{\text{T}}\text{DIC})$  in June and July in NCC compared with NwAC (Figure  
 808 13 and 14). Another explanation might be a consumption of  $\text{O}_2$  due to remineralisation and a delay in the  
 809 response of the  $c(\text{DIC})$  that was lowered during the two blooms. A fully functional  $\text{CO}_2$  optode in the second  
 810 part of the deployment would have helped to uncover the cause of the higher  $N(\text{DIC})$  than of  $N(\text{O}_2)$ .

811 Table 3 shows estimates of net community production ( $N$ ) in the Norwegian Sea (Falck and Anderson, 2005;  
 812 Falck and Gade, 1999; Kivimäe, 2007; Skjelvan et al., 2001). All these studies used low resolution datasets in  
 813 space and time. These datasets had data collected by several cruises in different years, Falck and Anderson  
 814 (2005) used historical data from 1960 to 2000 collected in the area from 62 to 70° N and from 1991 to 1994  
 815 collected all the year at OWSM. Skjelvan et al., (2001) used data collected from 67.5° N 9° E to 71.5° N 1° E  
 816 and along 74.5° N from 7 to 15° E from 1957 to 1970 and from 1991 to 1998. Kivimäe (2007) used the oxygen  
 817 measured all the year at OWSM from 1955 to 2005 and Table 3 shows estimates of net community production  
 818 ( $N$ ) in the Norwegian Sea. All other studies used ships to gather observations. The estimated  $N$  in of the four  
 819 other studies varied from 2.6 to 11.1  $\text{mol m}^{-2} \text{a}^{-1}$  for  $N(\text{O}_2)$  and was 3.4 for  $N(\text{DIC})$ . In our glider study, we  
 820 obtained between March and July  $N(\text{DIC})$  of 3.3  $\text{mol m}^{-2} \text{a}^{-1}$  and a  $N(\text{O}_2)$  of 4.2  $\text{mol m}^{-2} \text{a}^{-1}$ , in agreement with  
 821 these studies. The ratio of  $N(\text{O}_2)$  and  $N(\text{DIC})$  for an integration depth of 45 m gave a photosynthetic quotient  
 822 (PQ) of 1.3, in agreement with the Redfield ratio of  $1.45 \pm 0.15$  (Redfield, 1963; Anderson, 1995; Anderson and  
 823 Sarmiento, 1994; Laws, 1991). The  $N(\text{O}_2)$  estimate is influenced primarily by the air-sea exchange flux  $\Phi(\text{O}_2)$   
 824 (median: 34  $\text{mmol m}^{-2} \text{d}^{-1}$ ), followed by the inventory change (15  $\text{mmol m}^{-2} \text{d}^{-1}$ ). In contrast,  $N(\text{DIC})$  is  
 825 dominated by the inventory change ( $-29 \text{ mmol m}^{-2} \text{d}^{-1}$ ), followed by  $\Phi(\text{CO}_2)$  ( $-7.0 \text{ mmol m}^{-2} \text{d}^{-1}$ ). This reflects  
 826 the slower gas-exchange time constant of  $\text{CO}_2$  compared with  $\text{O}_2$ , due to DIC buffering. To compare our results  
 827 with previous studies we also used  $z_{\text{lim}} = 30 \text{ m}$  Falck and Gade (1999) used data collected all the year in all the  
 828 Norwegian Sea from 1955 to 1988. The estimated  $N$  in the 4 studies varies from 2.0 to 8.6  $\text{mol m}^{-2} \text{a}^{-1}$  for  $N(C_{\text{T}})$   
 829 and from 2.6 to 11.1  $\text{mol m}^{-2} \text{a}^{-1}$  for  $N(\text{O}_2)$ . In our study, we obtained an annual  $N(C_{\text{T}})$  of 0.9  $\text{mol m}^{-2} \text{a}^{-1}$  and a  
 830  $N(\text{O}_2)$  of 4  $\text{mol m}^{-2} \text{a}^{-1}$  in agreement with these studies. The larger  $N(\text{O}_2)$  compared with  $N(C_{\text{T}})$  should be  
 831 attributed to the large  $\Phi(\text{O}_2)$  that had an absolute median of 47  $\text{mmol m}^{-2} \text{d}^{-1}$  compared with  $\Phi(\text{CO}_2)$  absolute  
 832 median of 1.7  $\text{mmol m}^{-2} \text{d}^{-1}$ . Instead, the inventory changes were similar between  $N(\text{O}_2)$  and  $N(C_{\text{T}})$  with a median  
 833 of 12  $\text{mmol m}^{-2} \text{d}^{-1}$  and 7.6  $\text{mmol m}^{-2} \text{d}^{-1}$ , respectively. To compare our results with previous studies we used the  
 834 same  $z_{\text{lim}}$  of 30 m (Falck and Gade, 1999) and 100 m (Falck and Anderson, 2005; Kivimäe, 2007). The calculated  
 835  $N(C_{\text{T}}\text{DIC}; 30 \text{ m})$  was 3.1  $\text{mol m}^{-2} \text{a}^{-1}$ ,  $N(C_{\text{T}}\text{DIC}; 100 \text{ m})$  was 0.3.4  $\text{mol m}^{-2} \text{a}^{-1}$ ,  $N(\text{O}_2; 30 \text{ m})$  was 4.1  $\text{mol m}^{-2} \text{a}^{-1}$   
 836 and  $N(\text{O}_2; 100 \text{ m})$  was 3.7  $\text{mol m}^{-2} \text{a}^{-1}$ . In the case of The  $N(C_{\text{T}}; 30 \text{ m})$  and  $N(C_{\text{T}}\text{DIC}; 100 \text{ m})$  the values value is  
 837 in agreement with the value of 3.4  $\text{mol m}^{-2} \text{a}^{-1}$  given by Falck and Anderson (2005). However, the latter estimate  
 838 was for the entire year, whereas our estimate only covers the months from March to July.  $N(\text{O}_2)$  was similar for  
 839  $z_{\text{lim}} = 30 \text{ m}$  and 45 m, but lower for  $z_{\text{lim}} = 100 \text{ m}$  because of  $\text{O}_2$  consumption during organic matter  
 840 remineralisation below the euphotic zone. The PQ value at 30 was 1.3 and at 100 m decreased to 1.1. Extending  
 841  $N(\text{O}_2)$  to October increased  $N(\text{O}_2; 30 \text{ m})$  and  $N(\text{O}_2; 45 \text{ m})$  to 5.0 and 4.9  $\text{mol m}^{-2} \text{a}^{-1}$ , respectively. Instead,  $N(\text{O}_2;$

842 100 m) decreased to 3.6 mol m<sup>-2</sup> a<sup>-1</sup>, confirming the consumption of O<sub>2</sub> below the euphotic zone. The calculated  
843 were smaller to N(O<sub>2</sub>) until October was in agreement with the previous studies where N(C<sub>T</sub>) that varied from 2  
844 to 8.6 mol m<sup>-2</sup> a<sup>-1</sup>. The smallest value was for N(C<sub>T</sub>; 100 m) because it included the not productive layer located  
845 under the euphotic zone and the z<sub>mix</sub> where the remineralisation of the organic matter can increase C<sub>T</sub>. The  
846 calculated N(O<sub>2</sub>) was not affected by the selection of z<sub>lim</sub> because the changes were largely controlled by Φ(O<sub>2</sub>).  
847 However, the calculated N(O<sub>2</sub>) was in agreement with the previous studies where varied from between 2.6 to and  
848 11 mol m<sup>-2</sup> a<sup>-1</sup>.

849 Some of the previous N(C<sub>T</sub>DIC) estimates derived C<sub>T</sub>c(DIC) from other variables such as c(O<sub>2</sub>), c(PO<sub>4</sub><sup>3-</sup>),  
850 c(NO<sub>3</sub><sup>-</sup>), assuming Redfield ratios P:N:C:O<sub>2</sub> 1:16:106:138 (Redfield, 1963)(Redfield, 1963). During  
851 photosynthesis c(PO<sub>4</sub><sup>3-</sup>) and c(NO<sub>3</sub><sup>-</sup>) are taken up by phytoplankton to form organic matter and are released  
852 again after remineralisation of the organic matter giving an indication of NCP changes. Our N(C<sub>T</sub>DIC) estimate  
853 was 0.53.3 mol m<sup>-2</sup> a<sup>-1</sup> and is lower similar to 3.4 mol m<sup>-2</sup> a<sup>-1</sup> estimated by Falck and Anderson (2005) who used  
854 C<sub>T</sub> samples directly. The difference between our N(C<sub>T</sub>) and other studies is likely due to their use of the Redfield  
855 ratio assumption (Redfield, 1963) to convert N(O<sub>2</sub>) to N(C<sub>T</sub>). The carbon/nutrients ratios vary between water  
856 masses and during photosynthesis (Copin Montégut, 2000; Körtzinger et al., 2001; Osterroht and Thomas, 2000;  
857 Thomas et al., 1999). In deep waters, the release ratios vary for C<sub>T</sub>, c(PO<sub>4</sub><sup>3-</sup>), c(NO<sub>3</sub><sup>-</sup>) and c(O<sub>2</sub>) leading to  
858 different concentrations than the traditional Redfield ratio (Hupe and Karstensen, 2000; Minster and Boulahdid,  
859 1987; Shaffer, 1996). For example, during remineralisation, NO<sub>3</sub><sup>-</sup> and PO<sub>4</sub><sup>3-</sup> are released faster than C<sub>T</sub> leading  
860 to a C:P remineralisation ratio of 90 ± 15 at the base of the euphotic zone to about 125 ± 10 from to 1000 m to  
861 the bottom (Shaffer, 1996).

862 The difference of N(O<sub>2</sub>) and N(C<sub>T</sub>) is who used c(DIC) samples directly. The carbon/nutrient ratios vary between  
863 water masses and during photosynthesis (Thomas et al., 1999; Copin-Montégut, 2000; Osterroht and Thomas,  
864 2000; Körtzinger et al., 2001).

865 The difference of the annual N(O<sub>2</sub>) and N(DIC) with the previous studies can also be caused by the yearly  
866 variability of N in the Norwegian Sea. In fact, Kivimäe (2007) saw an annual variability of N(O<sub>2</sub>) from 1955 to  
867 2005 of between 4.7 mol m<sup>-2</sup> a<sup>-1</sup> to and 18.3 mol m<sup>-2</sup> a<sup>-1</sup> and of N(C<sub>T</sub>) of 3.6 mol m<sup>-2</sup> a<sup>-1</sup> to 14.0 mol m<sup>-2</sup> a<sup>-1</sup>. In  
868 order to understand what is causing these interannual changes, it is important to use available high resolution  
869 datasets capture inventory and air-sea changes. Also, this study showed that the Norwegian Sea spring and,  
870 summer and autumn N is strongly affected by time and location of sampling. For that reason, N estimated from  
871 low-resolution datasets make the result strongly dependant on the time and place of sampling. To quantify this  
872 interannual variability in N, more high-resolution studies are needed.

## 873 5 Conclusions

874 This study was, to the best of our knowledge, this study represents the first glider deployment of a CO<sub>2</sub>  
875 optode. During the deployment, the CO<sub>2</sub> optode performance was affected by drift, lag, lack of sampling in

876 the top 150 m after dive 400 (the 24 July 2014), and poor default calibration. We found that the optode response  
877 was better correlated together with  $c(\text{CO}_2)$  than  $p(\text{CO}_2)$ . Nevertheless, the optode was able to capture the spatial  
878 and temporal changes in the Norwegian Sea after recalibration with discrete samples collected along the glider  
879 section and nearby at OWSM during the deployment.

880  $C_T$  estimated from glider data had a standard deviation of  $10 \mu\text{mol kg}^{-1}$  and a mean bias of  $1.5 \mu\text{mol kg}^{-1}$   
881 compared with the discrete samples, while the  $\text{CO}_2$  fugacity  $f(\text{CO}_2)$  had a mean bias of  $(8 \pm 23) \mu\text{atm}$ . The dataset  
882 was used to calculate net community production  $N(\text{O}_2)$  and  $N(C_T)$  from inventory changes, air-sea flux, and  
883 entrainment. The two  $N$  values had maxima during the summer period of increased Chl  $a$  inventory of  $N(C_T) =$   
884  $(14 \pm 8.7) \text{ mmol m}^{-2} \text{ d}^{-1}$  and  $N(\text{O}_2) = (126 \pm 25) \text{ mmol m}^{-2} \text{ d}^{-1}$ . At the beginning of April, we sampled a smaller  
885 spring period of increased Chl  $a$  inventory with a  $N(C_T) = (23 \pm 4.2) \text{ mmol m}^{-2} \text{ d}^{-1}$  and  $N(\text{O}_2) = (94 \pm 24) \text{ mmol m}^{-2}$   
886  $\text{d}^{-1}$ . After the period of increased Chl  $a$  inventory,  $N(C_T)$  decreased due to remineralisation to  $(-4.5 \pm 5.2) \text{ mmol m}^{-2}$   
887  $\text{d}^{-1}$ , and  $N(\text{O}_2)$  to  $(0 \pm 1.5) \text{ mmol m}^{-2} \text{ d}^{-1}$ . The glider monitored two water masses (NwAC and NCC). The NCC-  
888 influenced one was characterised by a lower  $c(\text{O}_2)$  and  $C_T$  than the NwAC region.  $N(\text{O}_2)$  decreased to  $(3.9 \pm 7.3)$   
889  $\text{mmol m}^{-2} \text{ d}^{-1}$  driven by a decrease of  $c(\text{O}_2)$  under 30 m from 300 to 290  $\mu\text{mol kg}^{-1}$  and increased for  $N(C_T)$  to  
890  $(26 \pm 3.7) \text{ mmol m}^{-2} \text{ d}^{-1}$ . In particular, the  $N(\text{O}_2)$  changes were driven by the surface oxygen supersaturation  
891 making the seawater a source of oxygen. In contrast, the ocean was a sink of inorganic carbon during the  
892 summer, with a continuous  $\text{CO}_2$  flux from the atmosphere into the water.

893 This deployment optode shows the potential of using small, low energy consuming  $\text{CO}_2$  optodes these sensors on  
894 autonomous observing platforms like Seagliders to quantify the interactions between biogeochemical processes  
895 and the marine carbonate system at high spatiotemporal resolution. The deployment helped to uncover NCP and  
896 air-sea flux variability over a period of 8 months.

897 Despite all the problems (drift, lag and poor calibration), the  $\text{CO}_2$  optode data could be used to quantify  
898 dissolved inorganic carbon concentration variations. The temporal resolution sampling resolution was 106 s in  
899 the top 100 m (increasing to 381 s from 500 to 1000 m). This could be improved to less than 10 s, but this would  
900 reduce the length of the deployment due to the limited glider battery capacity. With better calibration and  
901 stability improvements, the  $\text{CO}_2$  optode could be routinely used to measure the carbonate system on gliders,  
902 floats and surface vehicles. Glider deployments up to 8 months are possible thanks to the sensor's low power  
903 consumption of 8 mW at 5 s sampling intervals and 7 mW at 60 s sampling intervals (Atamanchuk et al., 2014).  
904 Combined with other novel sensors that measure another DIC-related quantity such as  $A_T$  or  $c(\text{DIC})$ ,  $\text{CO}_2$   
905 optodes on gliders could help provide estimates of NCP, air-sea flux, respiration and remineralisation and  
906 aragonite saturation.

907 During our deployment we calculated  $\text{O}_2$  and DIC-based NCP over the spring and summer period. In the future,  
908 extended deployments could be used to estimate annual (full year) NCP. To have an accurate estimate of annual  
909 NCP, at least one additional glider deployment is needed to have continuous coverage (Binetti et al., 2020).

910 Similar deployments can be used in other areas of the globe to fill gaps in  $N(DIC)$  and  $N(O_2)$ . In particular, glider  
911 deployments have potential in under-sampled areas of the globe such as the Southern Ocean and the Arctic.  
912 Also, it can be used in well-studied areas such as North and Mediterranean Sea to reduce monitoring costs and  
913 compare NCP estimates with previous studies that used other sampling strategies.

914 *Data availability.* The glideglider data are available on Norwegian Marine Data Centre (NMDC) at  
915 <https://doi.org/10.21335/NMDC-1654657723>

916

917 *Competing interests.* The author declares authors declare that there is no conflict of interest.

918

919 *Acknowledgements.* Luca Possenti's PhD project is part of The Next Generation Unmanned Systems Science  
920 (NEXUSS) Centre for Doctoral Training which is funded by the Natural Environment Research Council (NERC)  
921 and the Engineering and Physical Science Research Council (EPSRC) [grant number NE/N012070/1]. We would  
922 like to thank the scientists, engineers, and crew that contributed to the glider mission and data collection along  
923 the glider transect and at Ocean Weather Station M (OWSM). We would also like to thank Kristin Jackson-  
924 Misje, who performed all the carbon analyses, as well as Michael Hemming and Bastien Queste for their initial  
925 contributions to the data analysis. We are grateful to the comments from the two anonymous reviewers and the  
926 Editor, which led to a greatly improved paper.

## 927 **6 References**

928 Alkire, M. B., Lee, C., D'Asaro, E., Perry, M. J., Briggs, N., Cetinić, I. and Gray, A.: Net community production  
929 and export from Seaglider measurements in the North Atlantic after the spring bloom, *J. Geophys. Res. Ocean.*,  
930 119(9), 6121–6139, 2014.

931 ~~Atamanchuk, D.: Development and use of an optical pCO<sub>2</sub> sensor in marine studies, 2013.~~

932 ~~Anderson, L. A.: On the hydrogen and oxygen content of marine phytoplankton, *Deep sea Res. part I Oceanogr.*~~  
933 ~~Res. Pap., 42(9), 1675–1680, 1995.~~

934 ~~Anderson, L. A. and Sarmiento, J. L.: Redfield ratios of remineralization determined by nutrient data analysis,~~  
935 ~~*Global Biogeochem. Cycles*, 8(1), 65–80, 1994.~~

936 Atamanchuk, D., Tengberg, A., Thomas, P. J., Hovdenes, J., Apostolidis, A., Huber, C. and Hall, P. O. J.:  
937 Performance of a lifetime-based optode for measuring partial pressure of carbon dioxide in natural waters,  
938 *Limnol. Oceanogr. Methods*, 12(2), 63–73, doi:10.4319/lom.2014.12.63, 2014.

939 Atamanchuk, D., Kononets, M., Thomas, P. J., Hovdenes, J., Tengberg, A. and Hall, P. O. J.: Continuous long-  
940 term observations of the carbonate system dynamics in the water column of a temperate fjord, *J. Mar. Syst.*, 148,  
941 272–284, doi:10.1016/j.jmarsys.2015.03.002, 2015a.

942 Atamanchuk, D., Tengberg, A., Aleynik, D., Fietzek, P., Shitashima, K., Lichtschlag, A., Hall, P. O. J. and Stahl,  
943 H.: Detection of CO<sub>2</sub> leakage from a simulated sub-seabed storage site using three different types of pCO<sub>2</sub>  
944 sensors, *Int. J. Greenh. Gas Control*, 38, 121–134, doi:10.1016/j.ijggc.2014.10.021, 2015b.

945 Bakker, D. C. E., Pfeil, B., Landa, C. S., Metzl, N., Brien, K. M. O., Olsen, A., Smith, K., Cosca, C., Harasawa,  
946 S. and Jones, S. D.: A multi-decade record of high-quality  $fCO_2$  data in version 3 of the Surface Ocean  
947  $CO_2$  Atlas (SOCAT), *Earth Syst. Sci. Data*, 383–413, doi:10.5194/essd-8-383-2016, 2016.

948 Benson, B. B. and Krause Jr, D.: The concentration and isotopic fractionation of oxygen dissolved in freshwater

949 and seawater in equilibrium with the atmosphere 1, *Limnol. Oceanogr.*, 29(3), 620–632,  
950 ~~1984~~<https://doi.org/10.4319/lo.1984.29.3.0620>, 1984.

951 Binetti, U., Kaiser, J., Damerell, G. M., Rumyantseva, A., Martin, A. P., Henson, S. and Heywood, K. J.: Net  
952 community oxygen production derived from Seaglider deployments at the Porcupine Abyssal Plain site (PAP;  
953 northeast Atlantic) in 2012–13, *Prog. Oceanogr.*, ~~183~~, ~~102293~~, *Oceanogr.*, 183, 102293,  
954 <https://doi.org/10.1016/j.pocean.2020.102293>, 2020.

955 Bittig, H. C. ~~and Körtzinger, A.:~~ Tackling ~~Oxygen Optode Drift~~ ~~oxygen optode drift~~: Near-Surface and In-Air  
956 ~~Oxygen Optode Measurements~~ ~~surface and in-air oxygen optode measurements~~ on a ~~Float~~ ~~Provide~~ ~~float provide~~  
957 an ~~Accurate in Situ Reference~~, ~~(November~~ ~~accurate in situ reference~~, *J. Atmos. Ocean. Technol.*, 32(8), 1536–  
958 1543, ~~doi:10.1175/JTECH-D-14-00162.1~~, <https://doi.org/10.1175/JTECH-D-14-00162.1>, 2015.

959 Bittig, H. C., Fiedler, B., Steinhoff, T. and Körtzinger, A.: ~~OCEANOGRAPHY : METHODS~~ A novel  
960 electrochemical calibration setup for oxygen sensors and its use for the stability assessment of Aanderaa optodes,  
961 ~~1~~, 921–933, ~~doi:10.4319/lom.2012.10.921~~, *Limnol. Oceanogr. Methods*, 10(11), 921–933,  
962 <https://doi.org/10.4319/lom.2012.10.921>, 2012.

963 von Bültzingslöwen, C., McEvoy, A. K., McDonagh, C., MacCraith, B. D., Klimant, I., Krause, C. and  
964 Wolfbeis, O. S.: Sol-gel based optical carbon dioxide sensor employing dual luminophore referencing for  
965 application in food packaging technology, *Analyst*, 127(11), 1478–1483,  
966 ~~2002~~<https://doi.org/10.1039/B207438A>, 2002.

967 Bushinsky, S. M., Takeshita, Y. and Williams, N. L.: Observing Changes in Ocean Carbonate Chemistry: Our  
968 Autonomous Future, *Curr. Clim. Chang. reports*, 5(3), 207–220, <https://doi.org/10.1007/s40641-019-00129-8>,  
969 2019.

970 Chu, S. N., Sutton, A. J., Alin, S. R., Lawrence-Slavas, N., Atamanchuk, D., Mickett, J. B., Newton, J. A.,  
971 Meinig, C., Stalin, S. and Tengberg, A.: Field evaluation of a low-powered, profiling ~~p-CO<sub>2</sub>~~ ~~pCO<sub>2</sub>~~ system in  
972 coastal Washington, ~~Limnol. Oceanogr.~~ ~~Limnology and Oceanography: Methods~~, ~~and~~ 18(6), pp.280-296,  
973 <https://doi.org/10.1002/lom3.10354>, 2020.

974 Copin-Montégut, C.: Consumption and production on scales of a few days of inorganic carbon, nitrate and  
975 oxygen by the planktonic community: results of continuous measurements at the Dyfamed Station in the  
976 northwestern Mediterranean Sea (May 1995), *Deep Sea Res. Part I Oceanogr. Res. Pap.*, 47(3), 447–477, ~~Pap.~~,  
977 47(3), 447–477, [https://doi.org/10.1016/S0967-0637\(99\)00098-9](https://doi.org/10.1016/S0967-0637(99)00098-9), 2000.

978 Degrandpre, M. D.: Measurement of Seawater pCO<sub>2</sub> Using a Renewable-Reagent Fiber Optic Sensor with  
979 Colorimetric Detection, , 1172(8), 331–337, doi:10.1021/ac00052a005, 1993.

980 Dickson, A. G.: Thermodynamics of the dissociation of boric acid in synthetic seawater from 273 ~~–15 to 318~~ ~~–15~~  
981 ~~K~~, ~~37(5)~~, 755–766, ~~15 to 318.15 K~~, *Deep Sea Research Part A. Oceanographic Research Papers*, 37(5), 755–  
982 766, [https://doi.org/10.1016/0198-0149\(90\)90004-F](https://doi.org/10.1016/0198-0149(90)90004-F), 1990.

983 ~~Dickson, A. G., Afghan, J. D. and Anderson, G. C.:~~ Reference materials for oceanic CO<sub>2</sub> analysis : a method for  
984 ~~the certification of total alkalinity~~, *Marine Chemistry*, 80, 185–197, [https://doi.org/10.1016/S0304-](https://doi.org/10.1016/S0304-4203(02)00133-0)  
985 ~~4203(02)00133-0~~, 2003.

986 Dlugokencky, E. J., Lang, P. M., Masarie, K. A., Crotwell, A. M. and Crotwell, M. J.: Atmospheric carbon  
987 dioxide dry air mole fractions from the NOAA ESRL Carbon Cycle Cooperative Global Air Sampling Network,  
988 1968–2014, NOAA ESRL Glob. Monit. Div. Boulder, CO, USA, 2015.

989 Ducklow, H. W. and Doney, S. C.: What Is the Metabolic State of the Oligotrophic Ocean?? A Debate, *Annual*

990 [Review of Marine Science 5](#), doi:10.1146/annurev-marine-121211-172331, 2013.

991 Falck, E. and Anderson, L. G.: The dynamics of the carbon cycle in the surface water of the Norwegian Sea,  
992 [Marine Chemistry](#), 94, 43–53, doi:10.1016/j.marchem.2004.08.009, 2005.

993 Falck, E. and Gade, G.: Net community production and oxygen fluxes in the Nordic Seas based on O<sub>2</sub> budget  
994 calculations, ~~13(4), 1117–1126~~, [Global Biogeochemical cycles](#), 13(4), 1117–1126,  
995 <https://doi.org/10.1029/1999GB900030>, 1999.

996 Fiedler, B., Fietzek, P., Vieira, N., Silva, P., Bittig, H. C. and Körtzinger, A.: In situ CO<sub>2</sub> and O<sub>2</sub> measurements  
997 on a profiling float, *J. Atmos. Ocean. Technol.*, 30(1), 112–126, doi:10.1175/JTECH-D-12-00043.1, 2013.

998 Foltz, G. R., Grodsky, S. A., Carton, J. A. and McPhaden, M. J.: Seasonal mixed layer heat budget of the tropical  
999 Atlantic Ocean, *J. Geophys. Res. Ocean.*, 108(C5), <https://doi.org/10.1029/2002JC001584>, 2003.

1000 Friedlingstein, P., Jones, M., O’Sullivan, M., Andrew, R., Hauck, J., Peters, G., Peters, W., Pongratz, J., Sitch, S.  
1001 and Le Quéré, C.: Global carbon budget 2019, *Earth Syst. Sci. Data*, 11(4), 1783–1838,  
1002 ~~2019~~ <https://doi.org/10.5194/essd-11-1783-2019>, 2019.

1003 Garcia, H. E. and Gordon, L. I.: Oxygen solubility in seawater: Better fitting equations, *Limnol. Oceanogr.*,  
1004 37(6), 1307–1312, <https://doi.org/10.4319/lo.1992.37.6.1307>, 1992.

1005 Gattuso, J.-P. and Hansson, L.: *Ocean acidification*, Oxford University Press., 2011.

1006 Gislefoss, J. S., Nydal, R., Slagstad, D., Sonninen, E. and Holme, K.: Carbon time series in the Norwegian sea, ~~;~~  
1007 ~~45, 433–460~~, [Deep Sea Research Part I: Oceanographic Research Papers](#), 45, 433–460,  
1008 [https://doi.org/10.1016/S0967-0637\(97\)00093-9](https://doi.org/10.1016/S0967-0637(97)00093-9), 1998.

1009 Gourcuff, C.: ANFOG Slocum CTD data correction, [IMOS](#), (March), 2014.

1010 Goyet, C., Walt, D. R. and Brewer, P. G.: Development of a fiber optic sensor for measurement of pCO<sub>2</sub> in sea  
1011 water: design criteria and sea trials, *Deep Sea Res. Part A. Oceanogr. Res. Pap.*, 39(6), 1015–1026, 1992.

1012 Hagebo, M. and Rey, F.: Storage of seawater for nutrients analysis, *Fisk. Hav.*, ~~4, 1, 12~~, [Hav., 4, 1, 12,  
1013 \[https://doi.org/10.1016/0198-0149\\(92\\)90037-T\]\(https://doi.org/10.1016/0198-0149\(92\)90037-T\), 1984.](#)

1014 Hansen, B. and Østerhus, S.: North Atlantic – Nordic Seas exchanges, [Progress in oceanography](#), 45, 109–208,  
1015 [https://doi.org/10.1016/S0079-6611\(99\)00052-X](https://doi.org/10.1016/S0079-6611(99)00052-X), 2000.

1016 Hardman-Mountford, N. J., Moore, G., Bakker, D. C. E., Watson, A. J., Schuster, U., Barciela, R., Hines, A.,  
1017 Moncoiffé, G., Brown, J., Dye, S., Blackford, J., Somerfield, P. J., Holt, J., Hydes, D. J. and Aiken, J.: An  
1018 operational monitoring system to provide indicators of CO<sub>2</sub>-related variables in the ocean, *ICES J. Mar. Sci.*,  
1019 65(8), 1498–1503, doi:10.1093/icesjms/fsn110, 2008.

1020 Haskell, W. Z., Hammond, D. E., Prokopenko, M. G., Teel, E. N., Seegers, B. N., Ragan, M. A., Rollins, N. and  
1021 Jones, B. H.: Net Community Production in a Productive Coastal Ocean From an Autonomous Buoyancy-Driven  
1022 Glider, *J. Geophys. Res. Ocean.*, 124(6), 4188–4207, <https://doi.org/10.1029/2019JC015048>, 2019.

1023 Hemsley, J. M.: *OBSERVATIONS PLATFORMS| Buoy*, 2015.

1024 Hemsley, V. S., Smyth, T. J., Martin, A. P., Frajka-williams, E., Thompson, A. F., Damerell, G. and Painter, S.  
1025 C.: Estimating Oceanic Primary Production Using Vertical Irradiance and Chlorophyll ~~Pro-f-iles~~ [Profiles](#) from  
1026 Ocean Gliders in the North Atlantic, ~~49(19), 11612-11621~~, doi:10.1021/acs.est.5b00608, 2015.

1027 Van Heuven, S., Pierrot, D., Rae, J. W. B., Lewis, E. and Wallace, D. W. R.: MATLAB program developed for  
1028 CO<sub>2</sub> system calculations, ORNL/CDIAC-105b. Carbon Dioxide Inf. Anal. Center, Oak Ridge Natl. Lab. US  
1029 Dep. Energy, Oak Ridge, Tennessee, 530, 2011.

1030 ~~Hupe, A. and Karstensen, J.: Redfield stoichiometry in Arabian Sea subsurface waters, [Global Biogeochem-](#)~~  
1031 ~~[Cycles](#), 14(1), 357–372, 2000.~~

1032 Jeansson, E., Olsen, A., Eldevik, T., Skjelvan, I., Omar, A. M., Lauvset, S. K., Nilsen, J. E. Ø., Bellerby, R. G.  
1033 J., Johannessen, T. and Falck, E.: The Nordic Seas carbon budget : Sources , sinks , and uncertainties, [Global](#)  
1034 [Biogeochemical Cycles](#), 25(2002), 1–16, doi:10.1029/2010GB003961, 2011.

1035 Kara, A. B., Rochford, P. A. and Hurlburt, H. E.: An optimal definition for ocean mixed layer depth, *J. Geophys.*  
1036 *Res. Ocean.*, 105(C7), 16803–16821, ~~2000~~<https://doi.org/10.1029/2000JC900072>, 2000.

1037 Kivimäe, C.: Carbon and oxygen fluxes in the Barents and Norwegian Seas: production, air-sea exchange and  
1038 budget calculations, ~~2007~~[PhD Dissertation, University of Bergen, 2007](#).

1039 Klimant, I., Huber, C., Liesch, G., Neurauder, G., Stangelmayer, A. and Wolfbeis, O. S.: Dual lifetime  
1040 referencing (DLR)—a new scheme for converting fluorescence intensity into a frequency-domain or time-  
1041 domain information, in *New Trends in Fluorescence Spectroscopy*, pp. 257–274, Springer.,  
1042 ~~2001~~[https://doi.org/10.1007/978-3-642-56853-4\\_13](https://doi.org/10.1007/978-3-642-56853-4_13), 2001.

1043 Körtzinger, A., Thomas, H., Schneider, B., Gronau, N., Mintrop, L. and Duinker, J. C.: At-sea intercomparison  
1044 of two newly designed underway pCO<sub>2</sub> systems—encouraging results, *Mar. Chem.*, 52(2), 133–145,  
1045 [https://doi.org/10.1016/0304-4203\(95\)00083-6](https://doi.org/10.1016/0304-4203(95)00083-6), 1996.

1046 Körtzinger, A., Koeve, W., Kähler, P. and Mintrop, L.: C: N ratios in the mixed layer during the productive  
1047 season in the northeast Atlantic Ocean, *Deep Sea Res. Part I Oceanogr. Res. Pap.*, 48(3), 661–688,  
1048 ~~2001~~[https://doi.org/10.1016/S0967-0637\(00\)00051-0](https://doi.org/10.1016/S0967-0637(00)00051-0), 2001.

1049 ~~Laws, E. A.: Photosynthetic quotients, new production and net community production in the open ocean, *Deep*~~  
1050 ~~*Sea Res. Part A. Oceanogr. Res. Pap.*, 38(1), 143–167, [https://doi.org/10.1016/0198-0149\(91\)90059-O](https://doi.org/10.1016/0198-0149(91)90059-O), 1991.~~

1051 Lee, K., Tong, L. T., Millero, F. J., Sabine, C. L., Dickson, A. G., Goyet, C., Park, G. H., Wanninkhof, R., Feely,  
1052 R. A. and Key, R. M.: Global relationships of total alkalinity with salinity and temperature in surface waters of  
1053 the world’s oceans, *Geophys. Res. Lett.*, 33(19), 1–5, doi:10.1029/2006GL027207, 2006.

1054 Lee, K., Kim, T., Byrne, R. H., Millero, F. J., Feely, R. A. and Liu, Y.: The universal ratio of boron to chlorinity  
1055 for the North Pacific and North Atlantic oceans, *Geochim. Cosmochim. Acta*, 74(6), 1801–1811,  
1056 doi:10.1016/j.gca.2009.12.027, 2010.

1057 Lockwood, D., Quay, P. D., Kavanaugh, M. T., Juranek, L. W., ~~and~~ Feely, R. A. ~~and~~ ~~À. E. C. À.:~~ High-  
1058 resolution estimates of net community production and air-sea ~~CO<sub>2</sub>~~ flux in the northeast Pacific, [Global](#)  
1059 [Biogeochemical Cycles](#), 26, 1–16, doi:10.1029/2012GB004380, 2012.

1060 Lueker, T. J., Dickson, A. G. and Keeling, C. D.: Ocean pCO<sub>2</sub> calculated from DIC, TA, and the Mehrbach  
1061 equations for K1 and K2: Validation using laboratory measurements of CO<sub>2</sub> in gas and seawater at equilibrium,  
1062 *Abstr. Pap. Am. Chem. Soc.*, 217, U848–U848, 2000.

1063 Martz, T. R., Connery, J. G. and Johnson, K. S.: Testing the Honeywell Durafet for seawater pH applications,  
1064 *Limnol. Oceanogr. Methods*, 8, 172–184, doi:10.4319/lom.2010.8.172, 2010.

1065 Medeot, N., Nair, R. and Gerin, R.: Laboratory Evaluation and Control of Slocum Glider C – T Sensors, [Journal](#)  
1066 [of Atmospheric and Oceanic Technology](#), 838–846, doi:10.1175/2011JTECHO767.1, 2011.

1067 Miloshevich, L.: Development and Validation of a Time-Lag Correction for Vaisala Radiosonde Humidity  
1068 Measurements, [Journal of Atmospheric and Oceanic Technology](#), 1305–1328, 2004.

1069 ~~Minster, J.-F. and Boulahdid, M.: Redfield ratios along isopycnal surfaces—a complementary study, *Deep Sea*~~  
1070 ~~*Res. Part A. Oceanogr. Res. Pap.*, 34(12), 1981–2003, 1987.~~

1071 Monteiro, P. M. S., Schuster, U., Hood, M., Lenton, A., Metzl, N., Olsen, A., Rogers, K., Sabine, C., Takahashi,  
1072 T. and Tilbrook, B.: A global sea surface carbon observing system: Assessment of changing sea surface CO<sub>2</sub> and  
1073 air-sea CO<sub>2</sub> fluxes, *Proc. Ocean.*, 9, 702–714, 2009.

1074 Naveira Garabato, A. C., Oliver, K. I. C., Watson, A. J. and Messias, M.: Turbulent diapycnal mixing in the  
1075 Nordic seas, *J. Geophys. Res. Ocean.*, 109(C12), <https://doi.org/10.1029/2004JC002411>, 2004.

1076 Neftel, A., Oeschger, H., Schwander, J., Stauffer, B. and Zumbunn, R.: Ice core sample measurements give  
1077 atmospheric  $\text{CO}_2$  content during the past 40,000 yr, *Nature*, 295(5846), 220–223,  
1078 <https://doi.org/10.1038/295220a0>, 1982.

1079 Neuer, S., Cianca, A., Helmke, P., Freudenthal, T., Davenport, R., Meggers, H. and Knoll, M.: *Progress in*  
1080 *Oceanography*-Biogeochemistry and hydrography in the eastern subtropical North Atlantic gyre . Results from  
1081 the European time-series station ESTOC, *Progress in Oceanography*, 72, 1–29,  
1082 doi:10.1016/j.pocean.2006.08.001, 2007.

1083 Nicholson, D., Emerson, S. and Eriksen, C. C.: Net community production in the deep euphotic zone of the  
1084 subtropical North Pacific gyre from glider surveys, *Limnol. Oceanogr.*, 53(5 PART 2), 2226–2236,  
1085 doi:10.4319/lo.2008.53.5\_part\_2.2226, 2008.

1086 Nicholson, D. P. and Feen, M. L.: Air calibration of an oxygen optode on an underwater glider, *Limnol.*  
1087 *Oceanogr. Methods*, 15(5), 495–502, doi:10.1002/lom3.10177, 2017.

1088 Nilsen, J. E. Ø. and Falck, E.: *Progress in Oceanography*-Variations of mixed layer properties in the Norwegian  
1089 Sea for the period 1948 – 1999, *Progress in Oceanography*, 70, 58–90, doi:10.1016/j.pocean.2006.03.014, 2006.

1090 Obata, A., Ishizaka, J. and Endoh, M.: Global verification of critical depth theory for phytoplankton bloom with  
1091 climatological in situ temperature and satellite ocean color data, *J. Geophys. Res. Ocean.*, 101(C9), 20657–  
1092 20667, <https://doi.org/10.1029/96JC01734>, 1996.

1093 Olsen, A., Key, R. M., Van Heuven, S., Lauvset, S. K., Velo, A., Lin, X., Schirnick, C., Kozyr, A., Tanhua, T.,  
1094 Hoppema, M., Jutterström, S., Steinfeldt, R., Jeansson, E., Ishii, M., Pérez, F. F. and Suzuki, T.: The global  
1095 ocean data analysis project version 2 (GLODAPv2) - An internally consistent data product for the world ocean,  
1096 *Earth Syst. Sci. Data*, 8(2), 297–323, doi:10.5194/essd-8-297-2016, 2016.

1097 Osterroht, C. and Thomas, H.: New production enhanced by nutrient supply from non-Redfield remineralisation  
1098 of freshly produced organic material, *J. Mar. Syst.*, 25(1), 33–46, *Syst.*, 25(1), 33–46,  
1099 [https://doi.org/10.1016/S0924-7963\(00\)00007-5](https://doi.org/10.1016/S0924-7963(00)00007-5), 2000.

1100 Pachauri, R. K. and Reisinger, A.: IPCC fourth assessment report, IPCC Fourth Assess. Rep., 1, 976 [online]  
1101 Available from:  
1102 [http://www.construible.es/construible%5Cbiblioteca%5Cpresentacion\\_informe\\_ipcc.pdf%5Cpapers2://publicacion/uuid/DD3ABB67-E411-4C0F-A29C-DA693B95B789](http://www.construible.es/construible%5Cbiblioteca%5Cpresentacion_informe_ipcc.pdf%5Cpapers2://publicacion/uuid/DD3ABB67-E411-4C0F-A29C-DA693B95B789), 2007.

1103 Peeters, F., Atamanchuk, D., Tengberg, A., Encinas-Fernández, J. and Hofmann, H.: Lake metabolism:  
1104 Comparison of lake metabolic rates estimated from a diel  $\text{CO}_2$ -and the common diel  $\text{O}_2$ -technique, *PLoS One*,  
1105 11(12), 2016-<https://doi.org/10.1371/journal.pone.0168393>, 2016.

1106 Plant, J. N., Johnson, K. S., Sakamoto, C. M., Jannasch, H. W., Coletti, L. J., Riser, S. C. and Swift, D. D.: Net  
1107 community production at Ocean Station Papa observed with nitrate and oxygen sensors on profiling floats,  
1108 *Global Biogeochem. Cycles*, 30(6), 859–879, <https://doi.org/10.1002/2015GB005349>, 2016.

1109 Quay, P., Stutsman, J. and Steinhoff, T.: Primary production and carbon export rates across the subpolar N.  
1110 Atlantic Ocean basin based on triple oxygen isotope and dissolved  $\text{O}_2$  and Ar gas measurements, *Global*  
1111 *Biogeochem. Cycles*, 26(2), *Cycles*, 26(2), <https://doi.org/10.1029/2010GB004003>, 2012.

1112 Le Quéré, C., Raupach, M. R., Canadell, J. G., Marland et al., G., Le Quéré et al., C., Le Quéré et al., C.,  
1113 Raupach, M. R., Canadell, J. G., Marland, G., Bopp, L., Ciais, P., Conway, T. J., Doney, S. C., Feely, R. A.,  
1114 Foster, P., Friedlingstein, P., Gurney, K., Houghton, R. A., House, J. I., Huntingford, C., Levy, P. E., Lomas, M.



1116 R., Majkut, J., Metzl, N., Ometto, J. P., Peters, G. P., Prentice, I. C., Randerson, J. T., Running, S. W.,  
1117 Sarmiento, J. L., Schuster, U., Sitch, S., Takahashi, T., Viovy, N., van der Werf, G. R. and Woodward, F. I.:  
1118 Trends in the sources and sinks of carbon dioxide, *Nat. Geosci.*, 2(12), 831–836, doi:10.1038/ngeo689, 2009.  
1119 Redfield, A. C.: The influence of organisms on the composition of seawater, *The sea*, 2, 26–77, 1963.  
1120 Rérolle, V. M. C., Floquet, C. F. A., Harris, A. J. K., Mowlem, M. C., Bellerby, R. R. G. J. and Achterberg, E.  
1121 P.: Development of a colorimetric microfluidic pH sensor for autonomous seawater measurements, *Anal. Chim.*  
1122 ~~*Acta*, 786, 124–131~~, *Acta*, 786, 124–131, <https://doi.org/10.1016/j.aca.2013.05.008>, 2013.  
1123 Reuer, M. K., Barnett, B. A., Bender, M. L., Falkowski, P. G. and Hendricks, M. B.: New estimates of Southern  
1124 Ocean biological production rates from O<sub>2</sub>/Ar ratios and the triple isotope composition of O<sub>2</sub>, *Deep Sea Res.*  
1125 *Part I Oceanogr. Res. Pap.*, 54(6), 951–974, *Pap.*, 54(6), 951–974, <https://doi.org/10.1016/j.dsr.2007.02.007>,  
1126 2007.  
1127 Rey, B. F.: 5 . Phytoplankton : the grass of the sea, ~~(ed)~~, 2001.  
1128 Sabine, C. L., Feely, R. A., Gruber, N., Key, R. M., Lee, K., Bullister, J. L., Wanninkhof, R., Wong, C. S. S.,  
1129 Wallace, D. W. R., Tilbrook, B., Millero, F. J., Peng, T.-H. T.-H., Kozyr, A., Ono, T., Rios, A. F., A., F. R.,  
1130 Gruber, N., Key, R. M., Lee, K., Bullister, J. L., Wanninkhof, R., Wong, C. S. S., Wallace, D. W. R., Tilbrook,  
1131 B., Millero, F. J., Peng, T.-H. T.-H., Kozyr, A., Ono, T. and Rios, A. F.: The oceanic sink for anthropogenic  
1132 CO<sub>2</sub>, *Science* ~~(80-)~~, 305(5682), 367–371, doi:10.1126/science.1097403, 2004.  
1133 Saderne, V., Fietzek, P. and Herman, P. M. J.: Extreme Variations of pCO<sub>2</sub> and pH in a Macrophyte Meadow of  
1134 the Baltic Sea in Summer: Evidence of the Effect of Photosynthesis and Local Upwelling, *PLoS One*, 8(4), 2–9,  
1135 doi:10.1371/journal.pone.0062689, 2013.  
1136 Saetre, R. and Ljoen, R.: THE NORWEGIAN COASTAL CURRENT, 1972.  
1137 Seguro, I., Marca, A. D., Painting, S. J., Shutler, J. D., Suggett, D. J. and Kaiser, J.: High-resolution net and  
1138 gross biological production during a Celtic Sea spring bloom, *Prog. Oceanogr.*, 177, 101885, *Oceanogr.*, 177,  
1139 101885, <https://doi.org/10.1016/j.pocean.2017.12.003>, 2019.  
1140 Seidel, M. P., Degrandpre, M. D. and Dickson, A. G.: A sensor for in situ indicator-based measurements of  
1141 seawater pH, *Marine chemistry*, 109, 18–28, doi:10.1016/j.marchem.2007.11.013, 2008.  
1142 ~~Shaffer, G.: Biogeochemical cycling in the global ocean 2. New production, Redfield ratios, and remineralization~~  
1143 ~~in the organic pump, , 101, 3723–3745, 1996.~~  
1144 Sharples, J., Ross, O. N., Scott, B. E., Greenstreet, S. P. R. and Fraser, H.: Inter-annual variability in the timing  
1145 of stratification and the spring bloom in the North-western North Sea, *Cont. Shelf Res.*, 26(6), 733–751,  
1146 2006, <https://doi.org/10.1016/j.csr.2006.01.011>, 2006.  
1147 Skjelvan, I., Falck, E., Anderson, L. G. and Rey, F.: Oxygen fluxes in the Norwegian Atlantic Current, *Mar.*  
1148 *Chem.*, 73(3–4), 291–303, doi:10.1016/S0304-4203(00)00112-2, 2001.  
1149 Skjelvan, I., Anderson, L. G., Falck, E. and Anders, K.: A Review of the Inorganic Carbon Cycle of the Nordic  
1150 Seas and Barents Sea ~~and Christoph through the strength area of 15–75~~, 2005.  
1151 Skjelvan, I., Falck, E., Rey, F. and Kringstad, S. B.: Inorganic carbon time series at Ocean Weather Station M in  
1152 the Norwegian Sea, *Biogeosciences*, 549–560, <https://doi.org/10.5194/bg-5-549-2008>, 2008.  
1153 Sprintall, J. and Roemmich, D.: Characterizing the structure of the surface layer in the Pacific Ocean, *J.*  
1154 *Geophys. Res. Ocean.*, 104(C10), 23297–23311, <https://doi.org/10.1029/1999JC900179>, 1999.  
1155 Sutton, A. J., Sabine, C. L., Meinig, C. and Feely, R. A.: A high-frequency atmospheric and seawater p CO<sub>2</sub>  
1156 data set from 14 open-ocean sites using a moored autonomous system, *Earth System Science Data*, 353–366,  
1157 doi:10.3334/CDIAC/OTG.TSM, 2014.

1158 Swift, J. H.: The arctic waters, in *The Nordic Seas*, pp. 129–154, Springer., 1986.

1159 Takahashi, T., Sutherland, S. C., Sweeney, C., Poisson, A., Metzl, N., Tilbrook, B., Bates, N., Wanninkhof, R.,  
1160 Feely, R. A., Sabine, C., Olafsson, J. and Nojiri, Y.: Global sea – air ~~CO<sub>2</sub>~~CO<sub>2</sub> flux based on climatological  
1161 surface ocean ~~pCO<sub>2</sub>~~pCO<sub>2</sub>, and seasonal biological and temperature effects, *Deep Sea Research Part II: Topical  
1162 Studies in Oceanography*, 49, 1601–1622, [https://doi.org/10.1016/S0967-0645\(02\)00003-6](https://doi.org/10.1016/S0967-0645(02)00003-6), 2002.

1163 Takahashi, T., Sutherland, S. C., Wanninkhof, R., Sweeney, C., Feely, R. A., Chipman, D. W., Hales, B.,  
1164 Friederich, G., Chavez, F., Sabine, C., Watson, A., Bakker, D. C. E., Schuster, U., Yoshikawa-Inoue, H., Ishii,  
1165 M., Midorikawa, T., Nojiri, Y., Körtzinger, A., Steinhoff, T., Hoppema, M., Olafsson, J., Arnarson, T. S.,  
1166 Johannessen, T., Olsen, A., Bellerby, R., Wong, C. S., Delille, B., Bates, N. R. and de Baar, H. J. W.:  
1167 Climatological mean and decadal change in surface ocean pCO<sub>2</sub>, and net sea–air CO<sub>2</sub> flux over the global  
1168 oceans, *Deep Sea Res. Part II Top. Stud. Oceanogr.*, 56(8), 554–577, doi:10.1016/j.dsr2.2008.12.009, 2009.

1169 Tengberg, A., Hovdenes, J., Andersson, H. J., Brocandel, O., Diaz, R. and Hebert, D.: *OCEANOGRAPHY :  
1170 METHODS*–Evaluation of a lifetime-based optode to measure oxygen in aquatic systems, *OCEANOGRAPHY :  
1171 METHODS*, (1964), 7–17, <https://doi.org/10.4319/lom.2006.4.7>, 2006.

1172 Thomas, H., Ittekkot, V., Osterroht, C. and Schneider, B.: Preferential recycling of nutrients—the ocean’s way to  
1173 increase new production and to pass nutrient limitation?, *Limnol. Oceanogr.*, 44(8), 1999–2004,  
1174 ~~1999-~~<https://doi.org/10.4319/lo.1999.44.8.1999>, 1999.

1175 Thomas, P. J., Atamanchuk, D., Hovdenes, J. and Tengberg, A.: The use of novel optode sensor technologies for  
1176 monitoring dissolved carbon dioxide and ammonia concentrations under live haul conditions, *Aquac. Eng.*, ~~77,~~  
1177 ~~89–96,~~*Eng.*, 77, 89–96, <https://doi.org/10.1016/j.aquaeng.2017.02.004>, 2017.

1178 Thompson, R. O. R. Y.: Climatological numerical models of the surface mixed layer of the ocean, *J. Phys.  
1179 Oceanogr.*, 6(4), 496–503, 1976.

1180 United States. National Environmental Satellite and Information Service, D., Monterey, G. I. and Levitus, S.:  
1181 Seasonal variability of mixed layer depth for the world ocean, US Department of Commerce, National Oceanic  
1182 and Atmospheric Administration ....., 1997.

1183 Wanninkhof, R.: *OCEANOGRAPHY : METHODS*–Relationship between wind speed and gas exchange over the  
1184 ocean revisited, *OCEANOGRAPHY : METHODS*, 351–362, doi:10.4319/lom.2014.12.351, 2014.

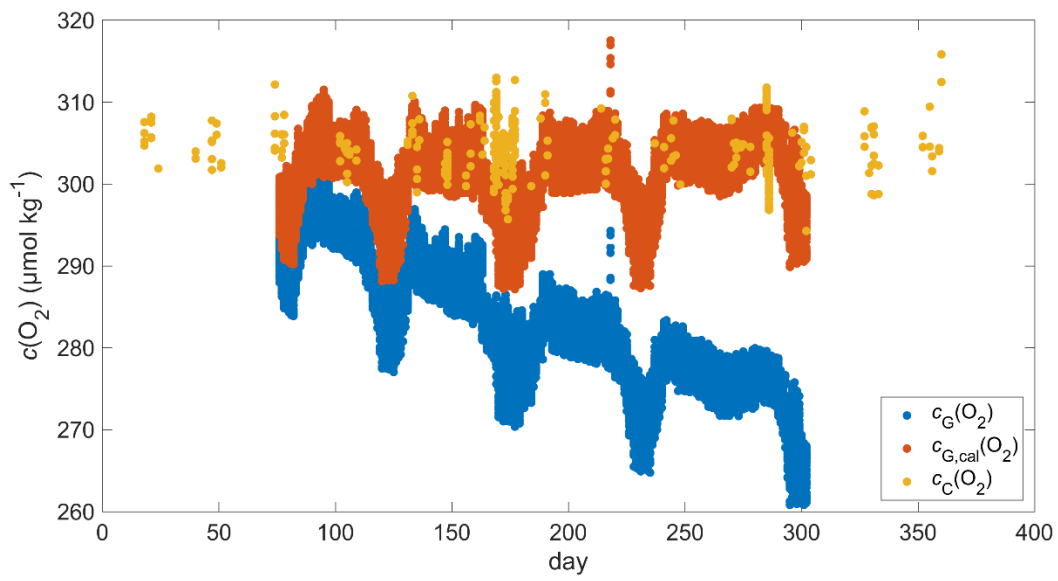
1185 Weiss, R. F.: Carbon dioxide in water and seawater: the solubility of a non-ideal gas, *Mar. Chem.*, 2(3), 203–  
1186 215, doi:10.1016/0304-4203(74)90015-2, 1974.

1187 Weiss, R. F. and Price, B. A.: Nitrous oxide solubility in water and seawater, *Mar. Chem.*, ~~8(4), 347–359,~~*Chem.*,  
1188 ~~8(4), 347–359,~~ [https://doi.org/10.1016/0304-4203\(80\)90024-9](https://doi.org/10.1016/0304-4203(80)90024-9), 1980.

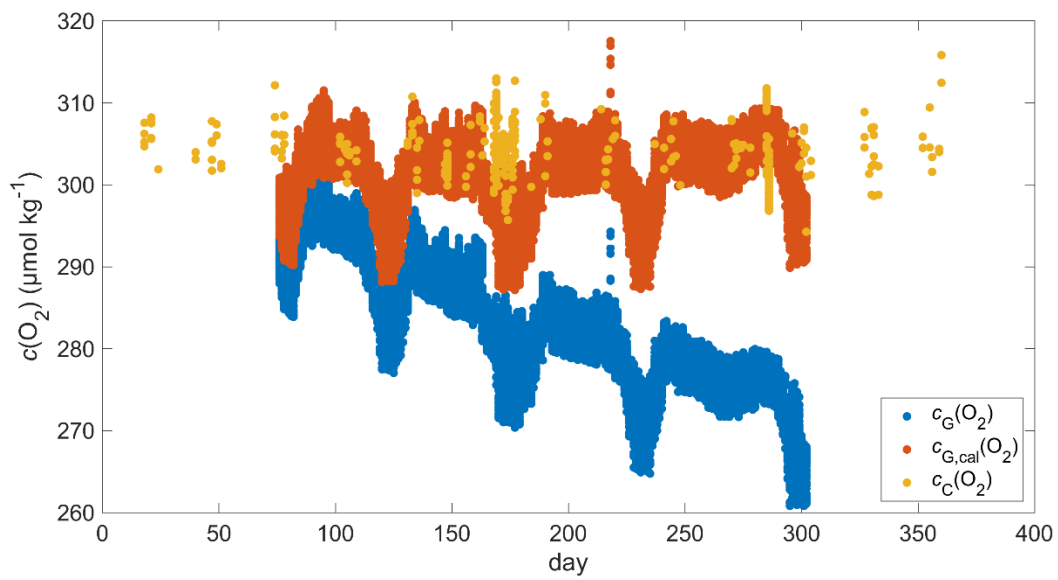
1189 Woolf, D. K. and Thorpe, S. A.: Bubbles and the air-sea exchange of gases in near-saturation conditions, *J. Mar.  
1190 Res.*, 49(3), 435–466, ~~1991-~~<https://doi.org/10.1357/002224091784995765>, 1991.

1191

1192 **7 Appendices**



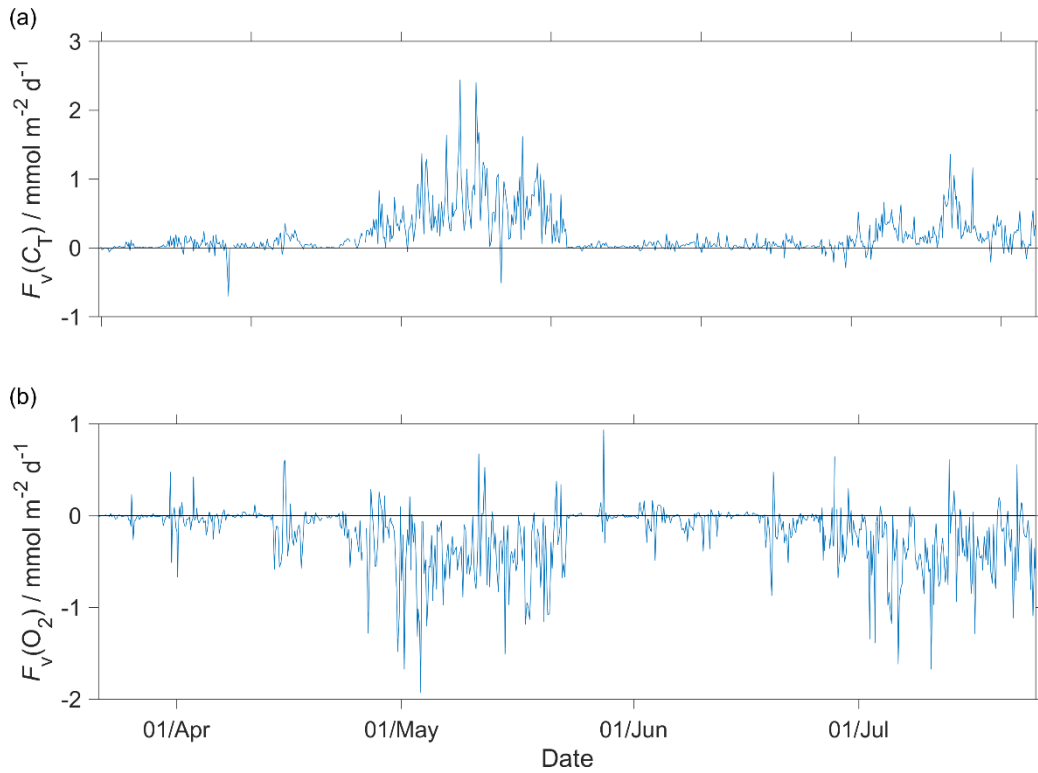
1193



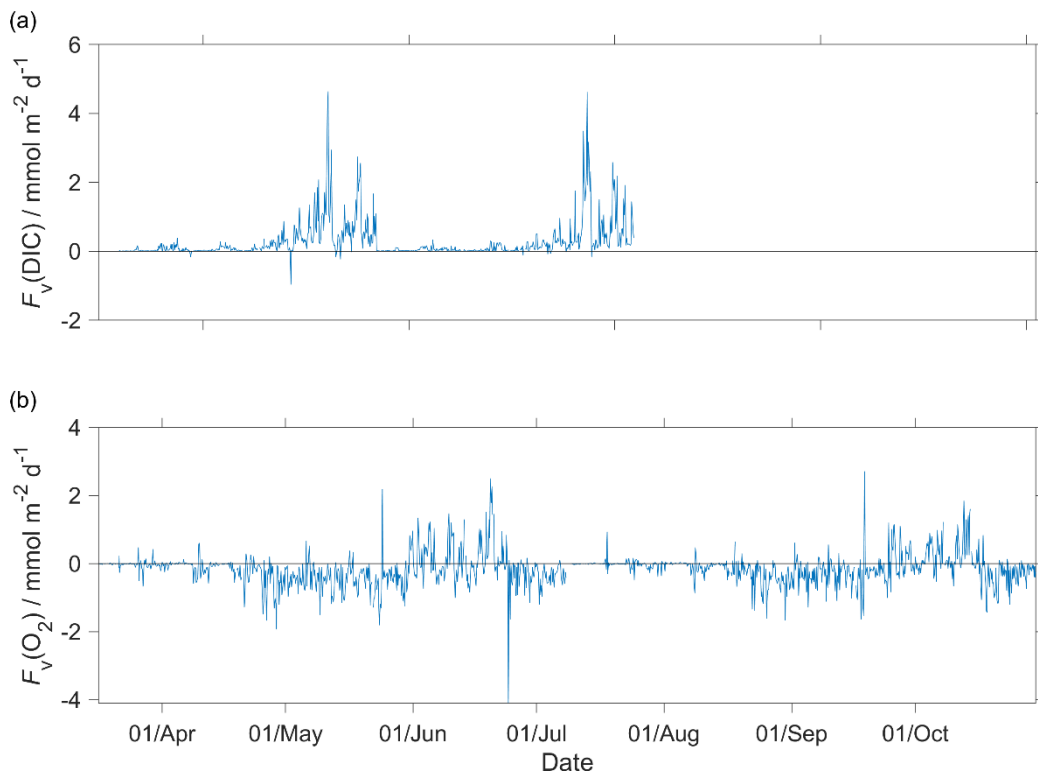
1194

1195 **Figure A1:** ~~discrete~~Discrete samples  $c_C(O_2)$  (yellow), raw glider oxygen  $c_G(O_2)$  (blue) and drift corrected glider  
 1196 oxygen  $c_{G,cal}(O_2)$  (red) for a potential density  $> 1028 \text{ kg m}^{-3}$  at depths less than 1000 m.

1197



1198



1199

1200 **Figure A2:** Diapycnal mixing ( $F_v$ ) calculated for the glider descent and ascent for a)  $\epsilon_{TC}(\text{DIC})$  and b)  $\text{O}_2$  at the  
 1201 mixed layer depth ( $z_{\text{mix}}$ ) when deeper than 45 m ( $z_{\text{lim}}$ ) and at  $z_{\text{lim}}$  when  $z_{\text{mix}}$  was shallower than 45 m. In the  
 1202 calculations we used a vertical eddy diffusivity ( $K_z$ ) of  $10^{-5} \text{ mm}^2 \text{ s}^{-2-1}$  (Naveira Garabato et al., 2004). (Naveira  
 1203 [Garabato et al., 2004](#)).